# Neutron Activation Analysis of eWaste using a Medical Cyclotron

by

Nathaniel Vitale

Faculty of Science & Environmental Studies

Lakehead University, Thunder Bay, Ontario

A dissertation submitted in partial fulfillment of

the requirements of the degree of

Master of Science

Chemistry Major

Graduate Program

# Table of contents

## Abstract

Neutron activation analysis (NAA) is an analytical technique that harnesses a decay product of certain radioactive isotopes. This works in a two-step process: neutron activation followed by gamma spectroscopy analysis. While a research reactor is typically used for NAA, a medical cyclotron can also be used as neutrons are produced as the byproduct of its radionuclide production. A potential source of these neutrons is from the reaction $^{18}O(p,n)^{18}F$, where a $H_2{}^{18}O$ target is irradiated by a proton beam to generate $^{18}F$ for radiotracer synthesis. This fact paired with its easier access compared to a research reactor demonstrates a potential benefit of using medical cyclotron for NAA.

This work focused on using a medical cyclotron to analyse electronic waste (eWaste) samples using NAA. A variety of elements were assessed, including aluminum, silicon, copper, iron, magnesium, tin, chromium, arsenic, cadmium, neodymium, gold, palladium, and nickel. Analysis of single-element calibration standards gave a high degree of linearity. A variety of multi-element samples were then prepared and analyzed. These included small circuit board fragments from a variety of eWaste, custom-made standards containing a selection of the previously mentioned elements, and heterogenous samples containing similar selections. Each of the samples were irradiated for 20 minutes or less and had their gamma rays collected via gamma spectroscopy for 10 minutes or less. Spectral data was analysed with InterSpec, with peak areas being corrected for radionuclide decay, neutron beam exposure, and gamma count time.

Across all the sixty-one gamma peaks analysed, approximately two thirds (62%) of the calculated masses were above the true or expected values for the element. Except for arsenic and palladium (35% higher and 40% lower, respectively), all NAA-determined elemental masses were within 26% of their expected value in the heterogeneous samples. These samples provided the most accurate assessment of this technique, as they were the only samples in which the elemental composition was known prior to NAA. Thus, the comparison of initial element masses to those determined through NAA had a high level of validity and accuracy.

## Acknowledgements

I would like to thank Dr. Campbell for all his help in developing an efficient procedure to both generate standard curves and analyse samples. This work could not have been done without his state-of-the-art “pneumatic transfer system” at the cyclotron facility, which provided the equipment necessary to safely and quickly preform neutron activation of a variety of samples. I would like to thank the Thunder Bay Regional Health Sciences Centre for providing access to their cyclotron and laboratory facilities. I would also like to thank Lakehead University for not only a laboratory to prepare samples but also access to the reagents necessary to generate the samples.

## List of Tables

## List of Figures

## Abbreviations

eV – Electronvolt = $1.602 \times 10^{-19}$ J

NAA – Neutron Activation Analysis

eWaste – Electronic Waste

FWHM – Full Width at Half Maximum

α – Alpha Particle

$\beta^-$ – Beta-Minus Particle

$\beta^+$ – Beta-Plus Particle

γ – Gamma Ray

ν – Neutrino

$\bar{\nu}$ – Anti-Neutrino

n – Neutron

p – Proton

# 1. Introduction

## 1.1. eWaste analysis

Electronic waste (eWaste) is an ever-growing concern as more electronic devices are manufactured. Many non-recycled old and/or broken electronics end up in landfills. This is a problem for two reasons. Discarded electronics contain toxic chemicals, comprised of elements such as bromine, lead, and arsenic. They also contain technologically valuable metals, such as gold, chromium, and palladium.[1] Given the significance of these elements, there has been a lot of work done to find effective methods for their recovery and subsequent reuse or proper disposal.[2] eWaste has been analysed through various methodologies over the years but one that has not been as thoroughly investigated is using neutron activation analysis (NAA). This study focused on assessing the effectiveness of using a cyclotron to preform NAA on eWaste and explored its strengths and limitations.

Common methods used to quantify the elements in eWaste are Inductively Coupled Plasma Mass Spectrometry (ICP-MS) and Inductively Coupled Plasma Optical Emission Spectroscopy (ICP-OES).[3] These techniques involve using concentrated acids (*i.e.* $H_2SO_4$, HCl, and $HNO_3$) to dissolve the sample and leach the elements of interest off the circuit boards. These techniques involve ionizing or exciting the compounds in the sample using plasma. For ICP-OES, these excited atoms will then release characteristic photons when they return to their ground state.[4] ICP-MS ionizes the sample and then separates the ions based on size and charge.[3] An example of the effectiveness of this method on eWaste analysis was demonstrated in a study by Schuster & Ebin in 2021, where it was successfully used to detect the indium concentration in LCD screens.[5] These methods are very useful, as they have high sensitivity, low detection limits, and can detect a vast array of elements.[4,5] The largest drawbacks however are the requirements that the solid sample be solubilized with acid. This alters the chemical properties of the sample, is more labour intensive and makes this method destructive. The solution also requires some dilution for the sample to be analysed, increasing the time to prepare samples.[4,5]

A study by Bookhagen et al.[1] from 2018 analyzed a variety of eWaste circuit board samples. Samples were prepared by grinding, followed by acid digestions, they analysed the elemental composition of the samples via ICP-OES and ICP-MS. They found that the most abundant elements in smartphone circuits were in decreasing order: copper, iron, silicon, nickel, tin, zinc, barium, aluminum, chromium, and calcium, which comprised 78% of the weight of the printed circuit boards. They also provided the relative mass percents of each element in their samples. The list of elements they reported informed the elements targeted as part of this study for analysis by NAA. From their results, copper, iron, silicon, nickel, tin, aluminum, and chromium were investigated along with gold, cadmium, arsenic, palladium, neodymium, and magnesium.

X-ray Fluorescence Spectroscopy (XRF) is another technique commonly used to analyse eWaste. This involves bombarding a sample with x-rays to eject K-shell electrons and using a spectrometer to detect the photons emitted by the sample when electrons move from the L- or M-shell to replace the K-shell vacancies.[3] A study by Otsuki et al.[6] in 2019 found that XRF was successful in the quantification of various metals in eWaste, including copper, iron, aluminum, and zinc. They mentioned however that XRF was unable to accurately quantify some metals (*e.g.* cadmium), leading to an overestimation of the mass.[6] While this technique is fast and non-destructive, it is predominately a surface analysis technique and experiences difficulties when analysing large, heterogenous samples.[3]

NAA has also been used to analyse eWaste.[3] As this technique is non-destructive it allows for repeated analysis under varied irradiation or counting conditions to maximize the data available. Using NAA also eliminates the need for expensive and potentially hazardous reagents in the sample preparation step. Samples can also be reanalyzed after decay by complementary techniques such as ICP-OES. All that is required is that the sample is small enough to fit into the vial being irradiated by the cyclotron's neutron beam, and subsequently, the gamma spectrometer. This technique allows for rapid and inexpensive results, while also being non-destructive and relatively safe.

In a study by Buczkó et al.[7] from 2025, they investigated eWaste using NAA with a research reactor. Both instrumental (INAA) and prompt gamma NAA (PGNAA) were utilized. Through their investigation, they were able to identify several elements, including copper, nickel, aluminum, silicon, iron, calcium, tin, and zinc. This study not only shows similar results to the ICP analysis of eWaste by Bookhagen et al.[1] but also demonstrates that NAA has the sensitivity to detect trace elements in eWaste, including cadmium and chromium. This provided additional support for this study to use the cyclotron to analyse eWaste samples with the goal that most, if not all, the elements that were focused on would be able to be detected and quantified effectively.

Buczkó et al.[7] irradiated their INAA samples from 20 minutes up to three hours. This was then followed by a delay of four or more days between the irradiation of their samples and their gamma collection. This was done to quantify the medium- and long-lived radioisotopes formed. To then test the detection limit of their analysis on these radioisotopes, they waited an additional few hours to few days before re-analysing. Given this delay, they were unable to detect the short-lived radioisotopes with INAA such as those produced by hydrogen, boron, carbon, oxygen, aluminum, silicon, and chlorine. They were however able to detect these elements when they analysed the samples via prompt NAA, as the gamma photons were detected from the compound nuclei as they formed. This demonstrates the impact of structuring the irradiation and analysis procedures around the long-lived radioisotopes, as opposed to the short-lived ones. For this study, while there were radioisotopes with half-lives ranging from a few minutes to a several days, it used a short irradiation time and minimal delay to analyse them. The irradiation time was also be limited to 20 minutes. While this did not generate as much signal as the three-hour irradiation in the paper, the low detection limits demonstrated by NAA allowed for the detection of any long-lived radioisotopes formed.

## 1.2. Neutron activation analysis

Neutron activation analysis (NAA) is a method of analysis used to both identify and quantify the presence of various elements in a sample.[8] It relies on the principle that each radioactive isotope emits characteristic gamma rays. These rays can be used to pick out a

particular radioisotope in a sample and provide insight as to which element it arose from. NAA generates these radioisotopes by bombarding stable atoms with neutrons, thus activating them.[9]

The history of NAA started back in 1910 when Carl Auer von Welsbach noticed that when he stored samples near the substance he termed “ionium”, which ended up being identified as $^{230}$Th, they too became radioactive. It turned out that the radioactive thorium was emitting alpha particles, leading to alpha-particle activation of the nearby samples.[9] George Hevesy and Hilde Levi built upon this discovery in 1935 when they published a paper on using thermal neutrons to irradiated samples containing dysprosium and europium.[10] They did this by combining a solution of $^{226}$Ra salt with finely ground beryllium powder. As the radium decayed through alpha emission, it irradiated the beryllium, causing the emission of neutrons, through the nuclear reaction $^{9}$Be(α,n)$^{12}$C.[10]

In 1938 Glenn Seaborg and John Livingood developed a method of using a cyclotron to irradiate samples as an improvement to the neutron-emitting radioisotope method. They bombarded an iron target with a deuteron beam with their cyclotron to produce neutrons, allowing for the production of radioisotopes including $^{60}$Co, $^{55}$Fe, $^{59}$Fe, $^{65}$Zn, and $^{131}$I. This research showed that there was real potential in developing and using this methodology, which was officially called radioactivation analysis by George Boyd in 1949.[9]

Up to this point in history, only (α, n) neutron sources and low-flux cyclotrons were being used for NAA. It wasn’t until the 1950s when nuclear reactors started to be used for NAA. This period of time also corresponded to the development of NaI(Tl) scintillation detectors and multichannel analysers (MCAs).[9] These technologies allowed for much more specialized detection of varying characteristic gamma rays, with a Full Width at Half Maximum (FWHM) of 50 keV, which is the width of the peak at half its max height. This resolution was improved by the invention of Ge(Li) detectors, which improved the resolution to 1-3 keV.[9] By the 1980s, more efficient intrinsic germanium detectors were developed, and the MCAs were moved from being hard-wired to being computer-based. It continues to be an essential tool in the fields of trace element analysis and the development and certification of reference standards.[9]

Since its invention, there have been many different types of NAA methods developed. NAA differs greatly depending on the energy of the neutrons irradiating the sample. In fast NAA, high energy (>0.5 MeV) neutrons are used to facilitate (n,n), (n,2n), (n,p), and (n,α) nuclear reactions, whereas thermal NAA uses thermal neutrons (<1 eV; average of 0.025 eV). In this type of analysis, only (n,γ) reactions can occur.[9] Since this study focused on utilizing an 18-24 MeV proton beam to generate the neutron flux, all of these reactions were possible. The high energy neutrons that were generated favoured the fast neutron reactions. There were however some thermal neutron reactions that occurred, as some fast neutrons became thermalized through inelastic scattering and neutron moderation.

The way NAA is used also depends on when the gamma rays are being analysed. In prompt NAA, the gamma rays are collected as the sample is being irradiated. These gamma rays are generated as the nuclear reaction is taking place (*e.g.* $^{197}Au(n,\gamma)^{198}Au$). In the case of delayed NAA, it is the gamma photons that the radioisotope emits as it decays that are measured. If the irradiated sample is analysed without post-irradiation chemical separation, it is called instrumental NAA. However, if specific radioisotopes are isolated from the sample before being analysed, it is known as radiochemical NAA.[9] This research focused on delayed instrumental NAA, as the irradiated samples were removed from the neutron beam and were subsequently analysed via gamma spectroscopy without purification. This was ideal, as many radioisotopes investigated had half-lives of hours or days. This also saved time and reduced costs by not requiring reagents or additional equipment to extract and purify the isotopes, determine the yield, or efficiency, or the chemical purification step(s).

Finally, depending on how the gamma activity is used to determine the abundance of each element of interest, either absolute, semi-absolute, or comparator/relative NAA can be used. In absolute NAA, the quantity of an analysed element can be mathematically determined using its cross section for the specific radioisotope produced, its decay factor, the time of irradiation, and the gamma activity. If the neutron flux can be kept constant (*i.e.* in a particular irradiation site in a research reactor), semi-absolute NAA can be used to calculate the element's abundance with only the activity needing to be measured. In comparator/relative NAA, a reference standard must be irradiated alongside the sample to compare their gamma activities

and identify the abundance of the elements.[9] This research used the comparator/relative NAA approach as standards of known composition were used to compare with the activity of the sample. Instead of irradiating a standard alongside the samples, several reference standards were created and irradiated in order to generate calibration curves. These curves were then compared to the gamma peak areas of the samples. Since the samples and the standards were not irradiated together, all were corrected for any variability in the irradiation and gamma analysis process to ensure an accurate comparison.

Regardless of the type of NAA used, one large drawback this technique has is nuclear interference. This occurs when a sample contains more than one element that forms the same radioisotope. This is an issue as the gamma signal produced for these species would be the sum of each element's contribution. This is most common in elements that have a Z-number within one or two of each other. Some examples of these are Si, Al, Mg, and Na. In this situation, the (n,p) or (n,α) reaction of one element will interfere with the (n,γ) reaction of another. To combat this, an interference factor can be calculated based on the ratio of thermal to fast-neutron flux, the quantity of the two interfering elements, as well as the cross-sections for the interfering nuclear reactions.[11] For this study, this issue was avoided by not including elements that have a similar Z-number in the same sample, with the exception of aluminum and silicon. For these elements, different radioisotopes were identified for each to prevent such difficulties.

NAA is mainly done using a research reactor, such as TRIGA and SLOWPOKE reactors. In a study from 1987, Grynpas et al. investigated human bone samples using reactor-based NAA.[12] The length of time spent irradiating the sample depended on the radioisotopes they were focusing on. For instance, when investigating the production of $^{20}$F, which has a half-life of 11.2 seconds, they utilized an irradiation time of 20 seconds, and a gamma spectrometer count time of 20 seconds. The short irradiation time is important, as short-lived radioisotopes will reach saturation quickly, limiting their quantity in longer irradiations. For the gamma analysis, a short count time allows for sufficient decay to occur without decreasing the signal to noise ratio by extending the collection for a longer period. For longer-lived radioisotopes (*e.g.* $^{24}$Na with a half-life of 14.96 hours), the irradiation was extended to 16 hours, with a count time of 33 minutes. This long irradiation was followed by a six-day delay in order to permit the short-lived

radioisotopes to decay, allowing for spectra of the longer-lived ones. This study signifies the importance of having a reasonable irradiation, delay, and count time for the isotopes being detected. For this study, most isotopes of interest had a half-life under an hour. Given this, the methods involved a 20-minute irradiation, followed by a two-to-10-minute delay, with a two-to-10-minute count time.

## 1.3. Using a cyclotron for neutron activation analysis

NAA continues to be used with cyclotron-accelerated deuteron beams. In a study by Kriváň & Münzel[13] in 1973 they used deuterons to bombard a beryllium target, causing a (d,n) reaction. Through this method they were able to create a neutron beam with energy up to 53 MeV, which allowed for a neutron beam with an energy greater than 35 MeV. This is much higher than the typical 14 MeV neutrons produced by neutron generators, such as $^{3}H(d,n)^{4}He$. They noticed that by varying the deuteron beam energy, they were able to tune the generated neutrons to have a peak energy close to the cross-section peak of their desired reactions. This allowed them to preferentially generate one radioisotope over another, a useful tool for their analysis. This study demonstrates the ability to not only generate a variety of neutron energies but also substantially high ones.

The sensitivity of using a cyclotron for NAA is also significantly better than using a typical 14 MeV neutron generator. In a study by Münzel et al.[14] in 1977, they were able to use a cyclotron to accelerate deuterons up to 45 MeV. They used these high-energy deuterons to generate neutrons for the NAA of oxygen through the nuclear reaction $^{16}O(n,p)^{16}N$. They were able to detect <1 μg of oxygen, which was over 100-times more sensitive than previously shown with a neutron generator. This high sensitivity was valuable in a study by Das et al.[15] in 2024, where they looked at the trace metals in lake water and sediment samples. They were able to identify nine heavy metals in water and lake sediment samples: chromium, iron, cobalt, nickel, copper, zinc, arsenic, cadmium, and lead. Their work being able to detect minute quantities of these important elements demonstrates great promise to use eWaste samples with similar elements. The concentration of these elements in eWaste however will be in higher concentrations, and thus, easier to detect.

In addition to high energy research cyclotrons being used for NAA, medical cyclotrons can also be used. The main difference between a medical cyclotron and a research cyclotron is that a medical cyclotron is set up to generate the radioisotopes typically via (p,n) reactions. A common example of this is the production of $^{18}F$ for radiotracer synthesis. This occurs through the $^{18}O(p,n)^{18}F$ nuclear reaction, where there is a $H_2{}^{18}O$ target instead of a beryllium target. This allows for neutrons to be generated for NAA while the cyclotron is being used for its daily operations.

Much of the interest in neutron activation in association with medical cyclotrons has been related to radiation safety. During routine operation the surfaces of the cyclotron vault, and the cyclotron itself, become activated by neutrons, where gamma spectroscopy is often used to identify the radionuclides present. In a study from 2019, Vichi et al.[16] studied the radioisotopes present in the concrete walls of two medical cyclotron vaults. One cyclotron was located in a hospital in Bologna, Italy, where a portable gamma spectrometer was used to collect data. The other cyclotron was located in a hospital in Bern, Switzerland, where core drilling samples were extracted. In both cases, the main long-lived radioisotopes identified were $^{152}Eu$, $^{54}Mn$, $^{60}Co$, $^{46}Sc$, and $^{134}Cs$. The activity measured was on average between 0.01-0.6 Bq/g concrete. This was determined to be above the safe operating levels based on European safety standards. They also determined that the amount of low-level radioactive waste that would need to be disposed of, given the potential decommissioning of these facilities, would be about 93 $m^3$ in the Bologna facility and about 58 $m^3$ in the Bern facility. While this activation was not desirable, it shows that these cyclotrons generated neutrons that could be used for NAA.

In a study by Benavente-Castillo et al.[17] from 2019, they investigated the neutron flux generated by a medical cyclotron during routine operation. Instead of analysing the activation in the vault's concrete walls, they instead set up metal-foil targets around the vault to not only assess the ability for NAA but assess if thermal, epithermal, and fast nuclear reactions were possible and their corresponding fluxes. This was of importance to better understand the ability for the neutron fluences to activate the equipment and bunker walls, to put appropriate safety measures in place for workers, given the radioisotopes produced through this process. The fluxes were measured through the placement of gold, indium, and nickel foils around the vault,

which were then analysed by gamma spectroscopy to analyse the respective thermal, epithermal, and fast neutron fluxes. It was found that the thermal flux was approximately 1.8 x $10^4$ $cm^{-2}$ $s^{-1}$, the epithermal flux was approximately 8.9 x $10^3$ $cm^{-2}$ $s^{-1}$, and the fast flux was approximately 5.4 x $10^4$ $cm^{-2}$ $s^{-1}$. In comparison, a SLOWPOKE research reactor can generate fluxes upwards of $10^{10}$ $cm^{-2}$ $s^{-1}$.[18] While the generated flux from a cyclotron is not as large as that generated by a research reactor, this study not only demonstrated that substantial neutron flux is emitted from a medical cyclotron, as it pertains to the potential risks of neutron activation, but if harnessed this flux can be used for irradiating and analysing other samples. This was significant to this study, as it demonstrated that medical cyclotrons generate significant neutron flux, with neutron energies capable of both thermal and fast NAA.

In a study by Campbell and Tikka[19] from 2022, they utilized a medical cyclotron for the NAA of gold, and silver samples. This paper discussed that while the gold samples could be irradiated during normal cyclotron operations and analysed later in the day, the half-life of the silver radioisotopes were much too short (<10 min) for this long of a delay. They described building and using a PVC tube track to insert and remove irradiation samples from the cyclotron vault. This allowed for the quick retrieval of samples containing short-lived radioisotopes.

This paper also described that when increasing the proton beam energy from 18 to 24 MeV, the activity generated from the radioisotopes also increased. Thus, irradiating samples with a proton beam at 24 MeV would not only give preference to the high-energy nuclear reactions but would also overall increase the signal. Another way to increase the signal is by increasing the irradiation time, as the study had only irradiated and collected the gamma spectra for about 10 minutes each. This study focused on irradiating samples for 20 minutes to generate more activity for the long-lived radioisotopes. Several gamma collections, ranging from a count time of two to 10 minutes were also used in this work to quickly observe the activity from the short-lived isotopes and give additional count time to measure the long-lived ones.

## 1.4. Radiochemistry

Radiochemistry is a branch of chemistry where time is of the essence. Radionuclides have a limited stability so they, and any pharmaceutical or tracer they are attached to, have a

pre-determined shelf life. Radiochemistry deals with both the stable and unstable versions of certain elements. These different versions of the element are known as the element's isotopes. All elements have many different isotopes, with the difference between them being the number of neutrons in their nucleus, and whether or not they are radioactive. For instance, $^{12}C$ is the most abundant isotope of carbon, with six protons and six neutrons. It is also one of the two stable isotopes of carbon, with the other being $^{13}C$. This contrasts with $^{11}C$, which is a radioactive isotope, with the same six protons but only five neutrons. Since this isotope is radioactive, it is referred to as a radioisotope or radionuclide.

### 1.4.1. Radioactivity

When an atom is radioactive, it's nucleus decays or disintegrates over time. This decay occurs when a nucleus contains either too many protons or neutrons. It undergoes decay to reach a more stable state. Different radioactive nuclides decay at different rates, as represented by their respective half-lives. Half-life is the amount of time that it takes for half of the radioactive atoms of a particular radionuclide to decay. A half-life can vary in length from a fraction of a second to trillions of years. Half-life is important as it lets you know how long your radioactive sample or product will last and, thus, how quickly you must make use of it.

### 1.4.2. Nuclear decay

There are many ways that a radionuclide can decay. The main types of decay are alpha, beta, and gamma. Alpha decay involves the release of an alpha particle, also known as a helium nucleus, with two protons and two neutrons (Equation 1.1):[20]

$$ {}^{A}_{Z}P \rightarrow {}^{A-4}_{Z-2}D + {}^{4}_{2}\alpha \qquad (1.1) $$

where *P* is the parent nucleus or the original radioactive atom, *D* is the daughter nucleus, *A* is the parent nucleus' mass number, *Z* is the parent nucleus' atomic number, and $\alpha$ is the alpha particle. In this decay, the daughter nucleus has two fewer protons and neutrons than the parent nucleus.

For beta decay, there are two forms: beta-plus and beta-minus. In beta-minus decay, a neutron decays into a proton while ejecting a beta-minus particle (an electron) and an antineutrino from the nucleus (Equation 1.2):[20]

$$ {}^{A}_{Z}P \rightarrow {}^{A}_{Z+1}D + \beta^{-} + \overline{\nu} \tag{1.2} $$

where $\beta^-$ is the beta-minus particle and $\overline{\nu}$ is the antineutrino. In this decay, the daughter nucleus has one more proton than the parent nucleus. Beta-plus decay is the opposite in that a proton decays into a neutron while ejecting a beta-plus particle (a positron or "antielectron") and a neutrino from the nucleus (Equation 1.3):[20]

$$ {}^{A}_{Z}P \rightarrow {}^{A}_{Z-1}D + \beta^{+} + \nu \tag{1.3} $$

where $\beta^+$ is the beta-plus particle and $\nu$ is the neutrino. In this decay, the daughter nucleus has one less proton than the parent nucleus.

Unlike alpha and beta decay, gamma decay does not result in a decrease in the number of protons or neutrons in the atom. Gamma decay occurs when a radioactive atom is in an excited state. These atoms will emit gamma photons to return to a lower-energy ground state. (Equation 1.4):[20]

$$ {}^{A}_{Z}P^{*} \rightarrow {}^{A}_{Z}P + \gamma \tag{1.4} $$

where $*$ represents the excited state of the parent atom and $\gamma$ is the gamma photon. Other forms of nuclear decay include electron capture, internal conversion, and spontaneous fission.[20]

There are many naturally occurring radioisotopes with a variety of half-lives (e.g., $^{14}C$ at 5700 years), but many useful radioisotopes for medical imaging or some other purposes have short half-lives and therefore do not exist in nature. If short-lived radionuclides are required for research or medical purposes, they would have to be made just prior to use. An important analytical technique that uses radionuclides is neutron activation analysis. This technique generates radionuclides through neutron activation, by placing samples within a flux of neutrons. These radionuclides are then used for medical applications or analysed to understand the composition of the material that is being investigated.[8]

## 1.5. Nuclear reactions

When bombarding an element with neutrons, nuclear reactions – *i.e.* reactions within the nucleus - occur. These reactions involve the absorption of a neutron by the target nucleus, forming an excited compound nucleus, which quickly decays into a product nucleus, as illustrated in Equation 1.5.[8,21,22]

$$ {}^{A}_{Z}T + {}^{1}_{0}n \rightarrow {}^{A+1}_{Z}E^{*} \rightarrow P + emitted\ particle \tag{1.5} $$

where *T* is the target nucleus, *n* is the neutron, $E^*$ is the excited nucleus, and *P* is the product nucleus. These reactions are written in the shorthand notation of T(*a*,*e*)P, where *a* is the particle being absorbed by the nucleus, and *e* is the particle being emitted.

Many different nuclear reactions can take place when the excited nucleus decays into the product nucleus, and as such, there are a variety of possible emitted particles. These may include alpha particles, neutrons, protons, and/or gamma photons. The most common reactions are (n,α), (n,p), (n,n), (n,2n), and (n,γ).[4] Both the (n,α) and (n,p) reactions lead to the conversion of one element into another. For the (n,α) reaction, an alpha particle is emitted, as per Equation 1.6.[22]

$$ {}^{A}_{Z}T + {}^{1}_{0}n \rightarrow {}^{A+1}_{Z}E^{*} \rightarrow {}^{A-3}_{Z-2}P + {}^{4}_{2}\alpha \tag{1.6} $$

For this reaction, the atomic number of the target nucleus decreases by two and its mass number decreases by three, converting it to an element with two fewer protons and one fewer neutron. An example of this reaction is $^{27}$Al(n,α)$^{24}$Na, where aluminum is converted to sodium by absorbing a neutron and emitting an alpha particle.

For the (n,p) reaction, a proton is emitted, as per Equation 1.7.[22]

$$ {}^{A}_{Z}T + {}^{1}_{0}n \rightarrow {}^{A+1}_{Z}E^{*} \rightarrow {}^{A}_{Z-1}P + {}^{1}_{1}p \tag{1.7} $$

For this reaction the atomic number is decreased by one and the mass number remains the same, converting it to an element with the one more neutron and one less proton. An example of this reaction is $^{58}$Ni(n,p)$^{58}$Co, where nickel is converted to cobalt through absorption of a neutron and emission of a proton.

Whereas the (n,α) and (n,p) reactions produce different elements, the (n,n), (n,2n), and (n,γ) reactions can yield a radioactive version of the same element. For the (n,n) reaction, a neutron is emitted, as per Equation 1.8.[22]

$$ {}^{A}_{Z}T + {}^{1}_{0}n \rightarrow {}^{A+1}_{Z}E^{*} \rightarrow {}^{Am}_{Z}T + {}^{1}_{0}n \quad (1.8) $$

For this reaction, the mass number and atomic number remain the same, producing a metastable version of target element. This metastable nucleus will undergo further decay in order to become more stable. An example of this reaction is $^{111}$Cd(n,n)$^{111m}$Cd, where cadmium-111 becomes metastable by both absorbing and emitting a neutron.

For the (n,2n) reaction, two neutrons are emitted, as per Equation 1.9.[22]

$$ {}^{A}_{Z}T + {}^{1}_{0}n \rightarrow {}^{A+1}_{Z}E^{*} \rightarrow {}^{A-1}_{Z}T + 2{}^{1}_{0}n \quad (1.9) $$

For this reaction, the mass number decreased by one while the atomic number remains the same. An example of this reaction is $^{63}$Cu(n,2n)$^{62}$Cu, where the copper becomes radioactive by absorbing one neutron and emitting two, leading to a radioisotope with one less neutron.

Finally, for the (n,γ) reaction, a gamma particle/photon is emitted, as per Equation 1.10.[22]

$$ {}^{A}_{Z}T + {}^{1}_{0}n \rightarrow {}^{A+1}_{Z}E^{*} \rightarrow {}^{A+1}_{Z}T + \gamma \quad (1.10) $$

For this reaction, the mass number increases by one while the atomic number remains the same. An example of this reaction is $^{197}$Au(n,γ)$^{198}$Au, where the gold becomes radioactive by absorbing one neutron and, instead of emitting any nucleons, only emits a gamma photon. This creates a radioisotope with one extra neutron.

## 1.6. Neutron sources

Different neutron sources produce neutrons of different energies from low energy (<1 eV) to high-energy (>1 MeV). In a situation where neutrons of varying energies exist, such as in a nuclear reactor, the varying quantities of neutrons with specific energies can be plotted in a neutron energy spectra. This spectra tends to group neutrons into three energy categories:

thermal (<1 eV), fast (>0.5 MeV), and intermediate/epithermal (1 eV to 0.5 MeV).[23] Depending on the energy of the neutrons, different reactions can take place. For (n,γ) reactions, thermal neutrons are required. These can either be generated directly via low-energy neutron generators[24], or by the thermalization of high-energy neutrons, as they lose energy when moving through the sample or a moderator. Other reactions, such as (n,α), (n,p), (n,n), and (n,2n), require higher energy neutrons from a high energy generator.

### 1.6.1. Nuclear reactor

Commonly, a nuclear reactor is used for neutron activation analysis (NAA), as it already produces neutrons as part of its operation. It does this first by producing incident neutrons with a neutron-generating radionuclide. These neutrons bombard uranium atoms, leading to fission. The fission is accompanied by the release of additional neutrons, which go on to bombard other uranium atoms, leading to a chain reaction. Since the magnitude of the neutron-flow is stable and reproduceable, this makes an excellent choice for NAA. Samples can be inserted into irradiation sites within the reactor to be irradiated by the neutrons. Since these sites can have different neutron energies, specific nuclear reactions can be selected for.[25] The main issue with this approach is the high cost and limited availability of using a nuclear reactor for NAA.[25]

### 1.6.2. Cyclotron

Cyclotrons are not normally used for NAA. Typically, they are used to generate proton-rich radioisotopes to be used in medicine and research. This occurs through the cyclotron creating a proton beam, which bombards the loaded sample. The most common radioisotope produced by cyclotrons is $^{18}F$ through the nuclear reaction $^{18}O(p,n)^{18}F$, with $[^{18}O]$-$H_2O$ being the source of the $^{18}O$.[19] As this is a (p,n) reaction, neutrons are produced as a by-product.[19] Typically, these neutrons exit the cyclotron and scatter within the vault until they are thermalized and absorbed by the concrete walls or other materials in the cyclotron vault. In some instances, the neutron bombardment of the vault has been measured and used to assess radiation safety.[16]

There have been a select few instances where these neutrons were used for NAA. In these instances, the neutrons were either produced unintentionally, as per the by-product of radionuclide generation, or intentionally for NAA. In the case of cyclotrons used for medical radionuclide production, these neutrons are commonly produced via the $^{18}O(p,n)^{18}F$ reaction.[19] In an intentional case of neutron generation, deuterons (deuterium nuclei) were bombarded upon a beryllium target, which resulted in a neutron beam capable of (n,p), (n,α), and (n,2n) nuclear reactions. That investigation used a deuteron beam with energies between 30-50 MeV, however, which are much higher than the average beam energies of other cyclotrons.[13]

Regardless of the intention behind the neutron generation, using a cyclotron for neutron activation analysis only requires that the sample of interest is placed behind the main target, exposing it to the neutron fluence. To maximize time and cost efficiency of running a cyclotron, using some form of sample transfer system into and out of the vault while the cyclotron is running is ideal. This allows for the quick and easy insertion and removal of a sample from the neutron beam, which is useful if the analysis of short-lived radioisotopes is desirable.

Overall, using a cyclotron for NAA is more accessible than a nuclear reactor, as they are more common among research facilities and hospitals. Also, if a NAA sample is placed in the neutron beam while the cyclotron is already being used for other medical or research purposes, the experiment is essentially free. A drawback is that it produces low neutron density, which results in comparatively long irradiation times to reach useful limits of detection.

## 1.7. Gamma spectroscopy

Once the NAA sample is irradiated by neutrons, it needs to be analysed to determine its activity and the quantity of its respective components. This is done through gamma spectroscopy. Most radioisotopes generate gamma rays with unique energies that can be used to identify them when they decay. An example is $^{198}Au$, which generates a characteristic gamma ray with an energy of 412 keV. The gamma rays detected in NAA are from decay of the produced radionuclide, so in this example, the peak at 412 keV is characteristic of $^{198}Au$ decay to $^{198}Hg$. This is a different energy than the gamma rays produced directly from any (n,γ) reaction, in

which the analysis of these photons is known as prompt gamma-ray neutron activation analysis.[26]

While gold demonstrates a straightforward example of elemental identification using NAA, there are some instances where it is not simple. The first case is when the radionuclide decays through beta-plus decay. As shown in Equation 1.3, beta-plus decay generates a beta-plus particle and a neutrino. The beta-plus particle is also known as a positron or an antielectron, the antimatter counterpart of the electron. When these particles are generated, they interact with nearby electrons and annihilate, generating gamma rays in the process. These gamma rays always carry a characteristic energy of 511 keV. For proton-rich radioisotopes, they favour beta-plus decay, generating positrons and the subsequent 511 keV peak. This is an issue for radionuclides such as $^{196}$Au and $^{80}$Br.

Another challenging case is when several elements generate the same radioisotope, termed nuclear interference. For example, in a NAA sample containing silicon, aluminum, magnesium, or sodium: $^{28}$Al can be generated by silicon and aluminum; $^{27}$Mg can be generated from silicon, aluminum, and magnesium; and $^{24}$Na can be generated by aluminum, magnesium, and sodium (Figure 1.7.1). The figure illustrates the stable isotopes (black circles) and their neutron activation products (white circles). The arrows denote the nuclear reaction, where green represents (n,γ) reactions, orange represents (n,p) reactions, and blue represents (n,α) reactions. For magnesium, $^{24}$Mg is the most abundant isotope and participates in the (n,p) reaction, whereas $^{26}$Mg participates in the (n,γ) reaction. $^{28}$Si is the most abundant isotope of silicon and participates in the (n,p) reaction, whereas $^{30}$Si participates in the (n,α) reaction.

This can create a substantial challenge when trying to differentiate between elements that are close to each other on the Periodic Table. To avoid identification issues pertaining to these cases, it is vitally important either to identify a unique radioisotope for each element being analysed or to avoid samples with elements leading to the same radionuclide products when irradiated.

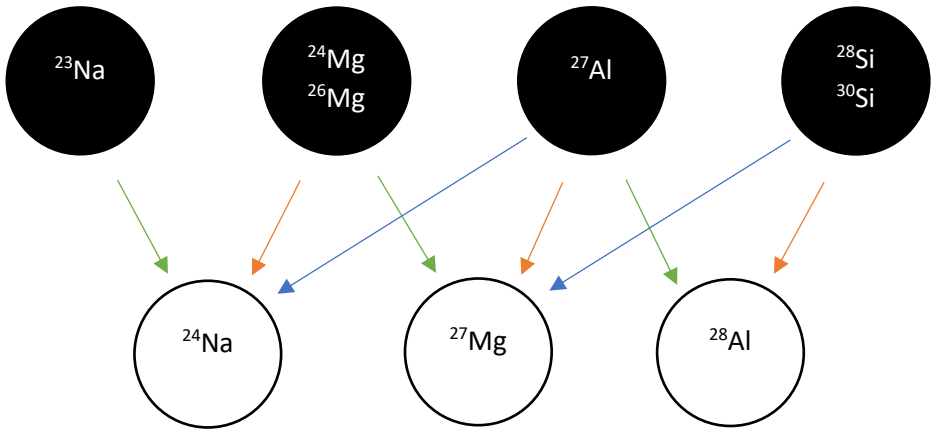


Figure 1.7.1. An illustration of the radioisotope interference that occurs when sodium, magnesium, aluminum, and silicon are analysed together via NAA.

Once a radioisotope is chosen per element of interest, gamma spectroscopy is quite straightforward. Count time may be modified to collect more signal, but isotopes with inherently short half-lives will decay quickly and limit the size of their peaks regardless of count time. Once the spectrum is collected, the integrated area under each peak can be used to quantify the element detected, through the generation of a standard curve. It is important however to correct the peak area for radionuclide decay, count time, and neutron beam exposure, as these may differ between samples.[19]

The size of the peaks is dependent on the measured activity of the radioisotope being investigated, as shown in Equation 1.11.

$$A = N\ x\ \sigma\ x\ \varphi\ x\ \left(1 - e^{-\lambda t}\right) \qquad (1.11)$$

where *A* is the activity of the radioisotope, *N* is the number of target atoms in the sample, σ is the activation cross section (*i.e.* the probability that the nucleus will absorb a bombarded neutron), φ is the neutron flux (*i.e.* the number of neutrons passing through a square-centimeter per second), $\lambda$ is the decay constant for the generated radioisotope, and *t* is the time the sample is being irradiated.[25]

## 1.8. Applications

Due to its simple nature, NAA has many applications. It has been used to generate reference standards for both the National Institute of Standards and Technology and the International Atomic Energy Agency.[8] Due to its non-destructive nature, it is commonly used in geochemistry and related fields. Since the samples do not need to be solubilized prior to analysis, NAA has shown great use in biological applications and in the analysis of minute materials, such as those of atmospheric and cosmic dust.[8] NAA has also been used to assist with a variety of analyses in the life sciences, some of which include atmospheric air quality monitoring; determination of halogen content in soil; food safety; workplace safety analysis; pharmaceutical and sorbent development; and the extraction of trace elements from ores, rocks, and production waste.[27]

# 2. Neutron activation analysis of eWaste using a medical cyclotron

## 2.1. Methods

### 2.1.1. Circuit board acquisition and preparation

A variety of electronic devices and components were acquired from Lakehead University's Shipping & Receiving department. These included a ThinkPad laptop, a stereo power amplifier, a DVD player, and computer components such as a hard drive disk, RAM sticks, and motherboards. Through percussive disassembly and meticulous circuit board breakdown with pliers, the samples were reduced to bags of fragments of about 1-6 $cm^2$ in size. Fragments of interest (*i.e*. those with a variety of electrical components) were further broken down with pliers to fit into 1-2 mL polypropylene cryovials. Since samples were not finely ground, they lacked homogeneity.

### 2.1.2. Standard calibration curve generation

A few fragments of interest were preliminarily analysed via neutron activation analysis to identify the radionuclides that they produced and the parent elements they represented. These fragments were individually transferred to 1 mL vials and placed into position via a custom-built pneumatic track system.[19] This system allowed for the vials to be positioned on the posterior end of the cyclotron target chamber, as to allow for the maximum neutron flux to exit the target chamber and irradiate the sample. The fragments were then analysed with a gamma spectrometer to collect gamma photon spectra. A Canberra HPGe (Model GC1020; Cryostat Model 7500S; Preamplifier Model 2002CSL;) and a Canberra DSL-LX MCA were operated with Genie 2000 (Version 3.3) gamma acquisition and analysis software. This detector was a p-type coaxial germanium detector, with a relative efficiency of 10%, and FWHM values of 1.00 keV at 122 keV and 2.00 keV at 1.3 MeV. It utilized digital electronics, and two inches of lead shielding surrounded the detector. Samples were directly placed on the detector. The generated spectra were then analysed with Interspec software (Version 1.0.8)[28] and compared to literature gamma peak data to label each significant peak.

For the analysis of the circuit samples, standard curves for silicon, tin, copper, bromine, and gold were generated at both 18 and 24 MeV cyclotron proton beam energies to test if a difference in beam energy would affect the detectability of the radioisotopes. Due to the gamma spectrometer experiencing a vacuum loss and required servicing from the manufacturer, these curves had to be repeated. The initial curves are in the Appendix, as they were used for the elemental quantification of the circuit board samples. New curves for these elements, as well as for chromium, nickel, palladium, neodymium, iron, and platinum were created at a cyclotron beam energy of 18 MeV. For each curve, three to six samples containing the element with varying masses were prepared, irradiated, and analysed via gamma spectroscopy. Following irradiation, the irradiated sample was transferred to a pre-weighed vial. This new vial was subsequently weighed after the gamma collection in case any of the sample remained in the irradiated vial. Each sample had an exposure of between 500 to 2000 µAmin (measured as proton beam time on $^{18}O$ target) and had their gamma spectrum collected between five and 10 minutes. The area of each peak of interest was corrected for sample exposure, decay, and gamma count time. To correct for variations in exposure, the area was divided by the exposure in µAh (µAmin / 60). For the count time correction, the area was divided by the count time in hours (count time / 3600). The decay correction was done by dividing the area by the decay correction factor (DCF), which is calculated in Equation 2.1. The DCF corrects for sample decay between the end of bombardment (EOB) and start of data collection as well as decay that occurs during counting. This is particularly important for radionuclides with short half-lives relative to the collection time.

$$DCF = \left(e^{-ln2 \times \frac{T1}{HL}}\right) \times \frac{\left(1 - e^{-ln2 \times \frac{T2}{HL}}\right)}{\left(ln2 \times \frac{T2}{HL}\right)} \quad (2.1)$$

T1 is the decay time in seconds, which occurs between the end of irradiation and the start of the gamma collection; T2 is the count time in seconds, and HL is the half-life in seconds. This equation originates from the combination of the equations for determining the decay and count factors: $e^{-\lambda tdet}$ and $1 - e^{-dtct}$, respectively. $\lambda$ is the decay constant of the radioisotope, which can also be represented as *ln2/HL*. "*tdet*" (time to detector) and "*tct*" (count time) are time

measurements, equivalent to T1 and T2, respectively. Equation 3.1 is calculating the fraction of the initial activity that remains after both the radioisotope's decay time while being transferred to the spectrometer (T1) and its decay time while in the spectrometer (T2). The corrected areas were plotted against the mass of the element of interest for each curve. A least squares regression line was added to each curve, with its y-intercept being set through the graph's origin.

### 2.1.3. Circuit board irradiation, spectroscopy, and analysis

A total of six circuit board fragments were analysed. Three were irradiated at 18 MeV, three at 24 MeV. Each sample was weighted and transferred to a 1 mL vial. Each sample was irradiated for about 2000 μAmin and its gamma spectrum was collected for about 20 minutes. The peaks for tin, copper, gold, bromine, and silicon were labelled, and their areas were corrected for sample irradiation, decay, and count times. Using the associated standard curve, the mass of each element was quantified by dividing the corrected peak area by the curve slope.

### 2.1.4. Preparation and analysis of custom eWaste standard

To better understand the effectiveness of this approach for elemental identification and quantification in eWaste, two custom standards were constructed. One contained four major elements found in eWaste: aluminum, iron, copper, and silicon (sample A). The other mixture contained the less-common, valuable and/or toxic elements: cadmium, chromium, gold, tin, arsenic, neodymium, nickel, magnesium, and palladium (sample B). The quantities of each compound that were used, along with the associated elemental concentration can be seen in Table 2.1.1.

Table 2.1.1. The composition of the custom eWaste standard, including both the mass of each component used and the relative elemental abundance.

| Sample | Element | Source Compound | Mass Compound (mg) | Element Concentration (mg/g) |
|---|---|---|---|---|
| A | Al | $Al_2O_3$ | 111 | 9.43 |
| | Si | $SiO_2$ | 219 | 16.4 |
| | Cu | $CuSO_4 \cdot 5H_2O$ | 1082 | 44.19 |
| | Fe | $FeCl_3$ | 1654 | 91.39 |
| B | Mg | $MgCl_2$ | 322 | 13.4 |
| | Sn | $SnCl_2 \cdot 2H_2O$ | 927 | 79.4 |
| | Cr | $Cr(NO_3)_3 \cdot 9H_2O$ | 517 | 10.9 |
| | As | $As_2O_3$ | 19 | 2.4 |
| | Cd | $Cd(NO_3)_2 \cdot 4H_2O$ | 46 | 2.8 |
| | Nd | $Nd_2O_3$ | 11 | 0.74 |
| | Au | $HAuCl_3$ | 3 | 1 |
| | Pd | Pd/C | 47 | 0.38 |
| | Ni | $Ni(NO_3)_2 \cdot 6H_2O$ | 1200 | 39.45 |

Compounds for each element were combined in a 250 mL round-bottom flask. Enough water was added to dissolve all water-soluble salts and assist with homogenizing the mixture. Approximately 3 g of the source compounds total were added, with approximately 3 g of activated carbon added as a “base”. The samples were then mixed further and dried on a Rotary Evaporator for about an hour. The dried mixtures were scraped off the walls of the flask and transferred to 1 mL vials for analysis. For each mixture, three sample vials were filled with varying masses: ~50 mg (A1 & B1), ~100 mg (A2 & B2), and ~200 mg (A3 & B3); see Table 2.1.1 for sample composition. Following irradiation, the samples were transferred to pre-weighed vials for collection of their gamma spectra. This was done to avoid any signals resulting from activation of the vial.

Each sample was irradiated for approximately 2000 μAmin and its gamma spectrum collected for two, five, and 10 minutes. The two-minute collection was done to make sure that the short-lived radioisotopes were detected before their decay. The five- and 10-minute collections were done to give additional time to detect the longer-lived radioisotopes. After

collection, each vial was re-weighed to determine the exact mass of the sample analysed. The spectra were analysed via InterSpec software, the peaks of interest were labelled, their areas were corrected for irradiation, decay, and count times, and masses were calculated using the standard curves. To improve precision, the masses were calculated using the corrected area from the 10-minute collection, where the signal-to-noise ratio was the highest. To determine the percent discrepancy associated with each mass calculation, the expected mass for each element (concentration multiplied by sample mass) was subtracted from the experimentally determined mass. This was then divided by each estimated mass to get each percent discrepancy (Equation 2.2).

$$\%\ Discrepancy\ = \frac{Experimentally\ Determined\ Mass - [Element]\ x\ Sample\ Mass}{[Element]\ x\ Sample\ Mass}\ x\ 100 \quad (2.2)$$

## 2.1.5. Preparation and analysis of heterogeneous mixtures

For a more accurate analysis, additional standard mixtures were created. Individual element mixtures were prepared and irradiated in their entirety. This was to minimize potential discrepancies resulting from uneven distribution of elements in a larger mixture. Two were made containing aluminum, iron, copper, and silicon (samples C1 & C2), and two were made containing cadmium, chromium, gold, arsenic, palladium, tin, nickel, neodymium, and magnesium (samples D1 & D2). The quantities of each compound that were used, along with the associated elemental concentration can be seen in Table 2.1.2.

Table 2.1.2. The composition of the heterogeneous standard.

| Sample | Element | Source Compound | Mass Compound (mg) | | Element Concentration (mg/g) | |
|---|---|---|---|---|---|---|
| | | | Subsample 1 | Subsample 2 | Subsample 1 | Subsample 2 |
| C | Si | $SiO_2$ | 12.67 | 35.20 | 126.1 | 140.5 |
| | Fe | $FeCl_3$ | 9.54 | 17.11 | 94.9 | 68.28 |
| | Cu | $CuSO_4 \cdot 5H_2O$ | 5.01 | 16.64 | 49.9 | 66.42 |
| | Al | $Al_2O_3$ | 13.76 | 31.86 | 136.9 | 127.1 |
| D | Mg | $MgCl_2$ | 8.99 | 31.73 | 31.7 | 47.82 |
| | Sn | $SnCl_2 \cdot 2H_2O$ | 0.84 | 2.16 | 3.0 | 3.25 |

| Sample | Element | Source Compound | Mass Compound (mg) | | Element Concentration (mg/g) | |
|---|---|---|---|---|---|---|
| | Cd | $Cd(NO_3)_2 \cdot 4H_2O$ | 9.69 | 6.74 | 34.2 | 10.2 |
| | Nd | $Nd_2O_3$ | 5.70 | 8.57 | 20.1 | 12.9 |
| | Ni | $Ni(NO_3)_2 \cdot 6H_2O$ | 11.59 | 35.44 | 40.84 | 53.42 |
| | As | $As_2O_3$ | 40.75 | 107.02 | 143.6 | 161.30 |
| | Cr | $Cr(NO_3)_3 \cdot 9H_2O$ | 7.99 | 10.93 | 28.2 | 16.47 |
| | Pd | Pd/C | 3.14 | 7.32 | 5.55 | 5.52 |
| | Au | Au wire | 2.90 | 22.40 | 10.2 | 33.76 |

Each of the four samples were created by measuring the compounds out into 1.5 mL vials without mixing. For the samples D1 and D2, the gold wire from the gold standard curve was used, as opposed to the $HAuCl_3$ used for the custom standards. An arbitrary amount of each compound was added to each sample, with samples C2 and D2 containing more of each compound than the samples C1 and D1, except for palladium, where the opposite was true. There was no need to pre-weigh additional empty vials for these samples as the vials were placed in the gamma spectrometer directly after being irradiated. There was also no activated carbon base or water added to these samples. To account for the gamma peaks of the irradiated vial, an empty vial was also irradiated as a reference. Since the gold wire from previous irradiations were used in these samples, they were analysed in the gamma spectrometer before being used to identify if they were still radioactive.

Each sample was irradiated for approximately 2000 μAmin and its gamma spectra collected for two, five, and 10 minutes. The spectra were analysed via InterSpec software, the peaks of interest were labelled, their areas were corrected for exposure, decay, and count time, and masses were calculated using the standard curves. To increase accuracy, the masses were calculated using the corrected area from the 10-minute collection, where the noise to signal ratio was the lowest. The peak areas from the previously irradiated gold and the irradiated vial were subtracted from the corresponding peaks in the samples before masses were calculated. To determine the percent discrepancy associated with each mass calculation, the experimentally determined mass of each element was subtracted by its expected mass (Table 2.1.2). This was then divided by each expected mass to get each percent discrepancy (Equation 2.3).

$$\%\ Discrepancy\ = \frac{Experimentally\ Determined\ Mass - Expected\ Mass}{Expected\ Mass}\ x\ 100 \qquad (2.3)$$

## 2.2. Results

### 2.2.1. Standard calibration curves

Most of the radionuclides used to generate the standard curves were produced via (n,p) or (n,γ) reactions. There were also a few generated via (n,α), (n,2n), and (n,n) reactions. As shown in Table 2.2.1, silicon, aluminum, and magnesium all produced some of the same radionuclides, namely $^{27}$Mg, $^{28}$Al, and $^{24}$Na. Thus, a unique radionuclide was focused on for each element. $^{29}$Al was selected for silicon detection, while $^{24}$Na was selected for both magnesium and aluminum. To avoid confusion in understanding whether the $^{24}$Na was from magnesium or aluminum in a sample, the two elements were analysed in separate samples.

Table 2.2.1. The collection of elements analysed, their specific stable isotopes present, and the radionuclide(s) detected to confirm their presence. Parent isotopes in bold indicate the isotope of focus for each element. Radionuclides in bold indicate those used to confirm elemental presence.

| Element | Source Compound | Parent Isotope | Radionuclide(s) Detected | | | | |
|---|---|---|---|---|---|---|---|
| | | | n,n | n,2n | n,γ | n,p | n,α |
| Si | $SiO_2$ | $^{28}$Si, $^{29}$**Si**, $^{30}$Si | | | $^{31}$Si | $^{28}$Al, **$^{29}$Al** | $^{27}$Mg |
| Fe | $FeCl_3$ | **$^{56}$Fe** | | | | **$^{56}$Mn** | |
| Cu | $CuSO_4\ 5H_2O$ | **$^{65}$Cu** | | | **$^{66}$Cu** | | |
| Al | $Al_2O_3$ | **$^{27}$Al** | | | $^{28}$Al | $^{27}$Mg | **$^{24}$Na** |
| Mg | $MgCl_2$ | **$^{24}$Mg**, $^{26}$Mg | | | $^{27}$Mg | **$^{24}$Na** | |
| Sn | $SnCl_2\ 2H_2O$ | $^{120}$Sn, **$^{122}$Sn, $^{124}$Sn** | | **$^{123m}$Sn** | **$^{123m}$Sn**, $^{125m}$Sn | | $^{117}$Cd |
| Cd | $Cd(NO_3)_2\ 4H_2O$ | **$^{111}$Cd** | **$^{111m}$Cd** | | | | |
| Nd | $Nd_2O_3$ | **$^{148}$Nd** | | | **$^{149}$Nd** | | |
| Ni | $Ni(NO_3)_2\ 6H_2O$ | **$^{58}$Ni** | | | | **$^{58}$Co** | |
| As | $As_2O_3$ | **$^{75}$As** | | | **$^{76}$As** | $^{75}$Ge | $^{72}$Ga |
| Cr | $Cr(NO_3)_3\ 9H_2O$ | **$^{52}$Cr** | | | | **$^{52}$V** | |
| Pd | Pd/C | **$^{109}$Pd** | **$^{109m}$Pd** | | | | |
| Au | $HAuCl_3$* | **$^{197}$Au** | | $^{196}$Au | **$^{198}$Au** | | |

| Element | Source Compound | Parent Isotope | Radionuclide(s) Detected | | | | |
|---|---|---|---|---|---|---|---|
| | | | n,n | n,2n | n,γ | n,p | n,α |
| Br | NaBr | **$^{79}$Br, $^{81}$Br** | | **$^{80}$Br** | **$^{80}$Br,** $^{82}$Br | | |
| Cl | Fe, Mg, Sn Salt | **$^{37}$Cl** | | | **$^{38}$Cl** | | |

*$HAuCl_3$ used for custom eWaste standards. Au wire used for standard curves and heterogeneous standards.

In all, 14 standard curves were generated, with a cyclotron proton beam energy of 18 MeV. The elements of interest were silicon, iron, copper, aluminum, magnesium, tin, cadmium, neodymium, nickel, arsenic, chromium, palladium, gold, and bromine. The bromine curve was used to analyse the circuit samples but was not used when analysing the custom eWaste standards or the heterogeneous standards, due to choosing different elements to include and analyse in these samples. There was no curve generated for chlorine, as it was not an element chosen for analysis. As seen in Fig. 2.2.1 to 2.2.14, all the standard curves are reasonably linear.

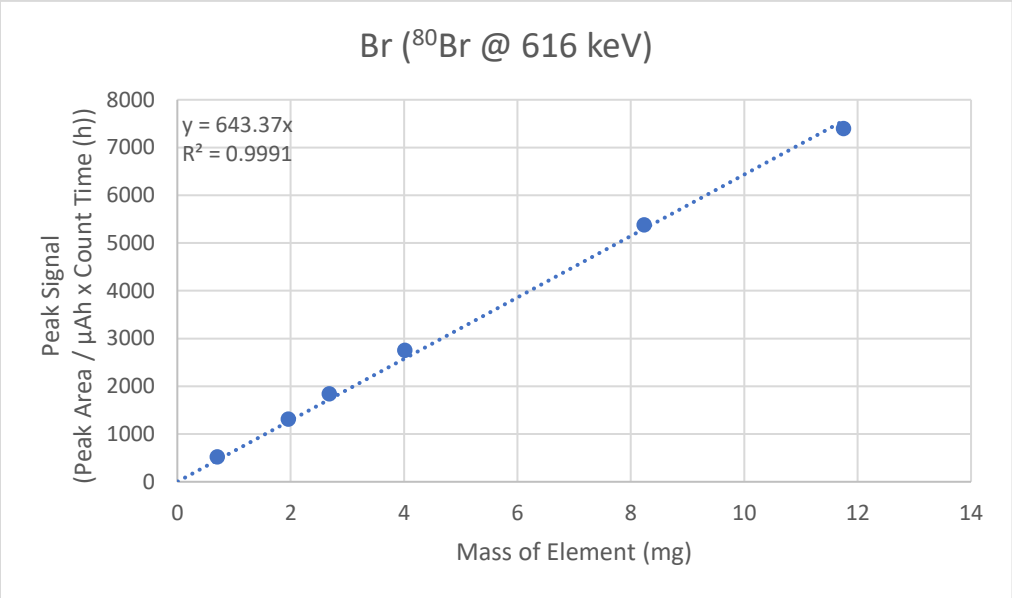


Fig. 2.2.1. Standard curve based on mass of bromine, in the form of NaBr. Peak area values corrected for proton beam exposure (µAh), spectrometer count time (h), and radionuclide decay (DCF). $T_{1/2}$ is 17.68 minutes.

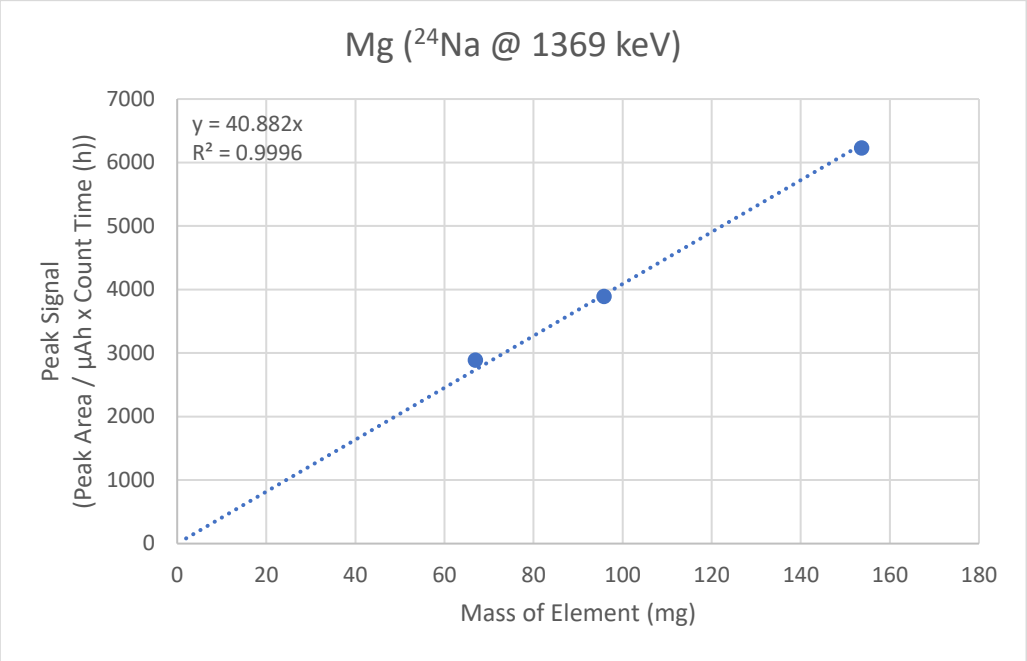


Fig. 2.2.2. Standard curve based on mass of magnesium, in the form of $MgCl_2$. Peak area values corrected for proton beam exposure (µAh), spectrometer count time (h), and radionuclide decay (DCF). $T_{1/2}$ is 14.96 hours.

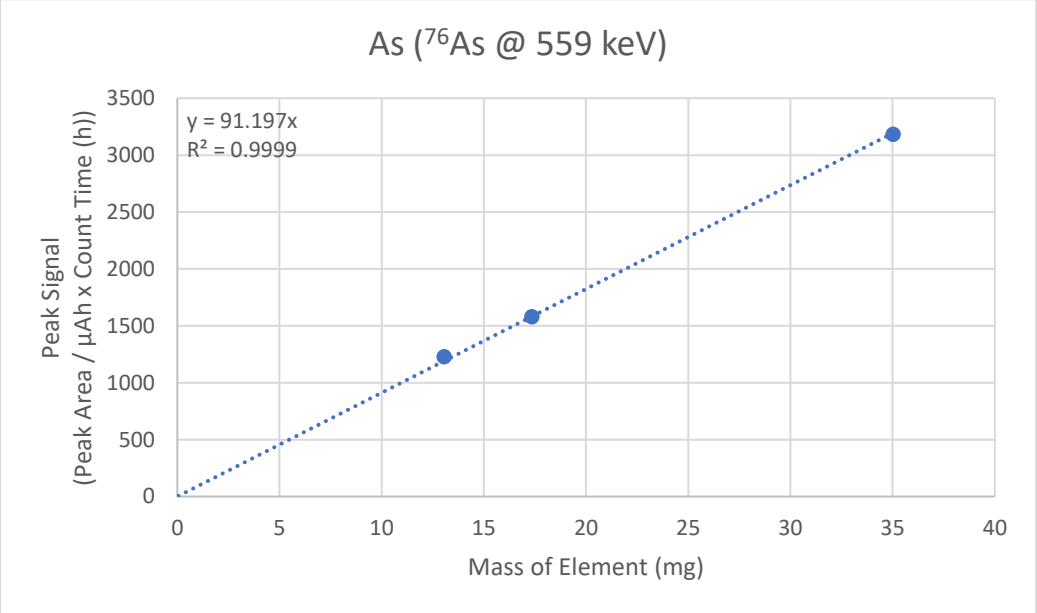


Fig. 2.2.3. Standard curve based on mass of arsenic, in the form of $As_2O_3$. Peak area values corrected for proton beam exposure (µAh), spectrometer count time (h), and radionuclide decay (DCF). $T_{1/2}$ is 26.25 hours.

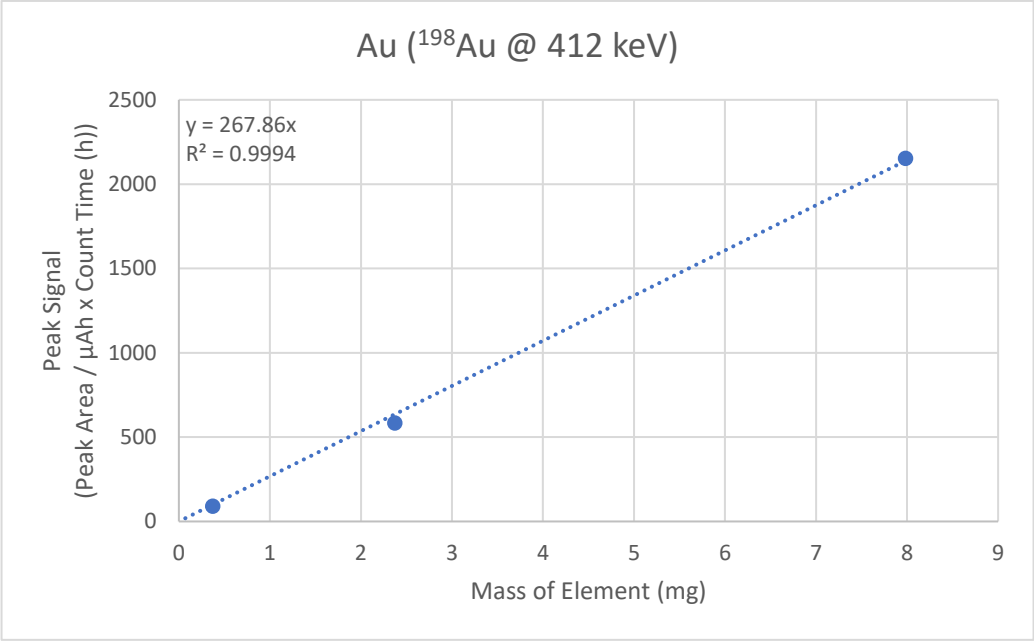


Fig. 2.2.4. Standard curve based on mass of gold, in the form of gold wire. Peak area values corrected for proton beam exposure (µAh), spectrometer count time (h), and radionuclide decay (DCF). $T_{1/2}$ is 2.69 days.

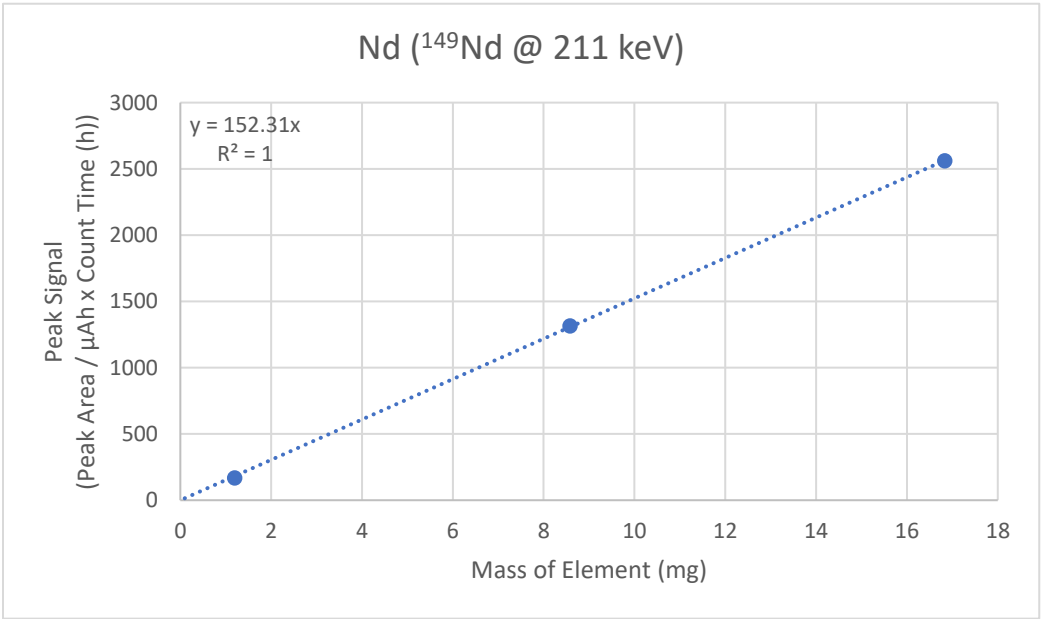


Fig. 2.2.5. Standard curve based on mass of neodymium, in the form of $Nd_2O_3$ Peak area values corrected for proton beam exposure (µAh), spectrometer count time (h), and radionuclide decay (DCF). $T_{1/2}$ is 1.73 hours.

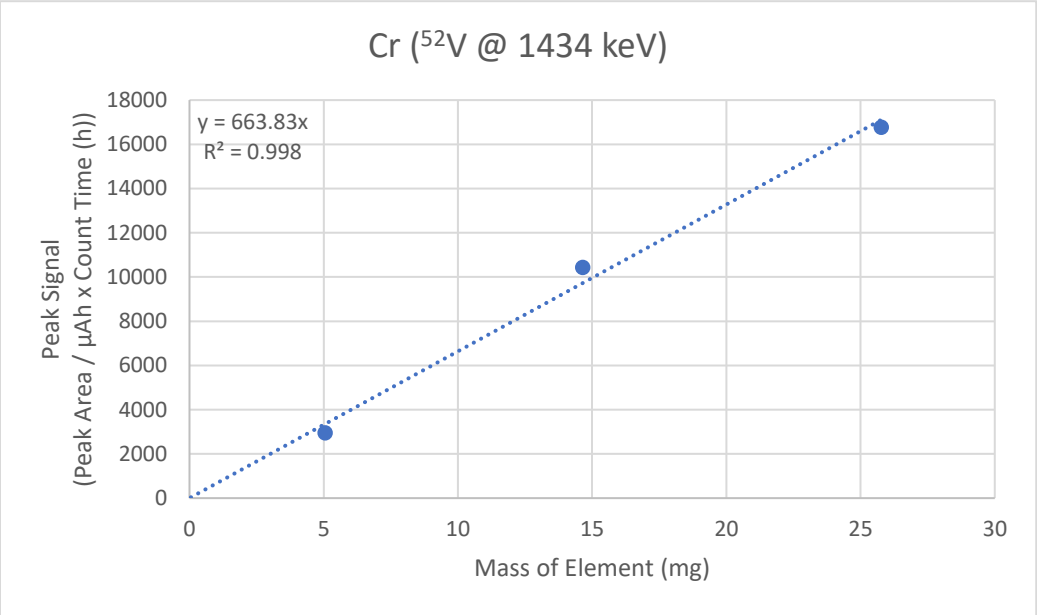


Fig. 2.2.6. Standard curve based on mass of chromium, in the form of $Cr(NO_3)_3 \cdot 9H_2O$. Peak area values corrected for proton beam exposure (µAh), spectrometer count time (h), and radionuclide decay (DCF). $T_{1/2}$ is 3.74 minutes.

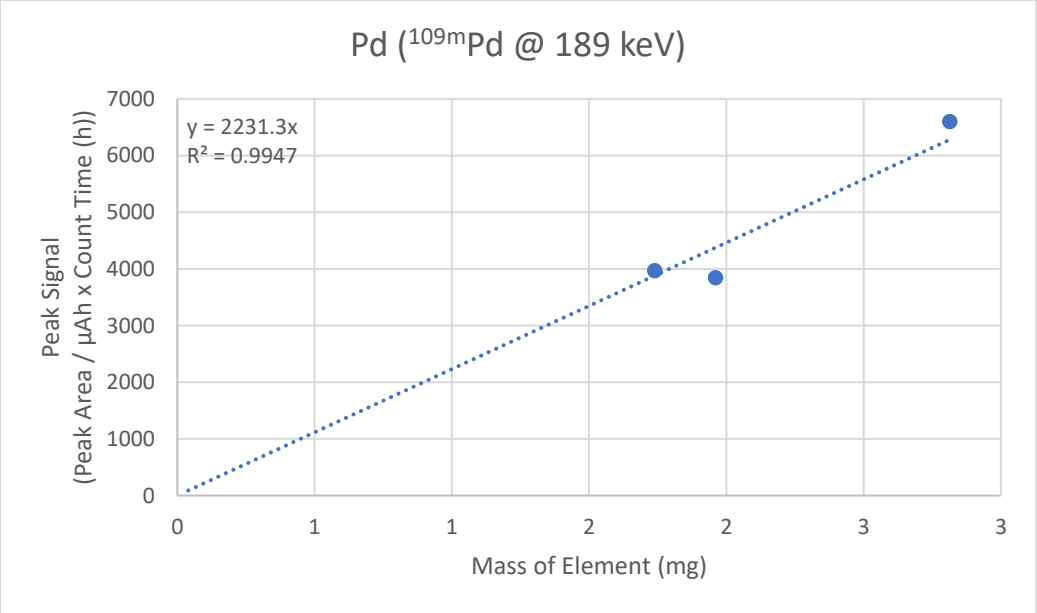


Fig. 2.2.7. Standard curve based on mass of palladium, in the form of 5% (w/w) palladium on carbon. Peak area values corrected for proton beam exposure (µAh), spectrometer count time (h), and radionuclide decay (DCF). $T_{1/2}$ is 4.70 minutes.

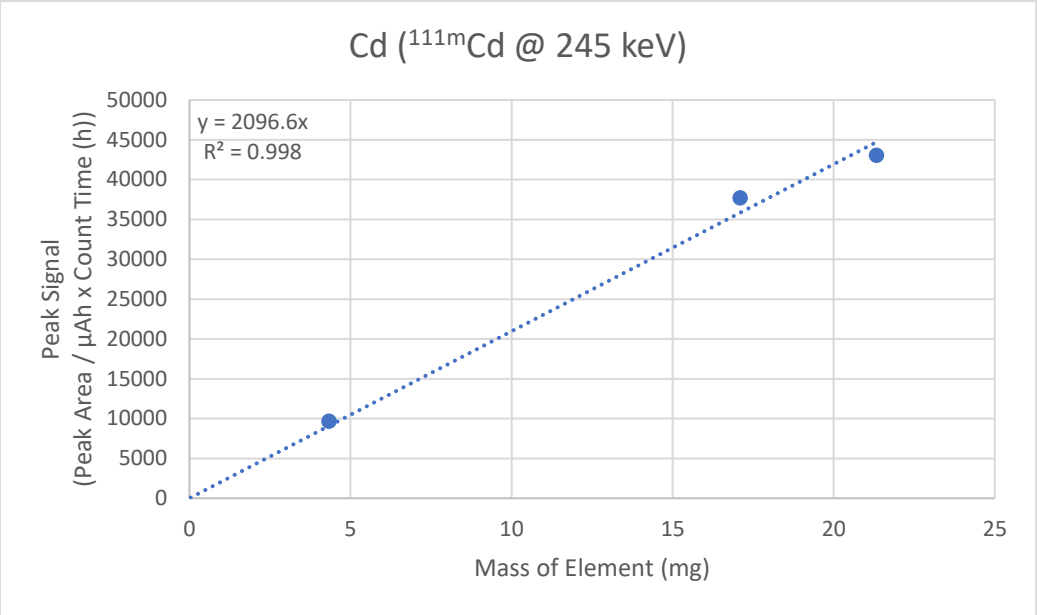


Fig. 2.2.8. Standard curve based on mass of cadmium, in the form of $Cd(NO_3)_2 \cdot 4H_2O$. Peak area values corrected for proton beam exposure (µAh), spectrometer count time (h), and radionuclide decay (DCF). $T_{1/2}$ is 48.50 minutes.

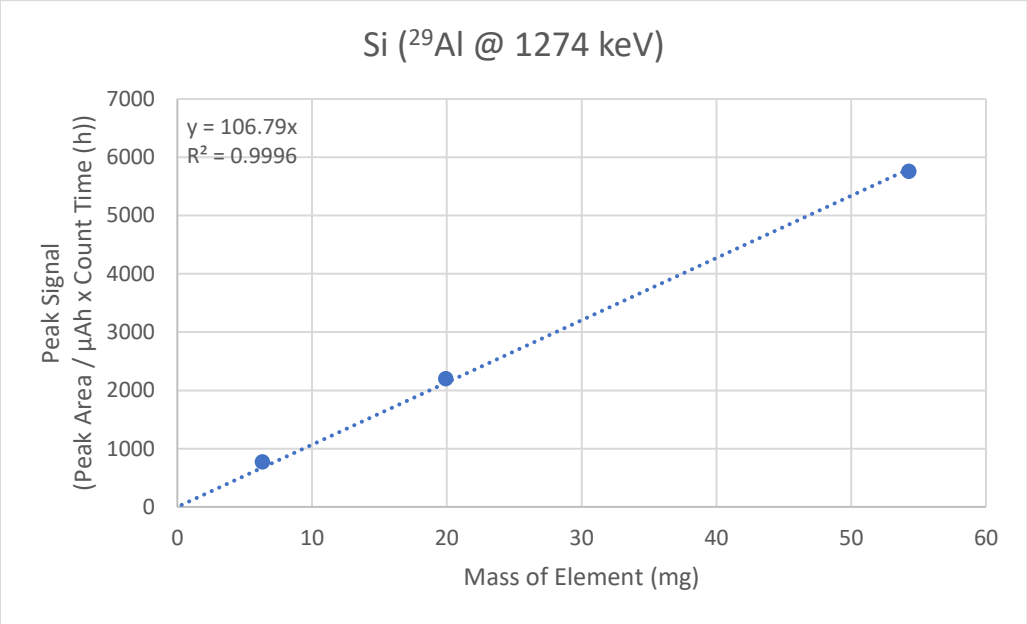


Fig. 2.2.9. Standard curve based on mass of silicon, in the form of $SiO_2$. Peak area values corrected for proton beam exposure (µAh), spectrometer count time (h), and radionuclide decay (DCF). $T_{1/2}$ is 6.56 minutes.

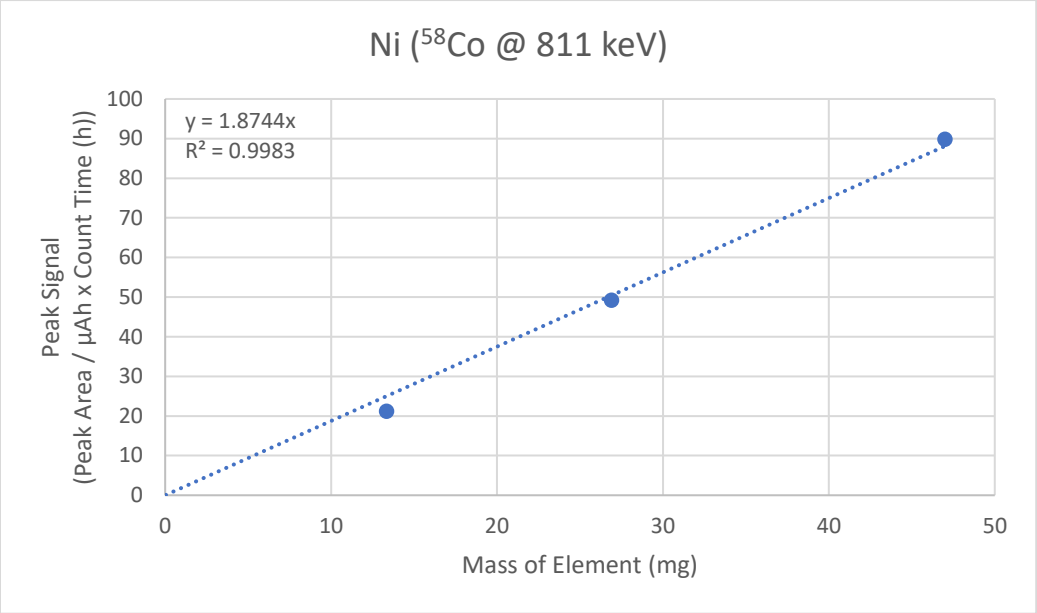


Fig. 2.2.10. Standard curve based on mass of nickel, in the form of $Ni(NO_3)_2 \cdot 6H_2O$. Peak area values corrected for proton beam exposure (µAh), spectrometer count time (h), and radionuclide decay (DCF). $T_{1/2}$ is 70.86 days.

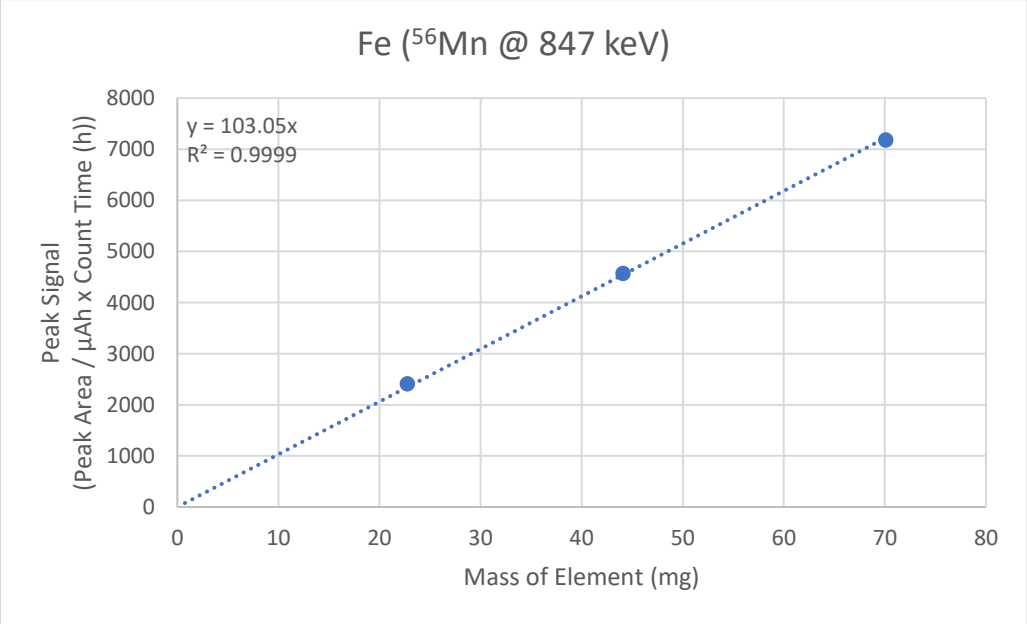


Fig. 2.2.11. Standard curve based on mass of iron, in the form of $FeCl_3$. Peak area values corrected for proton beam exposure (µAh), spectrometer count time (h), and radionuclide decay (DCF). $T_{1/2}$ is 2.58 hours.

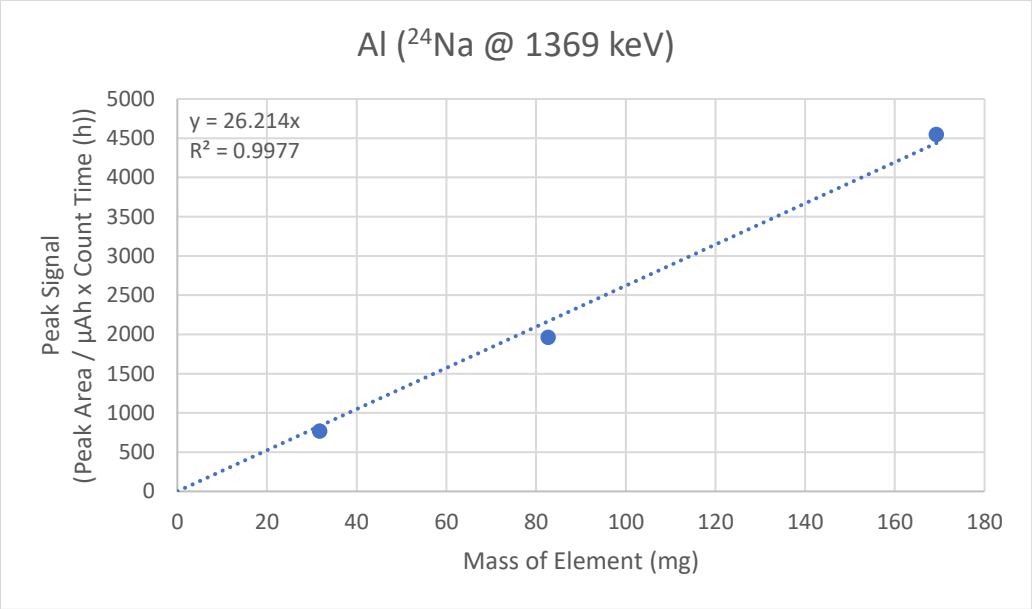


Fig. 2.2.12. Standard curve based on mass of aluminum, in the form of $Al_2O_3$. Peak area values corrected for proton beam exposure (µAh), spectrometer count time (h), and radionuclide decay (DCF). $T_{1/2}$ is 14.96 hours.

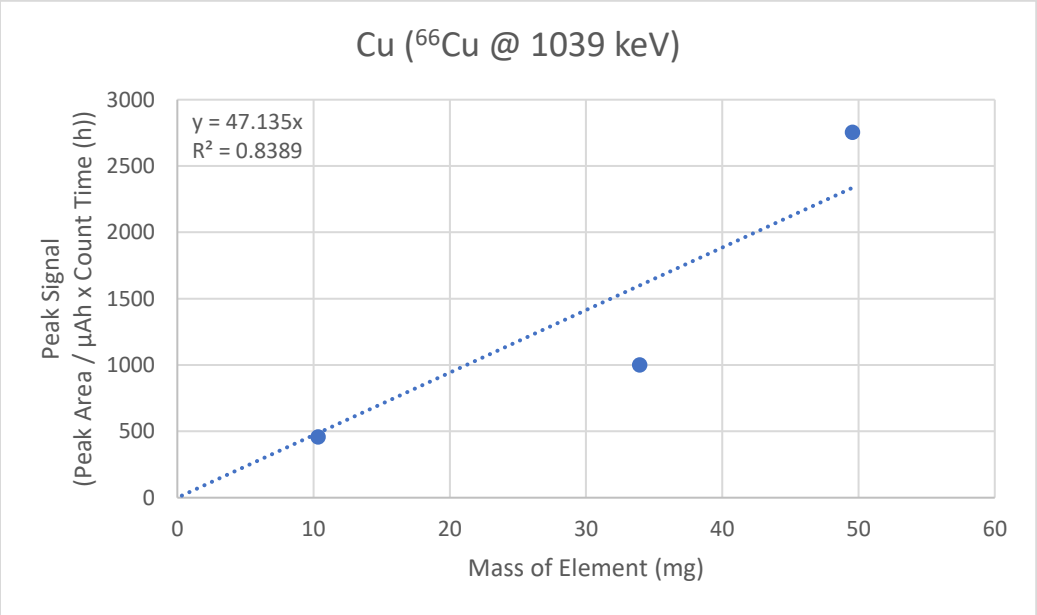


Fig. 2.2.13. Standard curve based on mass of copper, in the form of $CuSO_4 \cdot 5H_2O$. Peak area values corrected for proton beam exposure (µAh), spectrometer count time (h), and radionuclide decay (DCF). $T_{1/2}$ is 5.12 minutes.

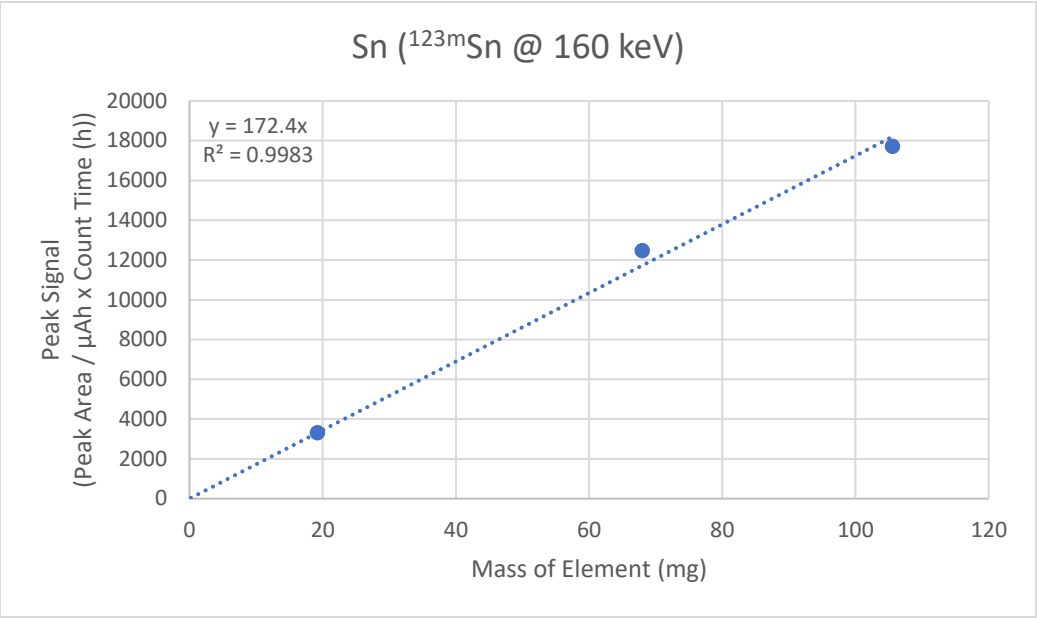


Fig. 2.2.14. Standard curve based on mass of tin, in the form of $SnCl_2 \cdot 2H_2O$. Peak area values corrected for proton beam exposure (µAh), spectrometer count time (h), and radionuclide decay (DCF). $T_{1/2}$ is 40.06 minutes.

## 2.2.2. Circuit board analysis

A total of six circuit board samples were analysed via neutron activation analysis, with masses ranging from 200-500 mg. Many peaks were identified in each board, including those of $^{123m}$Sn, $^{125m}$Sn, $^{198}$Au, $^{80}$Br, $^{82}$Br, $^{27}$Mg, $^{66}$Cu, $^{29}$Al, $^{24}$Na, and $^{28}$Al (Fig. 2.2.15-22). The peak energy for each identified radionuclide, as well as their mode of production can be found in Table 2.2.2. Silicon, tin, and copper were identified in all samples, while bromine was only found in five, and gold in two. Circuit boards #1, 2, and 3 were irradiated while operating the cyclotron at a proton beam energy of 24 MeV, while circuit boards #5, 7, and 8 were irradiated while operating the cyclotron at a proton beam energy of 18 MeV to determine if the difference in beam energy would affect which radioisotopes were detectable.

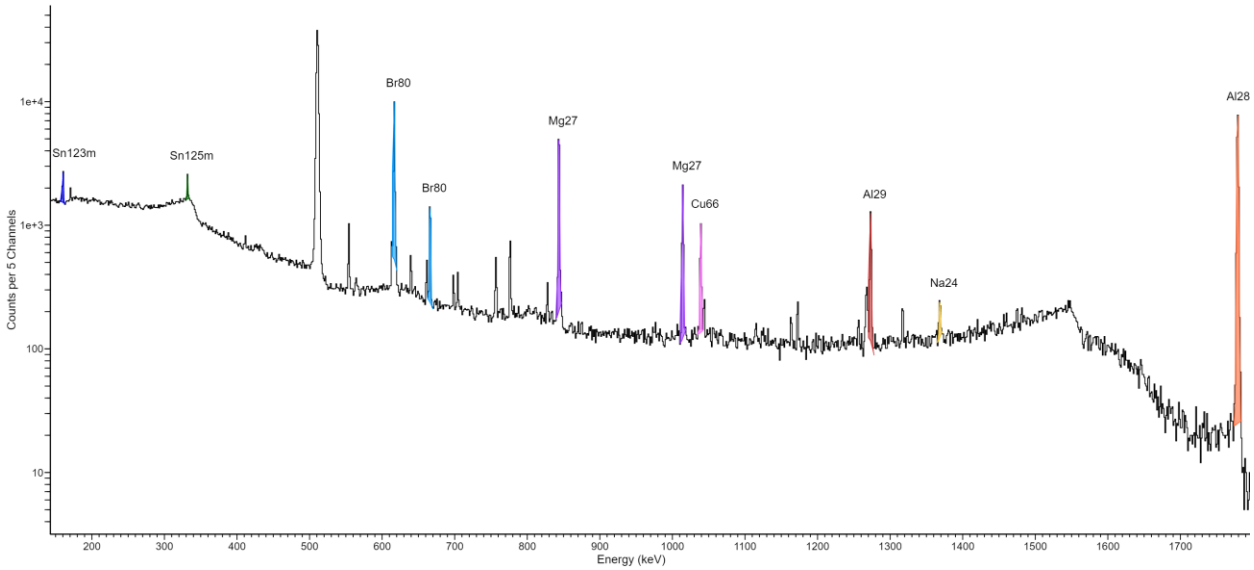


Fig. 2.2.15. Gamma spectrum for circuit board #1. Cyclotron operated at 24 MeV. Count time of 20 minutes and decay time of four minutes. Sample placed directly on detector. Peaks of interest are labelled with radionuclide symbol. The unlabelled peak at 511 keV is from positron-electron annihilation and thus not specific to the decay of a particular radionuclide.

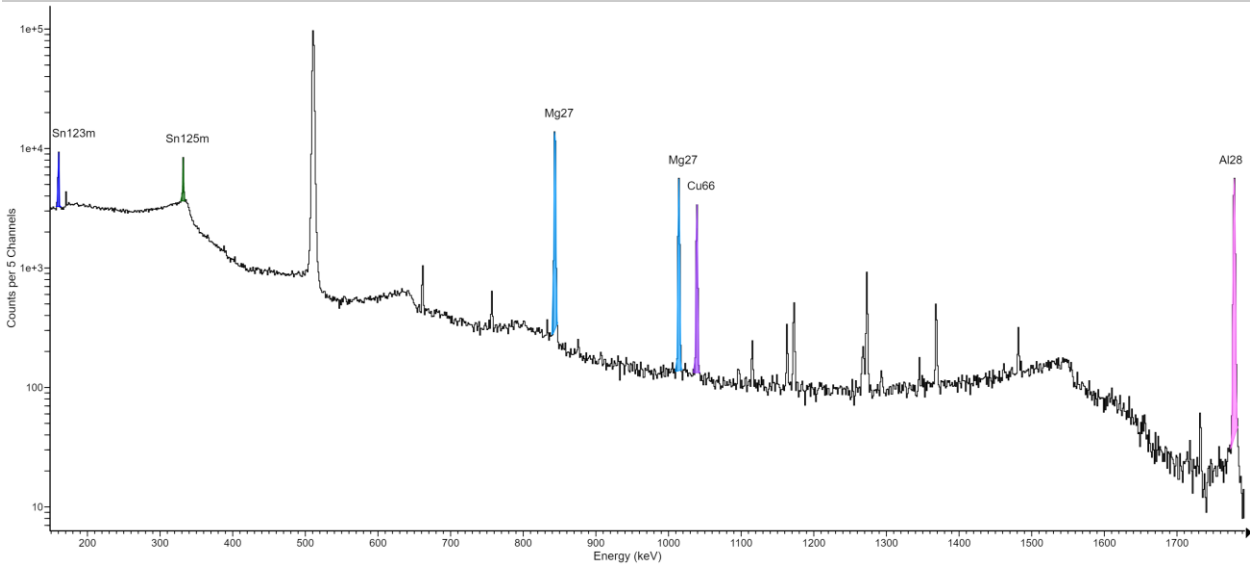


Fig. 2.2.16. Gamma spectrum for circuit board #2. Cyclotron operated at 24 MeV. Count time of 20 minutes and decay time of five minutes. Sample placed directly on detector. Peaks of interest are labelled with radionuclide symbol.

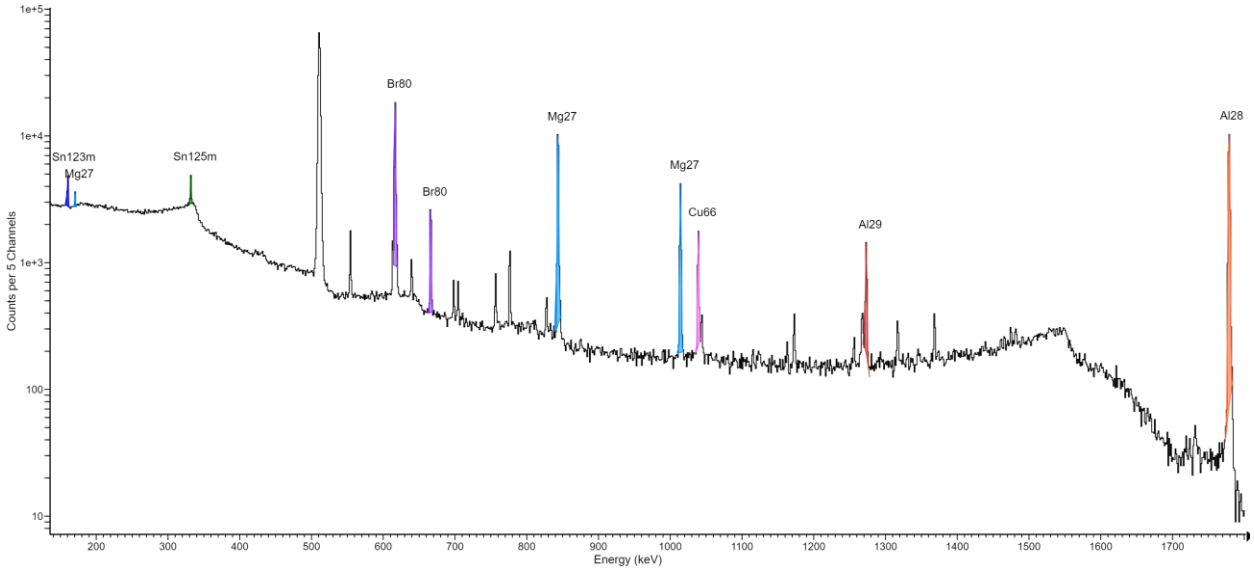


Fig. 2.2.17. Gamma spectrum for circuit board #3. Cyclotron operated at 24 MeV. Count time of 15 minutes and decay time of four minutes. Sample placed directly on detector. Peaks of interest are labelled with radionuclide symbol.

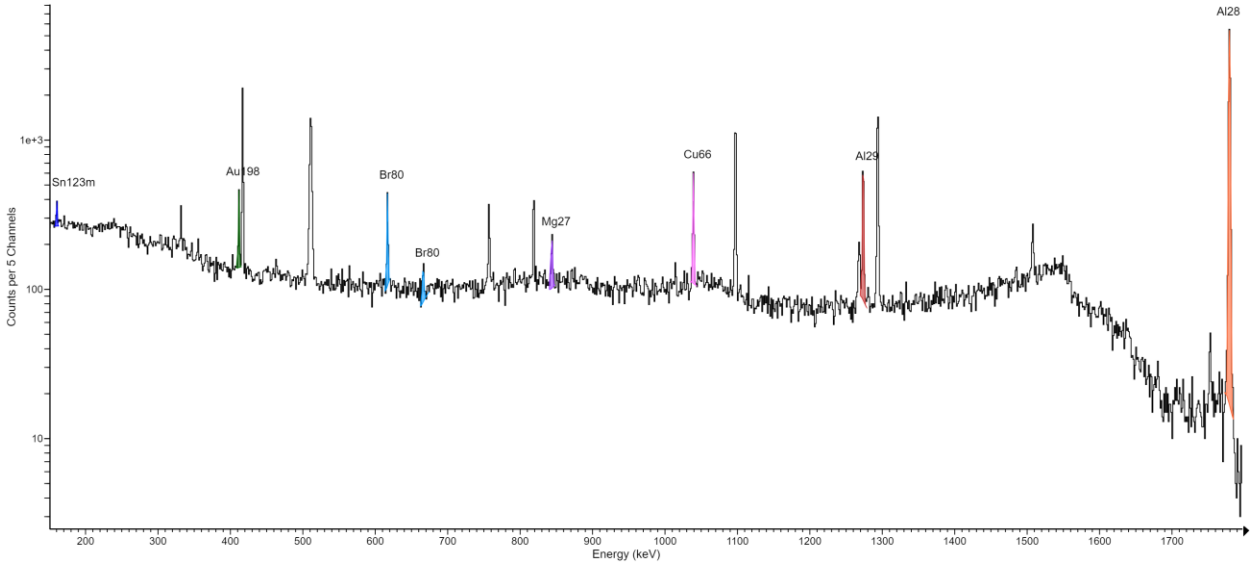


Fig. 2.2.18. Gamma spectrum for circuit board #5. Cyclotron operated at 18 MeV. Count time of 20 minutes and decay time of three minutes. Sample placed directly on detector. Peaks of interest are labelled with radionuclide symbol.

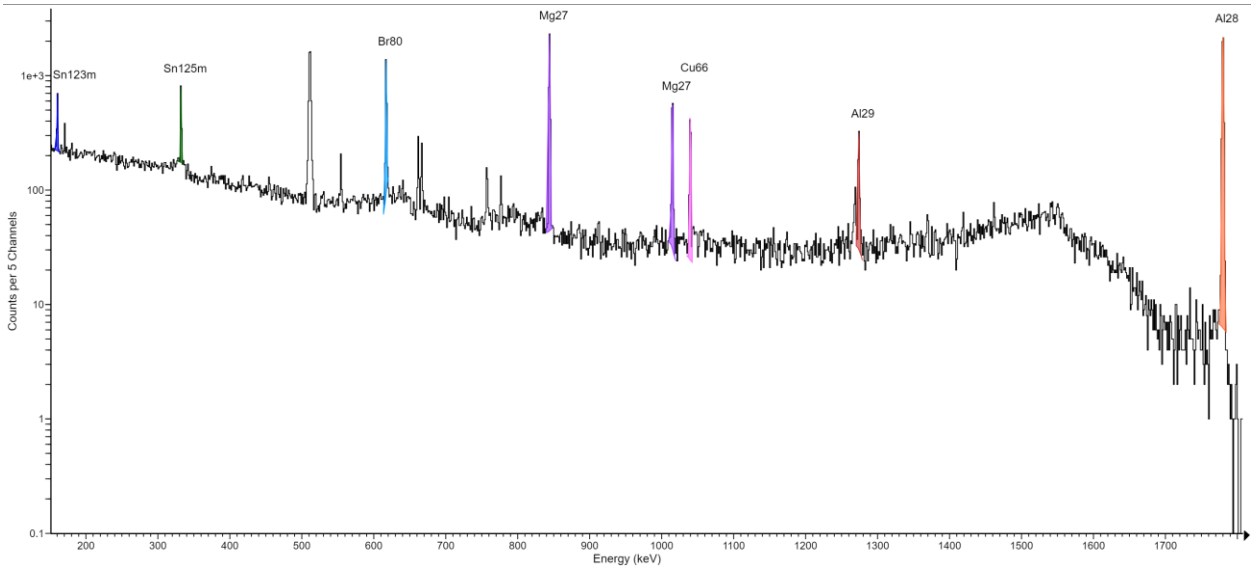


Fig. 2.2.19. Gamma spectrum for circuit board #7. Cyclotron operated at 18 MeV. Count time of 20 minutes and decay time of three minutes. Sample placed directly on detector. Peaks of interest are labelled with radionuclide symbol.

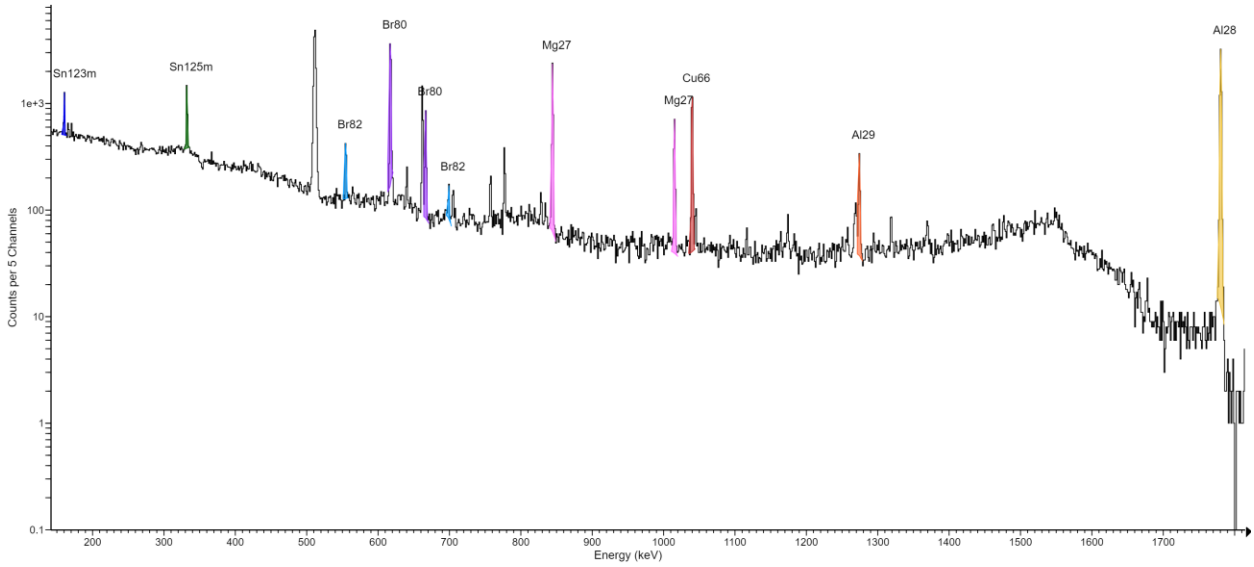


Fig. 2.2.20. Gamma spectrum for circuit board #8. Cyclotron operated at 18 MeV. Count time of 20 minutes and decay time of two minutes. Sample placed directly on detector. Peaks of interest are labelled with radionuclide symbol.

Table 2.2.2. All substantial peaks from tested circuit boards, including peak energy and intensity, radionuclide detected, half-life, and reaction of production.

| keV (Intensity) | Nuclide | Half Life | Reaction |
|---|---|---|---|
| 160.29 (85.7) | $^{123m}$Sn | 40.06 min | $^{122}$Sn(n,γ)$^{123m}$Sn / $^{124}$Sn(n,2n)$^{123m}$Sn |
| 170.61 (0.8) | $^{27}$Mg | 9.46 min | $^{26}$Mg(n,γ)$^{27}$Mg / $^{27}$Al(n,p)$^{27}$Mg / $^{30}$Si(n,α)$^{27}$Mg |
| 331.95 (97.2) | $^{125m}$Sn | 9.52 min | $^{124}$Sn(n,γ)$^{125m}$Sn |
| 411.80 (95.6) | $^{198}$Au | 2.69 days | $^{197}$Au(n,γ)$^{198}$Au |
| 510.96 (100) | Non-Specific | | Positron Annihilation / Electron Capture |
| 554.78 (70.9) | $^{82}$Br | 1.47 days | $^{81}$Br(n,γ)$^{82}$Br |
| 617.29 (6.7) | $^{80}$Br | 17.68 min | $^{79}$Br(n,γ)$^{80}$Br / $^{81}$Br(n,2n)$^{80}$Br |
| 666.81 (1.1) | $^{80}$Br | 17.68 min | $^{79}$Br(n,γ)$^{80}$Br / $^{81}$Br(n,2n)$^{80}$Br |
| 843.80 (71.8) | $^{27}$Mg | 9.46 min | $^{26}$Mg(n,γ)$^{27}$Mg / $^{27}$Al(n,p)$^{27}$Mg / $^{30}$Si(n,α)$^{27}$Mg |
| 1014.50 (28) | $^{27}$Mg | 9.46 min | $^{26}$Mg(n,γ)$^{27}$Mg / $^{27}$Al(n,p)$^{27}$Mg / $^{30}$Si(n,α)$^{27}$Mg |
| 1038.81 (7.4) | $^{66}$Cu | 5.12 min | $^{65}$Cu(n,γ)$^{66}$Cu |
| 1273.52 (90.6) | $^{29}$Al | 6.56 min | $^{29}$Si(n,p)$^{29}$Al |
| 1368.79 (100) | $^{24}$Na | 14.96 hours | $^{24}$Mg(n,p)$^{24}$Na / $^{27}$Al(n,α)$^{24}$Na |
| 1779.30 (100) | $^{28}$Al | 2.24 min | $^{27}$Al(n,γ)$^{28}$Al / $^{28}$Si(n,p)$^{28}$Al |

Even though they were roughly the same size and mass, circuit 5 had six times the amount of gold that circuit 1 did, with a concentration of gold also being about five times larger, when accounting for the sample masses (Table 2.2.3). All circuits had a tin concentration of about 0.06-0.4 wt%, a bromine concentration of about 0.03-0.7 wt%, a copper concentration of about 1.5-4.5 wt%, and a silicon concentration of about 1-22 wt%. Out of circuits 1-8, circuit 2 had the highest concentration of tin, while circuit 5 had the least; circuits 1 and 2 had a lot more bromine than circuits 3-8; circuits 2 and 8 had the most copper; and circuits 1 and 3 had the most silicon.

Table 2.2.3. Quantity of several elements detected in seven circuit board fragments. Both the masses (mg) and mass percents of tin, gold, bromine, copper, and silicon were determined using the standard curves generated. Circuits 1, 2, and 3 were irradiated with a proton beam energy of 24 MeV, while circuits 5, 7, and 8 were irradiated at 18 MeV.

| Sample | Mass (g) | Tin (mg, wt%) | Gold (mg, wt%) | Bromine (mg, wt%) | Copper (mg, wt%) | Silicon (mg, wt%) |
|---|---|---|---|---|---|---|
| Circuit 1 | 0.212 | 0.37, 0.17 | 0.05, 0.02 | 1.33, 0.626 | 4.82, 2.27 | 46.29, 21.8 |
| Circuit 2 | 0.434 | 1.76, 0.405 | | | 19.36, 4.46 | 32.62, 7.52 |

| Sample | Mass (g) | Tin (mg, wt%) | Gold (mg, wt%) | Bromine (mg, wt%) | Copper (mg, wt%) | Silicon (mg, wt%) |
|---|---|---|---|---|---|---|
| Circuit 3 | 0.398 | 0.68, 0.17 | | 2.76, 0.694 | 8.37, 2.10 | 53.04, 13.3 |
| Circuit 5 | 0.311 | 0.18, 0.057 | 0.30, 0.096 | 0.10, 0.033 | 4.68, 1.50 | 7.74, 2.49 |
| Circuit 7 | 0.261 | 0.62, 0.24 | | 0.43, 0.16 | 4.70, 1.80 | 3.67, 1.41 |
| Circuit 8 | 0.302 | 0.94, 0.31 | | 0.11, 0.036 | 11.82, 3.92 | 3.18, 1.05 |

### 4.2.3. Custom standard analysis

For samples A1, A2, and A3, as the sample size and gamma spectrometer count time increased, so did the size of the peaks (Fig. 2.2.21-23). The peaks of interest for these samples were that of $^{56}$Mn at 847 keV, $^{66}$Cu at 1039 keV, $^{29}$Al at 1273 keV, and $^{24}$Na at 1369 keV. These radionuclides were used to identify the presence of iron, copper, silicon, and aluminum, respectively.

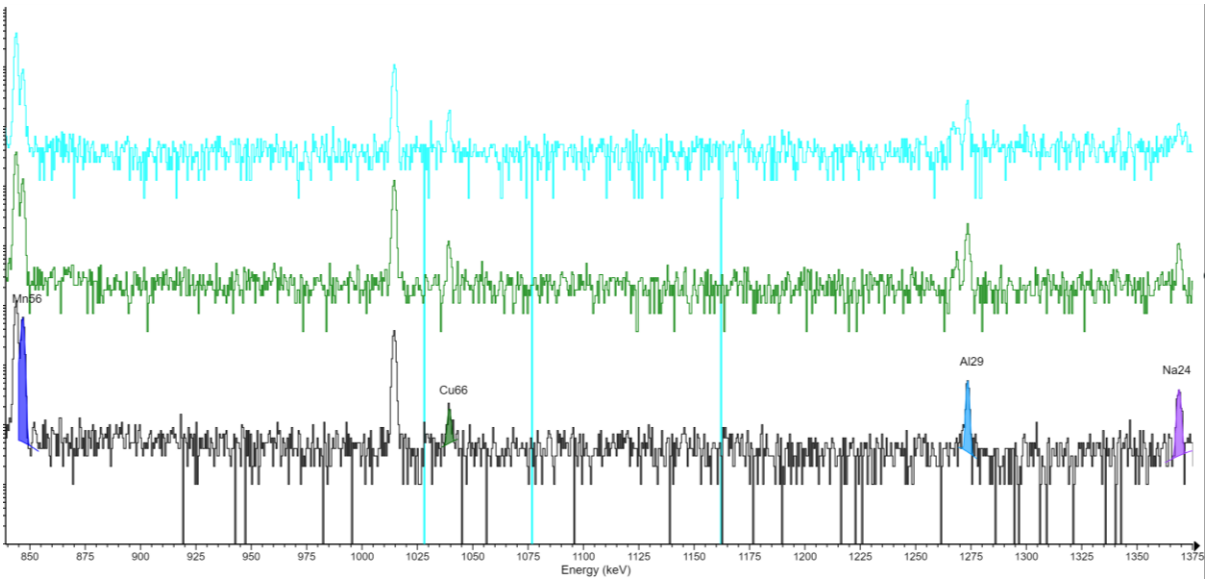


Fig. 2.2.21. Gamma spectra of sample A1. Cyclotron operated at 18 MeV. Count time of two (blue), five (green), and 10 (black) minutes. Decay time of four, seven, and 12 minutes, respectively. Sample placed directly on detector. Peaks of interest are labelled with radionuclide symbol.

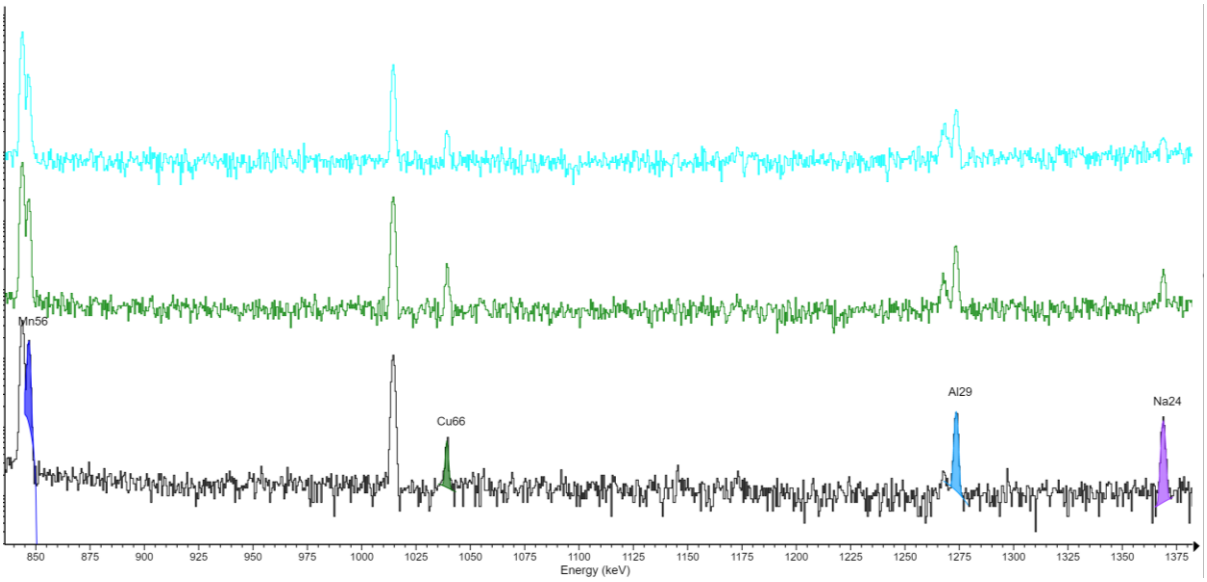


Fig. 2.2.22. Gamma spectra of sample A2. Cyclotron operated at 18 MeV. Count time of two (blue), five (green), and 10 (black) minutes. Decay time of three, five, and 11 minutes, respectively. Sample placed directly on detector. Peaks of interest are labelled with radionuclide symbol.

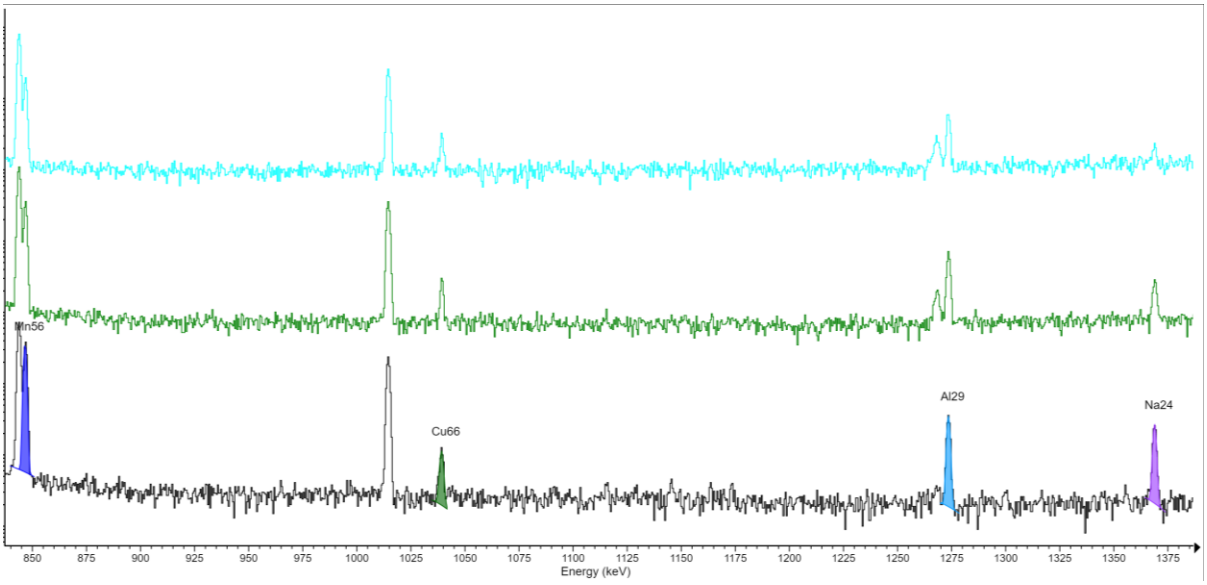


Fig. 2.2.23. Gamma spectra of sample A3. Cyclotron operated at 18 MeV. Count time of two (blue), five (green), and 10 (black) minutes. Decay time of two, five, and 11 minutes, respectively. Sample placed directly on detector. Peaks of interest are labelled with radionuclide symbol.

In addition to the four peaks of interest, there were several other peaks identified in the spectra from these samples (Fig. 2.2.24). These included three peaks for $^{27}$Mg at 170 keV, 844 keV, and 1015 keV; the annihilation 511 keV peak, indicative of positron decay and electron capture; $^{38}$Cl at 1643 keV; $^{28}$Al at 1779 keV; and $^{56}$Mn at 1811 keV. The respective reactions of production for these radionuclides are listed in Table 2.2.4.

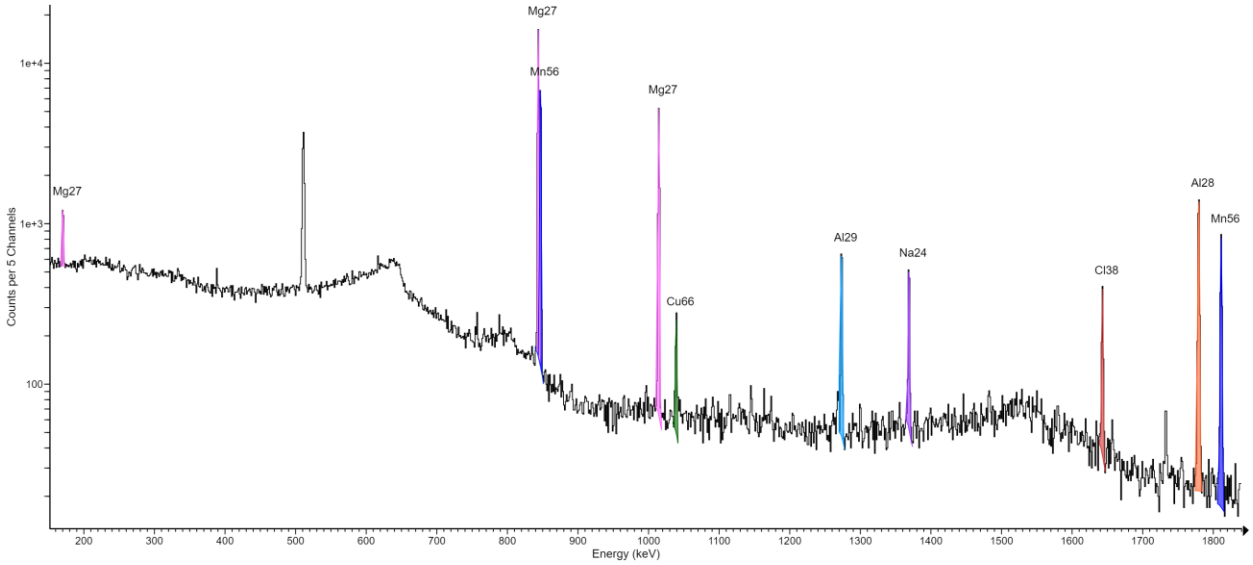


Fig. 2.2.24. Gamma spectrum of sample A3. Cyclotron operated at 18 MeV. Count time of 10 minutes and decay time of 11 minutes. Sample placed directly on detector. All substantial peaks are labelled with radionuclide symbol.

Table 2.2.4. All substantial peaks from sample A3, including peak energy and intensity, radionuclide detected, half-life, and reaction of production.

| keV (Intensity) | Nuclide | Half Life | Reaction |
|---|---|---|---|
| 170.59 (0.8) | $^{27}$Mg | 9.46 min | $^{27}$Al(n,p)$^{27}$Mg / $^{30}$Si(n,α)$^{27}$Mg |
| 510.99 (100) | Non-Specific | | Positron Annihilation / Electron Capture |
| 843.82 (71.8) | $^{27}$Mg | 9.46 min | $^{27}$Al(n,p)$^{27}$Mg / $^{30}$Si(n,α)$^{27}$Mg |
| 846.83 (98.9) | $^{56}$Mn | 2.57 hours | $^{56}$Fe(n,p)$^{56}$Mn |
| 1014.54 (28) | $^{27}$Mg | 9.46 min | $^{27}$Al(n,p)$^{27}$Mg / $^{30}$Si(n,α)$^{27}$Mg |
| 1039.18 (7.4) | $^{66}$Cu | 5.12 min | $^{65}$Cu(n,γ)$^{66}$Cu |
| 1273.53 (90.6) | $^{29}$Al | 6.56 min | $^{29}$Si(n,p)$^{29}$Al |
| 1368.86 (100) | $^{24}$Na | 14.96 hours | $^{27}$Al(n,α)$^{24}$Na |
| 1642.98 (31.9) | $^{38}$Cl | 37.24 min | $^{37}$Cl(n,γ)$^{38}$Cl |
| 1779.33 (100) | $^{28}$Al | 2.24 min | $^{27}$Al(n,γ)$^{28}$Al / $^{28}$Si(n,p)$^{28}$Al |
| 1811.14 (27.2) | $^{56}$Mn | 2.57 hours | $^{56}$Fe(n,p)$^{56}$Mn |

For samples B1, B2, and B3, there were a total of nine peaks of interest in their respective gamma spectra (Fig. 2.2.25-27). These included $^{123m}$Sn at 160 keV, $^{109m}$Pd at 189 keV, $^{149}$Nd at 211 keV, $^{111m}$Cd at 245 keV, $^{198}$Au at 412 keV, $^{76}$As at 559 keV, $^{58}$Co at 811 keV, $^{24}$Na at 1369 keV, and $^{52}$V at 1434 keV. As the size of the sample increased from 50 to 200 mg, the size of each peak increased as expected. This was also true of the length of count time. This can be seen in Fig. 2.2.25. As the mass of the sample and the count time increased, the number of identifiable peaks also increased. For example, for sample B1 only five of the nine peaks gave sufficient signal to be easily identifiable (Fig. 2.2.25). These were the peaks for tin, cadmium, gold, sodium, and vanadium. For sample B2 a two-minute collection led to six peaks being easily detectible, adding palladium (Fig. 2.2.26). A five-minute collection gave eight peaks, adding those of neodymium and arsenic. A 10-minute collection assisted in the labelling of all nine peaks, adding cobalt. For sample B3, a two-minute collection led to tin, cadmium, gold, arsenic, sodium, and vanadium being easily identified (Fig. 2.2.27). When increased to five minutes, palladium was added. Then for 10 minutes, neodymium and cobalt were added. It shall be noted that even though fewer peaks were labelled at lower masses and count times, all nine peaks were identified in every spectrum but only labelled as per described.

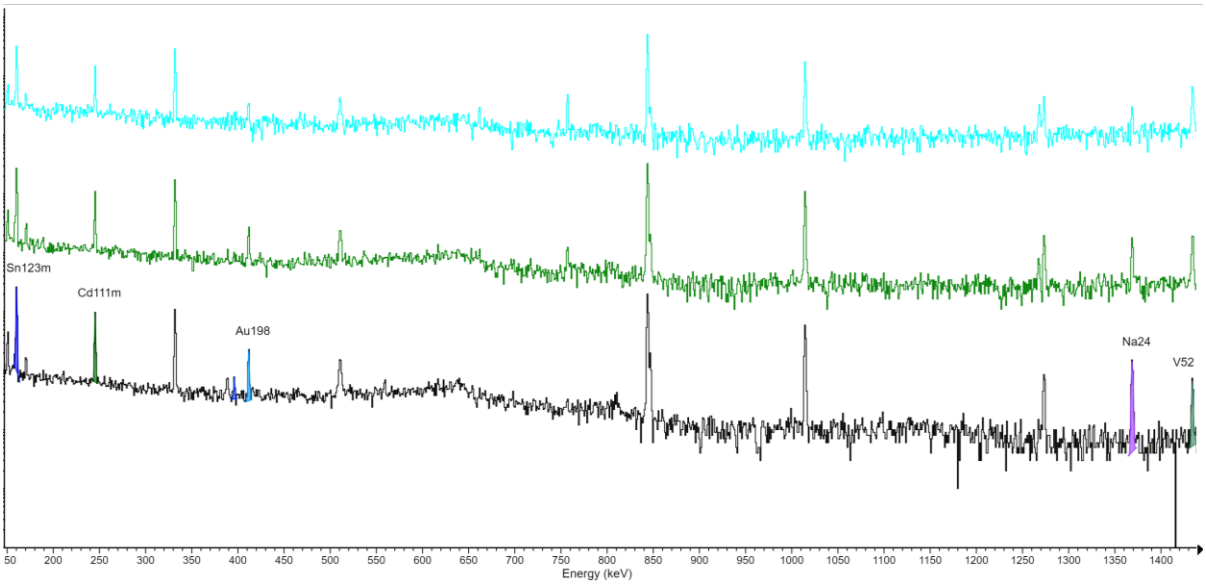


Fig. 2.2.25. Gamma spectra of sample B1. Cyclotron operated at 18 MeV. Count time of two (blue), five (green), and 10 (black) minutes. Decay time of two, five, and 10 minutes, respectively. Sample placed directly on detector. Peaks of interest are labelled with radionuclide symbol.

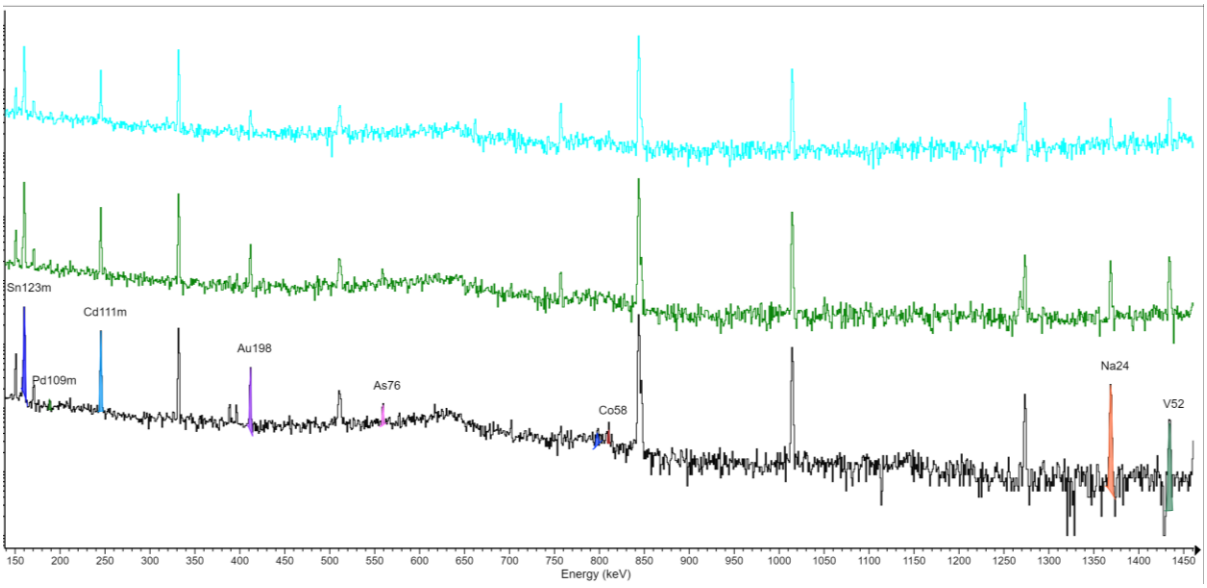


Fig. 2.2.26. Gamma spectra of sample B2. Cyclotron operated at 18 MeV. Count time of two (blue), five (green), and 10 (black) minutes. Decay time of three, seven, and 12 minutes, respectively. Sample placed directly on detector. Peaks of interest are labelled with radionuclide symbol.

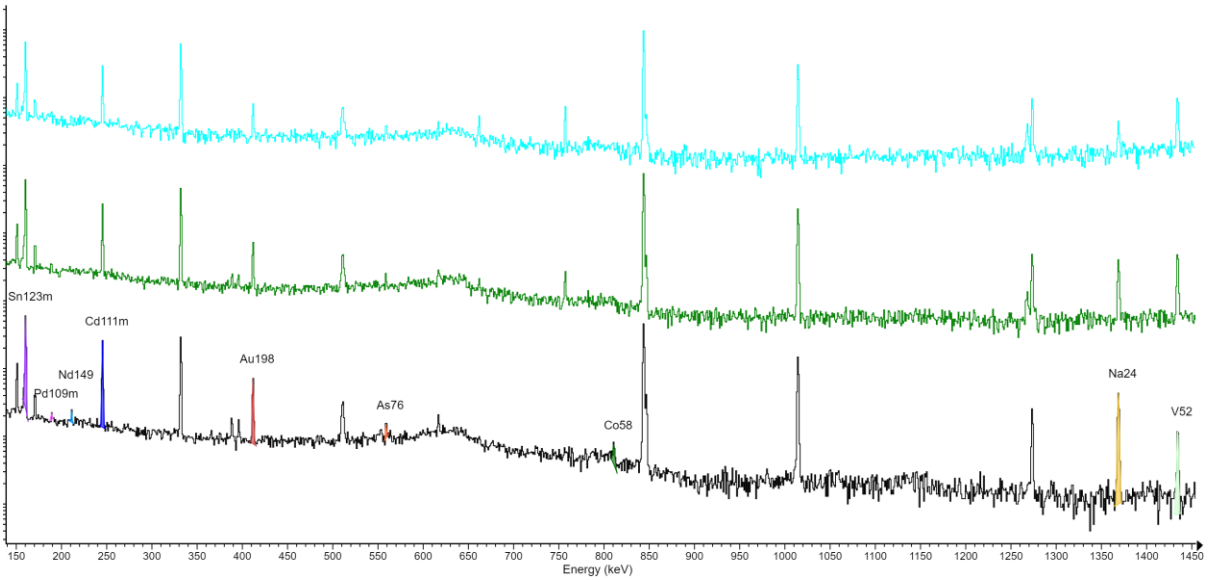


Fig. 2.2.27. Gamma spectra of sample B3. Cyclotron operated at 18 MeV. Count time of two (blue), five (green), and 10 (black) minutes. Decay time of four, seven, and 12 minutes, respectively. Sample placed directly on detector. Peaks of interest are labelled with radionuclide symbol.

In addition to the nine peaks of interest previously mentioned, additional peaks were identified (Fig. 2.2.28). These included another $^{111m}$Cd peak at 151 keV; $^{27}$Mg peaks at 171, 844, and 1015 keV; $^{125m}$Sn at 332 keV; the annihilation 511 keV, indicative of positron decay and/or electron capture; and $^{38}$Cl at 1643 keV (Table 2.2.5). The 847 keV peak of $^{56}$Mn, the 1274 keV peak of $^{29}$Al, and the 1779 keV peak of $^{28}$Al were also identified and are labelled in bold.

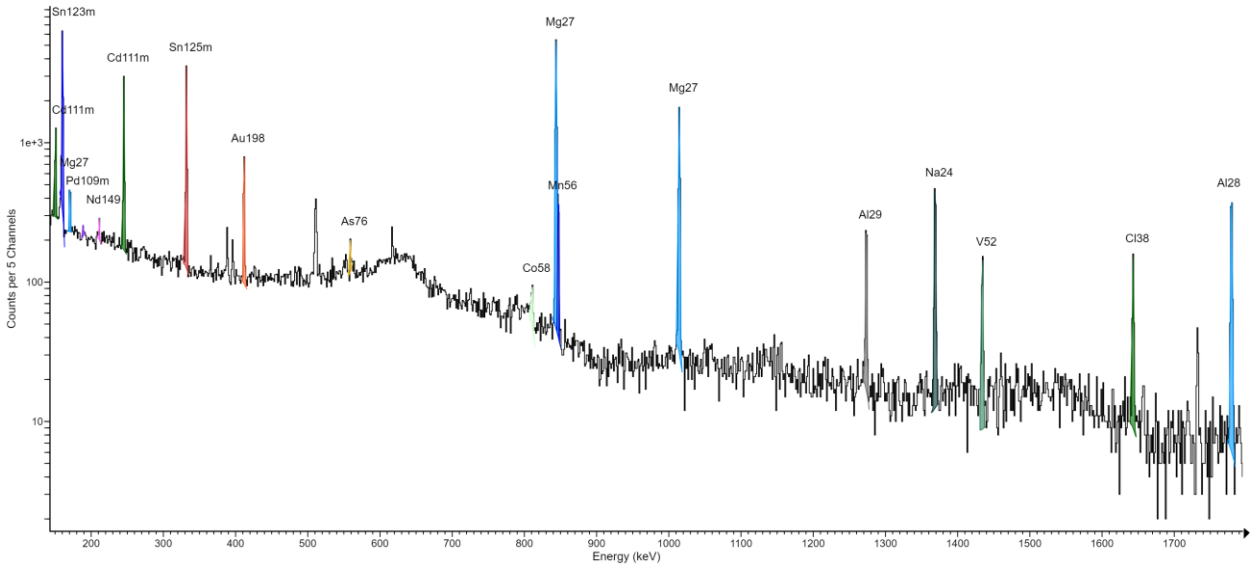


Fig. 2.2.28. Gamma spectrum of sample B3. Cyclotron operated at 18 MeV. Count time of 10 minutes and decay time of 12 minutes. Sample placed directly on detector. All substantial peaks are labelled with radionuclide symbol.

Table 2.2.5. All substantial peaks from sample B3, including peak energy and intensity, radionuclide detected, half-life, and reaction of production. Radionuclides in bold indicate those that should not have been present in the sample.

| keV (Intensity) | Nuclide | Half Life | Reaction |
|---|---|---|---|
| 150.76 (29.14) | $^{111m}$Cd | 48.50 min | $^{111}$Cd(n,n)$^{111}$Cd |
| 160.29 (85.7) | $^{123m}$Sn | 40.06 min | $^{122}$Sn(n,γ)$^{123m}$Sn / $^{124}$Sn(n,2n)$^{123m}$Sn |
| 170.61 (0.8) | $^{27}$Mg | 9.46 min | $^{26}$Mg(n,γ)$^{27}$Mg / $^{27}$Al(n,p)$^{27}$Mg / $^{30}$Si(n,α)$^{27}$Mg |
| 189.15 (55.9) | $^{109m}$Pd | 4.70 min | $^{108}$Pd (n,γ) $^{109m}$Pd / $^{110}$Pd (n,2n) $^{109m}$Pd |
| 211.23 (25.9) | $^{149}$Nd | 1.73 hours | $^{148}$Nd(n,γ)$^{149}$Nd |
| 245.35 (94) | $^{111m}$Cd | 48.50 min | $^{111}$Cd(n,n)$^{111m}$Cd (n,n) |
| 331.95 (97.2) | $^{125m}$Sn | 9.52 min | $^{124}$Sn(n,γ)$^{125m}$Sn |
| 411.80 (95.6) | $^{198}$Au | 2.69 days | $^{197}$Au(n,γ)$^{198}$Au |
| 510.96 (100) | Non-Specific | | Positron Annihilation / Electron Capture |
| 558.97 (45) | $^{76}$As | 1.09 days | $^{75}$As(n,γ)$^{76}$As |
| 810.89 (99.45) | $^{58}$Co | 70.86 days | $^{58}$Ni(n,p)$^{58}$Co |
| 843.80 (71.8) | $^{27}$Mg | 9.46 min | $^{26}$Mg(n,γ)$^{27}$Mg / $^{27}$Al(n,p)$^{27}$Mg / $^{30}$Si(n,α)$^{27}$Mg |
| **846.78 (98.87)** | **$^{56}$Mn** | **2.58 hours** | **$^{56}$Fe(n,p)$^{56}$Mn** |
| 1014.50 (28) | $^{27}$Mg | 9.46 min | $^{26}$Mg(n,γ)$^{27}$Mg / $^{27}$Al(n,p)$^{27}$Mg / $^{30}$Si(n,α)$^{27}$Mg |
| **1273.52 (90.6)** | **$^{29}$Al** | **6.56 min** | **$^{29}$Si(n,p)$^{29}$Al** |
| 1368.79 (100) | $^{24}$Na | 14.96 hours | $^{24}$Mg(n,p)$^{24}$Na / $^{27}$Al(n,α)$^{24}$Na |
| 1434.33 (100) | $^{52}$V | 3.74 min | $^{52}$Cr(n,p)$^{52}$V |

| keV (Intensity) | Nuclide | Half Life | Reaction |
|---|---|---|---|
| 1643.04 (31.9) | $^{38}$Cl | 37.24 min | $^{37}$Cl(n,γ)$^{38}$Cl |
| **1779.30 (100)** | **$^{28}$Al** | **2.24 min** | **$^{27}$Al(n,γ)$^{28}$Al / $^{28}$Si(n,p)$^{28}$Al** |

With all the identified peaks, the masses of the elements of interest were identified for each of the six samples (Table 2.2.6). In 24 of the 39 mass calculations, the calculated mass was larger than the expected mass. The percent discrepancy found in the masses were also quite large, with some reaching as large as 310%. The elements with the largest discrepancy were silicon with ~141%, aluminum with ~219%, and gold with ~259%. Silicon's and aluminum's discrepancy increased as the sample size increased from 50 mg to 100 mg, whereas gold's discrepancy decreased. Copper with ~6%, iron with ~11%, and arsenic with ~17% were the elements with the lowest average percent discrepancy. Iron's and copper's discrepancy decreased as the mass of the sample increased, whereas arsenic's discrepancy increased.

Table 2.2.6. The experimentally determined mass of each analysed element in the samples, in addition to the expected mass, mass difference, and percent discrepancy.

| Sample | Element | Calculated Mass (mg) | Expected Mass (mg) | Mass Difference (mg) | Percent Discrepancy (%) |
|---|---|---|---|---|---|
| A1 | Si | 1.50 | 0.85 | 0.64 | 86 |
| | Fe | 3.66 | 4.74 | -1.08 | 20.3 |
| | Cu | 2.02 | 2.29 | -0.28 | 12 |
| | Al | 1.20 | 0.49 | 0.72 | 150 |
| A2 | Si | 4.49 | 1.66 | 2.83 | 170. |
| | Fe | 9.88 | 9.24 | 0.64 | 6.9 |
| | Cu | 4.73 | 4.47 | 0.27 | 6.0 |
| | Al | 3.46 | 0.95 | 2.50 | 260 |
| A3 | Si | 9.32 | 3.50 | 5.82 | 166 |
| | Fe | 20.70 | 19.48 | 1.22 | 6.27 |
| | Cu | 9.43 | 9.42 | 0.01 | 0.1 |
| | Al | 7.00 | 2.01 | 4.99 | 248 |
| B1 | Mg | 1.49 | 0.77 | 0.73 | 95 |
| | Sn | 4.33 | 4.54 | -0.22 | 4.8 |
| | Cd | 0.13 | 0.16 | -0.03 | 20 |
| | Nd | 0.09 | 0.04 | 0.05 | 100 |
| | Ni | 7.85 | 2.26 | 5.59 | 248 |

| Sample | Element | Calculated Mass (mg) | Expected Mass (mg) | Mass Difference (mg) | Percent Discrepancy (%) |
|---|---|---|---|---|---|
| | As | 0.13 | 0.14 | -0.01 | 1 |
| | Cr | 0.47 | 0.63 | -0.16 | 25 |
| | Pd | 0.03 | 0.02 | 0.01 | 40 |
| | Au | 0.23 | 0.06 | 0.18 | 300 |
| B2 | Mg | 2.09 | 1.40 | 0.69 | 49 |
| | Sn | 6.96 | 8.31 | -1.35 | 16.2 |
| | Cd | 0.21 | 0.29 | -0.07 | 30 |
| | Nd | 0.11 | 0.08 | 0.03 | 40 |
| | Ni | 4.86 | 4.13 | 0.73 | 18 |
| | As | 0.27 | 0.25 | 0.02 | 10 |
| | Cr | 0.88 | 1.14 | -0.26 | 23 |
| | Pd | 0.04 | 0.04 | 0.00 | 0 |
| | Au | 0.40 | 0.10 | 0.29 | 280 |
| B3 | Mg | 3.42 | 3.11 | 0.31 | 10. |
| | Sn | 10.22 | 18.46 | -8.24 | 44.6 |
| | Cd | 0.35 | 0.64 | -0.29 | 46 |
| | Nd | 0.21 | 0.17 | 0.04 | 20 |
| | Ni | 7.34 | 9.17 | -1.83 | 19.9 |
| | As | 0.33 | 0.55 | -0.22 | 40. |
| | Cr | 1.38 | 2.54 | -1.16 | 45.8 |
| | Pd | 0.04 | 0.09 | -0.05 | 50 |
| | Au | 0.66 | 0.23 | 0.42 | 180 |

### 2.2.4. Heterogeneous mixture analysis

These samples contained the same selection of elements found in the custom standards, but their relative proportions differed. For samples C1 and C2, there were the same main four peaks of interest: $^{56}$Mn, $^{66}$Cu, $^{29}$Al, and $^{24}$Na (Fig. 2.2.29-30). As the sample mass and gamma count time increased, so did the peak size for each of the four radionuclides. There were no spectra where the peaks were challenging to find and label.

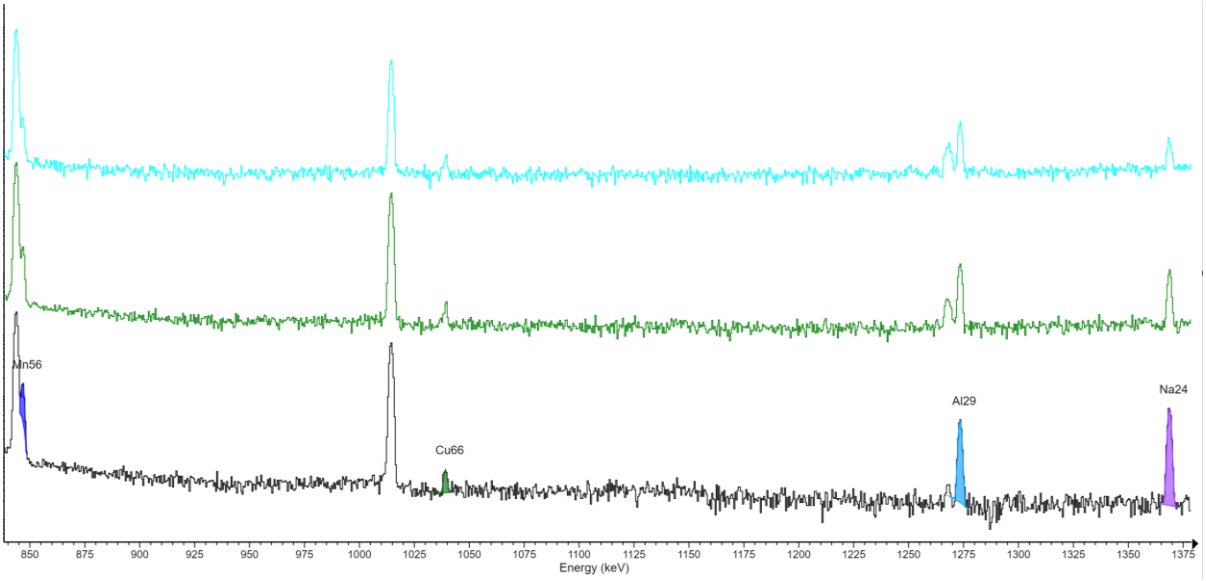


Fig. 2.2.29. Gamma spectra of sample C1. Cyclotron operated at 18 MeV. Count time of two (blue), five (green), and 10 (black) minutes. Decay time of three, six, and 12 minutes, respectively. Sample placed directly on detector. Peaks of interest are labelled with radionuclide symbol.

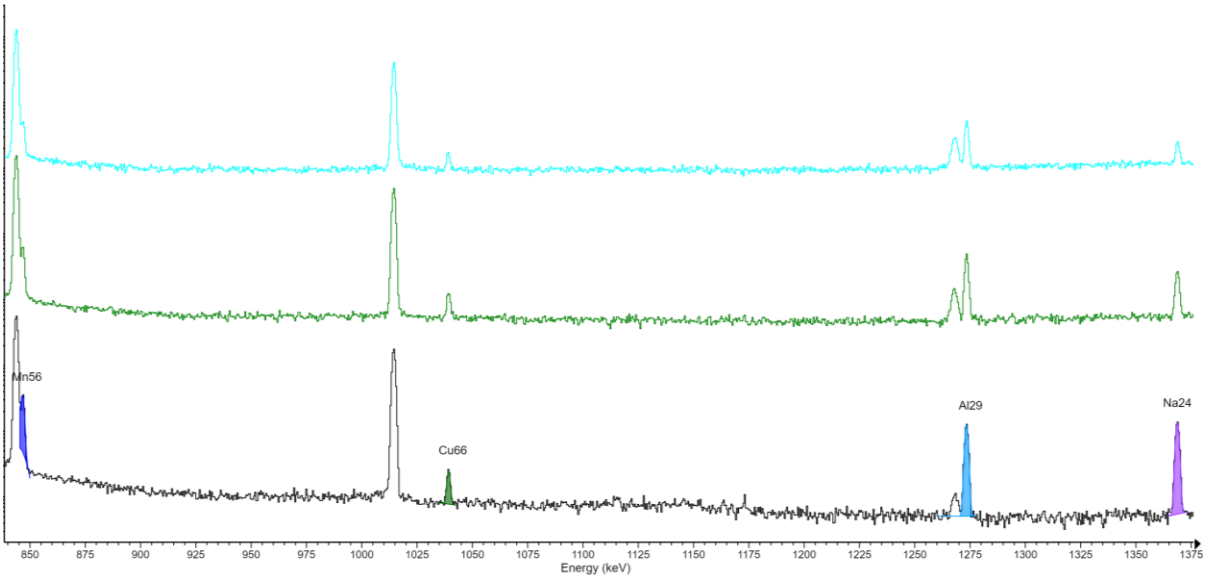


Fig. 2.2.30. Gamma spectra of sample C2. Cyclotron operated at 18 MeV. Count time of two (blue), five (green), and 10 (black) minutes. Decay time of two, five, and 11 minutes, respectively. Sample placed directly on detector. Peaks of interest are labelled with radionuclide symbol.

Other than the main four peaks of interest, additional peaks were identified and labelled in the two samples (Fig. 2.2.31), *i.e.* $^{27}$Mg, $^{38}$Cl, and $^{28}$Al. The annihilation peak at 511 keV was also present. The peak energy and reaction of production of each radionuclide peak can be found in Table 2.2.7.

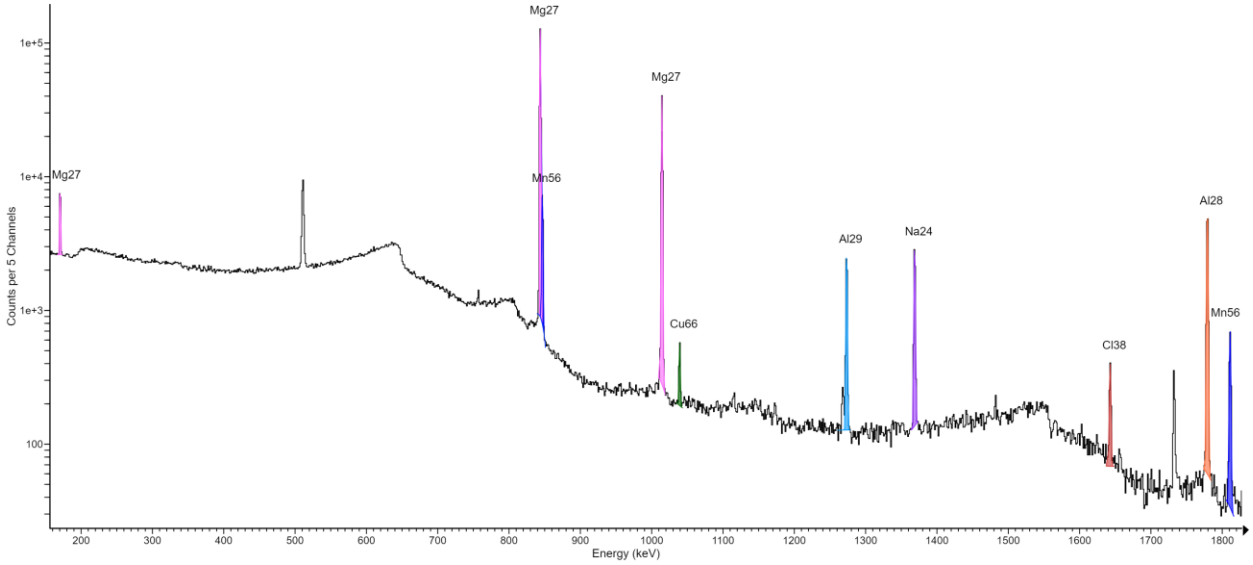


Fig. 2.2.31. Gamma spectrum of sample C2. Cyclotron operated at 18 MeV. Count time of 10 minutes and decay time of 11 minutes. Sample placed directly on detector. All substantial detected peaks are labelled with radionuclide symbol.

Table 2.2.7. All substantial peaks from sample C2, including peak energy and intensity, radionuclide detected, half-life, and reaction of production.

| keV (Intensity) | Nuclide | Half Life | Reaction |
|---|---|---|---|
| 170.59 (0.8) | $^{27}$Mg | 9.46 min | $^{27}$Al(n,p)$^{27}$Mg / $^{30}$Si(n,α)$^{27}$Mg |
| 510.99 (100) | Non-Specific | | Positron Annihilation / Electron Capture |
| 843.82 (71.8) | $^{27}$Mg | 9.46 min | $^{27}$Al(n,p)$^{27}$Mg / $^{30}$Si(n,α)$^{27}$Mg |
| 846.83 (98.9) | $^{56}$Mn | 2.57 hours | $^{56}$Fe(n,p)$^{56}$Mn |
| 1014.54 (28) | $^{27}$Mg | 9.46 min | $^{27}$Al(n,p)$^{27}$Mg / $^{30}$Si(n,α)$^{27}$Mg |
| 1039.18 (7.4) | $^{66}$Cu | 5.12 min | $^{65}$Cu(n,γ)$^{66}$Cu |
| 1273.53 (90.6) | $^{29}$Al | 6.56 min | $^{29}$Si(n,p)$^{29}$Al |
| 1368.86 (100) | $^{24}$Na | 14.96 hours | $^{27}$Al(n,α)$^{24}$Na |
| 1642.98 (31.9) | $^{38}$Cl | 37.24 min | $^{37}$Cl(n,γ)$^{38}$Cl |
| 1779.33 (100) | $^{28}$Al | 2.24 min | $^{27}$Al(n,γ)$^{28}$Al / $^{28}$Si(n,p)$^{28}$Al |
| 1811.14 (27.2 | $^{56}$Mn | 2.57 hours | $^{56}$Fe(n,p)$^{56}$Mn |

Before sample D1 could be analysed, a gamma spectrum was generated to detect any residual radionuclides remaining from the previous irradiation and analysis of some of the compounds used in both the heterogeneous standard and the standard curves. The only element that was detectable was gold, represented by both a $^{196}$Au peak at 356 keV and a $^{198}$Au peak at 412 keV (Fig. 2.2.32). All nine elements of interest were successfully identified in sample D1 after a 10-minute collection. For the two- and five-minute collections, the peak for $^{58}$Co (Ni) was below its detection limit. The other elements ($^{123m}$Sn, $^{109m}$Pd, $^{149}$Nd, $^{111m}$Cd, $^{198}$Au, $^{76}$As, $^{24}$Na, or $^{52}$V) were clearly identifiable.

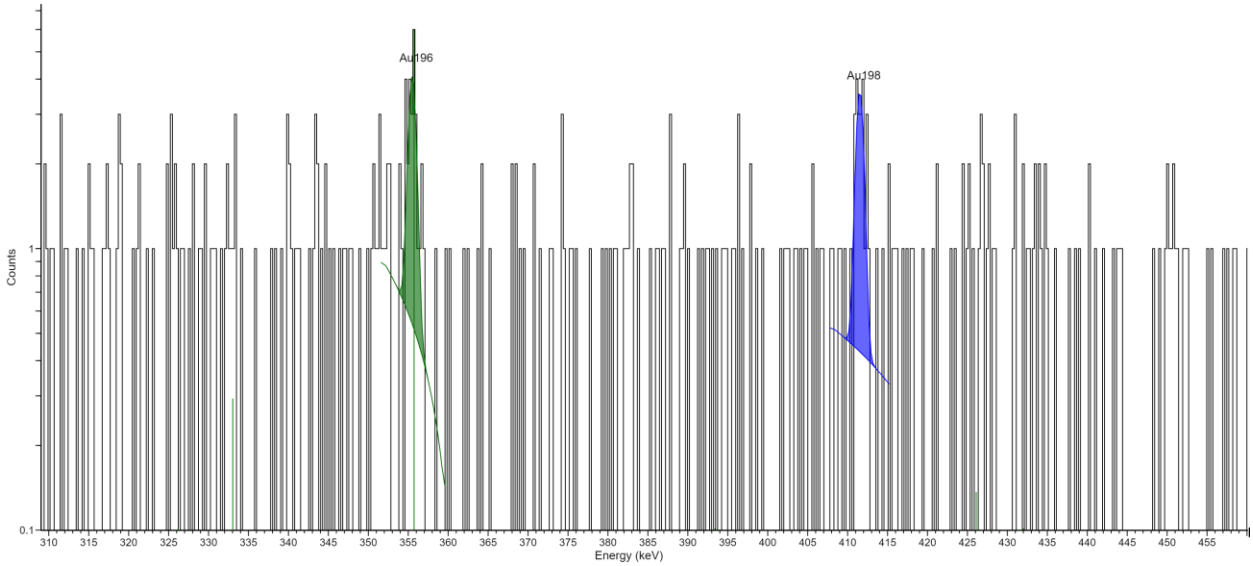


Fig. 2.2.32. Gamma spectrum of residual $^{196}$Au and $^{198}$Au activity in sample D1 prior to re-irradiation. Cyclotron operated at 18 MeV. Count time of 10 minutes. Sample placed directly on detector. Peaks of interest are labelled with radionuclide symbol.

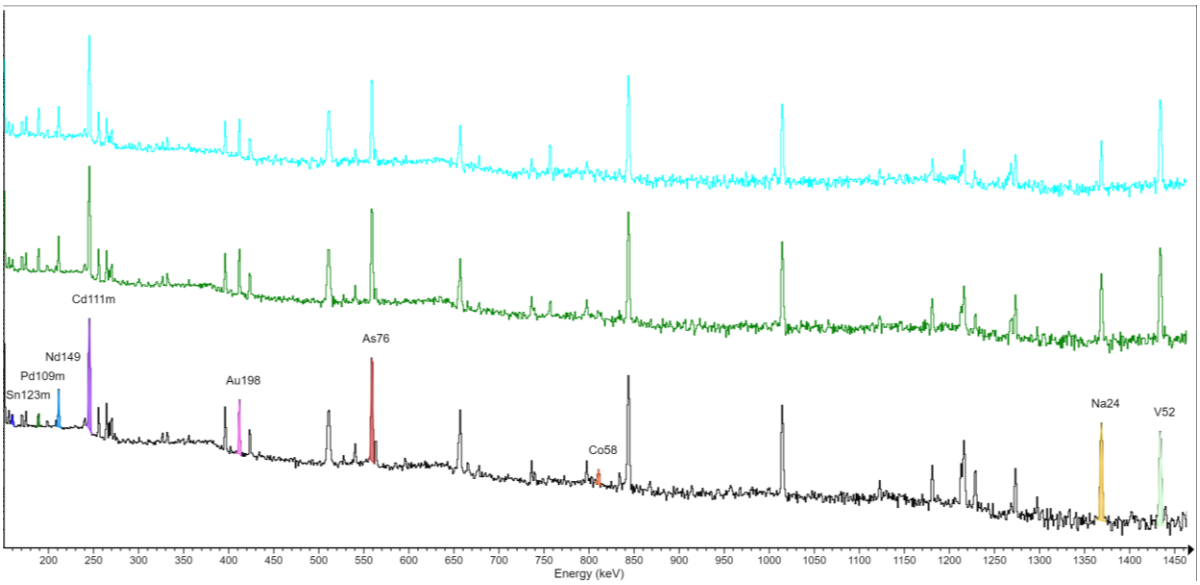


Fig. 2.2.33. Gamma spectra of sample D1. Cyclotron operated at 18 MeV. Count time of two (blue), five (green), and 10 (black) minutes. Decay time of three, five, and 11 minutes, respectively. Sample placed directly on detector. Peaks of interest are labelled with radionuclide symbol.

For sample D2, a similar pre-irradiation analysis was done to identify any residual radionuclides in the prepared sample. Once again, only gold was identified in the form of $^{196}$Au and $^{198}$Au peaks (Fig. 2.2.34). Since this sample contained a larger amount of gold compared to D1, the gold peaks were much larger compared to the background noise. There were no difficulties identifying all nine peaks of interest in any of the spectra, regardless of the count time.

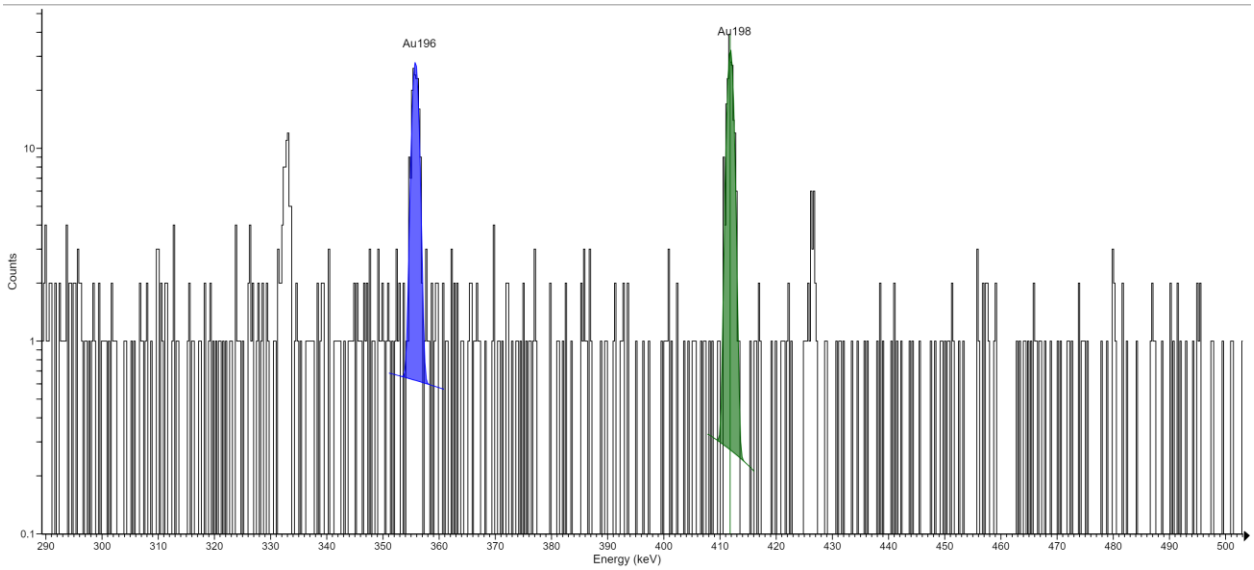


Fig. 2.2.34. Gamma spectrum of residual $^{196}$Au and $^{198}$Au activity in sample D2 prior to re-irradiation. Cyclotron operated at 18 MeV. Count time of 10 minutes. Sample placed directly on detector. Peaks of interest are labelled with radionuclide symbol.

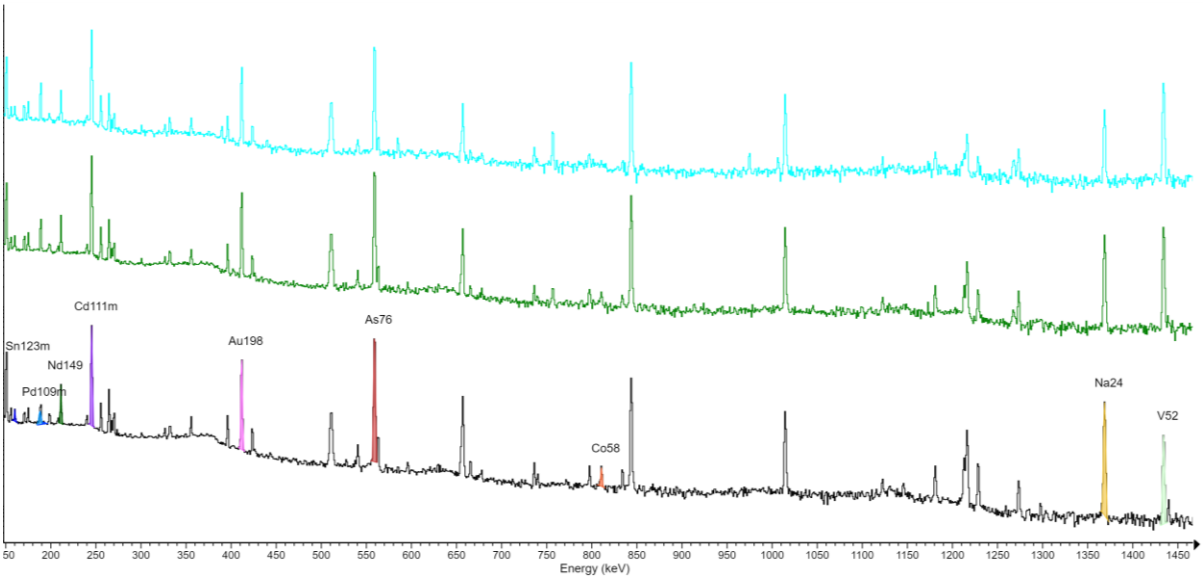


Fig. 2.2.35. Gamma spectra of sample D2. Cyclotron operated at 18 MeV. Count time of two (blue), five (green), and 10 (black) minutes. Decay time of two, five, and 10 minutes, respectively. Sample placed directly on detector. Peaks of interest are labelled with radionuclide symbol.

There were numerous additional peaks identified and labelled for this sample (Fig. 2.2.36). These were $^{27}$Mg, $^{75}$Ge, $^{117}$Cd, $^{196}$Au, $^{125m}$Sn, $^{72}$Ga, $^{38}$Cl, and $^{28}$Al. There were a secondary peaks identified for $^{149}$Nd at 114 keV, $^{111m}$Cd at 151 keV, and $^{76}$As at 657 keV. The peak energies and reactions of production for all other radionuclides can be seen in Table 2.2.8.

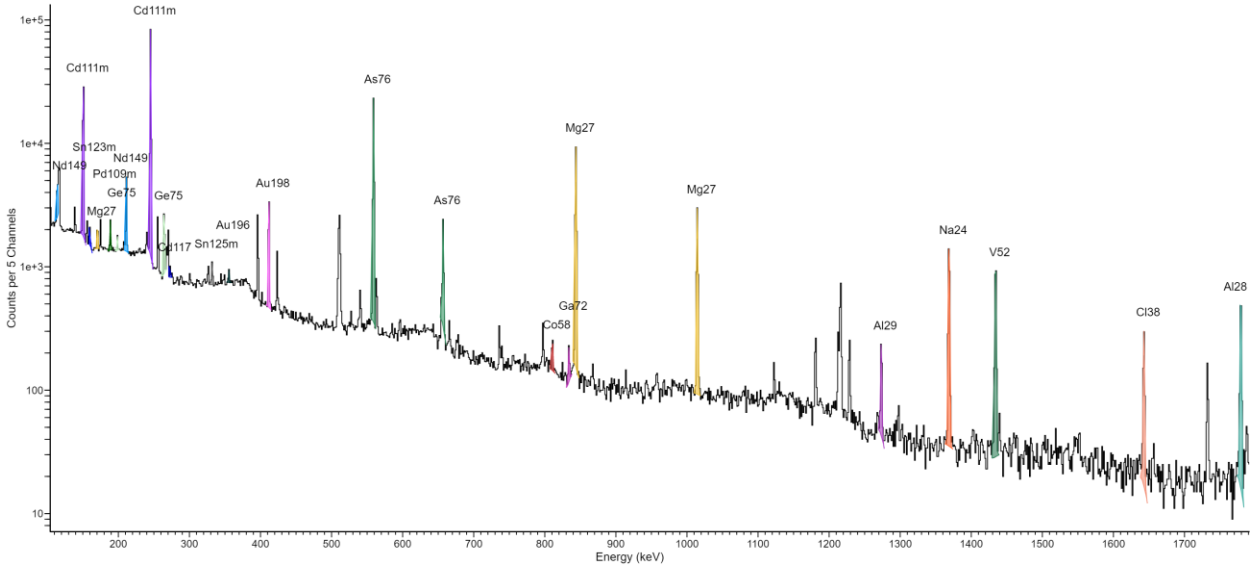


Fig. 2.2.36. Gamma spectrum of sample D2. Cyclotron operated at 18 MeV. Count time of 10 minutes and decay time of 10 minutes. Sample placed directly on detector. All substantial detected peaks are labelled with radionuclide symbol.

Table 2.2.8. All substantial peaks from sample D2, including peak energy and intensity, radionuclide detected, half-life, and reaction of production.

| keV (Intensity) | Nuclide | Half Life | Reaction |
|---|---|---|---|
| 114.22 (19.17) | $^{149}$Nd | 1.73 hours | $^{148}$Nd(n,γ)$^{149}$Nd |
| 150.75 (29.14) | $^{111m}$Cd | 48.50 min | $^{111}$Cd(n,n)$^{111}$Cd |
| 160.22 (85.7) | $^{123m}$Sn | 40.06 min | $^{122}$Sn(n,γ)$^{123m}$Sn / $^{124}$Sn(n,2n)$^{123m}$Sn |
| 170.68 (0.8) | $^{27}$Mg | 9.46 min | $^{26}$Mg(n,γ)$^{27}$Mg / $^{27}$Al(n,p)$^{27}$Mg / $^{30}$Si(n,α)$^{27}$Mg |
| 188.78 (55.9) | $^{109m}$Pd | 4.70 min | $^{108}$Pd (n,γ) $^{109m}$Pd / $^{110}$Pd (n,2n) $^{109m}$Pd |
| 198.67 (1.19) | $^{75}$Ge | 1.38 hours | $^{75}$As(n,p)$^{75}$Ge |
| 211.28 (25.9) | $^{149}$Nd | 1.73 hours | $^{148}$Nd(n,γ)$^{149}$Nd |
| 245.34 (94) | $^{111m}$Cd | 48.50 min | $^{111}$Cd(n,n)$^{111}$Cd |
| 264.60 (11.4) | $^{75}$Ge | 1.38 hours | $^{75}$As(n,p)$^{75}$Ge |
| 273.32 (27.9) | $^{117}$Cd | 2.49 hours | $^{120}$Sn(n,α) $^{117}$Cd |
| 332.32 (97.2) | $^{125m}$Sn | 9.52 min | $^{124}$Sn(n,γ)$^{125m}$Sn |
| 355.65 (86.95) | $^{196}$Au | 6.17 days | $^{197}$Au(n,2n)$^{196}$Au |
| 411.74 (95.6) | $^{198}$Au | 2.69 days | $^{197}$Au(n,γ)$^{198}$Au |

| keV (Intensity) | Nuclide | Half Life | Reaction |
|---|---|---|---|
| 510.91 (100) | Non-Specific | | Positron Annihilation / Electron Capture |
| 559.05 (45) | $^{76}$As | 1.09 days | $^{75}$As(n,γ)$^{76}$As |
| 656.99 (6.17) | $^{76}$As | 1.09 days | $^{75}$As(n,γ)$^{76}$As |
| 810.72 (99.45) | $^{58}$Co | 70.86 days | $^{58}$Ni(n,p)$^{58}$Co |
| 834.11 (95.45) | $^{72}$Ga | 14.10 hours | $^{75}$As(n,α) $^{72}$Ga |
| 843.75 (71.8) | $^{27}$Mg | 9.46 min | $^{26}$Mg(n,γ)$^{27}$Mg / $^{27}$Al(n,p)$^{27}$Mg / $^{30}$Si(n,α)$^{27}$Mg |
| 1014.47 (28) | $^{27}$Mg | 9.46 min | $^{26}$Mg(n,γ)$^{27}$Mg / $^{27}$Al(n,p)$^{27}$Mg / $^{30}$Si(n,α)$^{27}$Mg |
| 1273.42 (90.6) | $^{29}$Al | 6.56 min | $^{29}$Si(n,p)$^{29}$Al |
| 1368.74 (100) | $^{24}$Na | 14.96 hours | $^{24}$Mg(n,p)$^{24}$Na / $^{27}$Al(n,α)$^{24}$Na |
| 1434.22 (100) | $^{52}$V | 3.74 min | $^{52}$Cr(n,p)$^{52}$V |
| 1642.89 (31.9) | $^{38}$Cl | 37.24 min | $^{37}$Cl(n,γ)$^{38}$Cl |
| 1779.24 (100) | $^{28}$Al | 2.24 min | $^{27}$Al(n,γ)$^{28}$Al / $^{28}$Si(n,p)$^{28}$Al |

Due to the heterogeneous nature of the four samples, each sample was run in the gamma spectrometer without being transferred to a new vial after being irradiated. This prevented the transfer of the irradiated samples to non-irradiated vials, leading to potential gamma photon contributions from the vial. To remove any influence that this may have had on the results, an empty vial was also irradiated and analysed for 10 minutes (Fig. 2.2.37). The peaks identified were $^{27}$Mg at 171, 844, and 1014 keV, $^{29}$Al at 1273 keV, $^{24}$Na at 1369 keV, and $^{28}$Al at 1779 keV (Table 2.2.9). The 511 keV peak was also present.

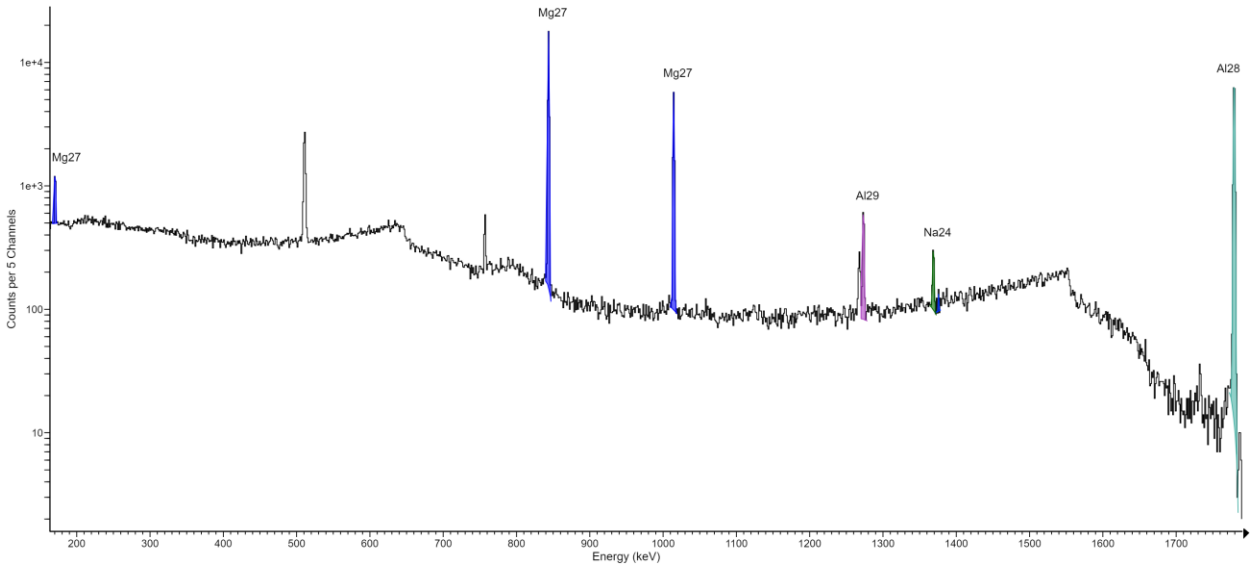


Fig. 2.2.37. Gamma spectrum of an empty sample vial. Cyclotron operated at 18 MeV. Count time of 10 minutes and decay time of one minute. Sample placed directly on detector. All substantial detected peaks are labelled with radionuclide symbol. The unlabelled peak is the annihilation 511 keV peak.

Table 2.2.9. All substantial peaks from the empty sample vial, including peak energy and intensity, radionuclide detected, and reaction of production.

| keV (Intensity) | Nuclide | Reaction |
|---|---|---|
| 170.59 (0.8) | $^{27}$Mg | $^{27}$Al(n,p)$^{27}$Mg / $^{30}$Si(n,α)$^{27}$Mg |
| 510.93 | Non-Specific | Positron Annihilation / Electron Capture |
| 843.74 (71.8) | $^{27}$Mg | $^{27}$Al(n,p)$^{27}$Mg / $^{30}$Si(n,α)$^{27}$Mg |
| 1014.44 (28) | $^{27}$Mg | $^{27}$Al(n,p)$^{27}$Mg / $^{30}$Si(n,α)$^{27}$Mg |
| 1273.44 (90.6) | $^{29}$Al | $^{29}$Si(n,p)$^{29}$Al |
| 1368.79 (100) | $^{24}$Na | $^{27}$Al(n,α)$^{24}$Na |
| 1779.19 (100) | $^{28}$Al | $^{27}$Al(n,γ)$^{28}$Al / $^{28}$Si(n,p)$^{28}$Al |

Using all these data, the elemental masses for the four samples were calculated. A total of 16 out of the 26 masses calculated were above their respective expected values (Table 2.2.10). This led to percent discrepancies up to 50%. The elements with the lowest average percent discrepancy are magnesium with ~1%, silicon with ~5%, neodymium with 6%, copper with ~9%, cadmium with 10%, and chromium with 11%. The elements with the largest average percent discrepancy are palladium with ~40% and arsenic with ~35%. When comparing the percent discrepancy of the “small” samples (C1 & D1) to their “large” counterparts (C2 & D2),

the following elements showed an increase in discrepancy when increasing sample size: silicon, iron, copper, aluminum, tin, cadmium, chromium, palladium, and gold. The other elements showed the opposite trend, with their percent discrepancy decreasing as the sample size increased: magnesium, neodymium, nickel, and arsenic.

Table 2.2.10. The experimentally determined mass of each analysed element of each sample, in addition to the actual mass, mass difference, and percent discrepancy. Elements in bold have approximated masses, due to gamma spectra contamination from the irradiated vial.

| Sample | Element | Calculated Mass (mg) | Actual Mass (mg) | Mass Difference (mg) | Percent Discrepancy (%) |
|---|---|---|---|---|---|
| C1 | **Si** | **12.94** | **12.67** | **0.27** | **2.2** |
| | Fe | 8.30 | 9.54 | -1.24 | 13.0 |
| | Cu | 4.75 | 5.01 | -0.26 | 5.2 |
| | **Al** | **16.09** | **13.76** | **2.33** | **16.9** |
| C2 | **Si** | **38.14** | **35.20** | **2.94** | **8.35** |
| | Fe | 19.54 | 17.11 | 2.43 | 14.2 |
| | Cu | 18.75 | 16.64 | 2.10 | 12.6 |
| | **Al** | **39.42** | **31.86** | **7.56** | **23.7** |
| D1 | **Mg** | **9.20** | **8.99** | **0.21** | **2.3** |
| | Sn | 0.95 | 0.84 | 0.11 | 13 |
| | Cd | 10.44 | 9.69 | 0.75 | 7.7 |
| | Nd | 6.13 | 5.70 | 0.43 | 7.5 |
| | Ni | 17.13 | 11.59 | 5.54 | 47.8 |
| | As | 59.24 | 40.75 | 18.49 | 45.37 |
| | Cr | 8.75 | 7.99 | 0.76 | 9.5 |
| | Pd | 0.97 | 1.57 | -0.60 | 38 |
| | Au | 2.61 | 2.90 | -0.29 | 9.9 |
| D2 | **Mg** | **31.59** | **31.73** | **-0.14** | **0.43** |
| | Sn | 1.74 | 2.16 | -0.42 | 19 |
| | Cd | 7.55 | 6.74 | 0.81 | 12 |
| | Nd | 8.89 | 8.57 | 0.32 | 3.7 |
| | Ni | 33.98 | 35.44 | -1.47 | 4.14 |
| | As | 132.87 | 107.02 | 25.85 | 24.15 |
| | Cr | 9.66 | 10.93 | -1.27 | 11.6 |
| | Pd | 2.09 | 3.66 | -1.57 | 42.9 |
| | Au | 13.68 | 22.40 | -8.72 | 38.9 |

## 2.3. Discussion

### 2.3.1. Identification of elements

The following elements were identified in the eWaste samples: silicon, aluminum, copper, iron, tin, magnesium, chromium, cadmium, neodymium, gold, arsenic, palladium, and nickel. Of these elements, all but two had at least one unique radionuclide activation product, leading to a gamma ray with a unique energy. As demonstrated in Table 2.2.1, there are a variety of interference between the neutron-activated isotopes of silicon, aluminum, and magnesium. Silicon and aluminum share $^{28}$Al, aluminum and magnesium share $^{24}$Na, and all these elements share $^{27}$Mg. Conveniently, $^{29}$Al was only detected in the presence of silicon, which can be used for its unambiguous detection even in the presence of the other two elements. For aluminum and magnesium, there were no consistently present, well defined and unique peaks for either element, and thus, the elements could not be distinguished in any sample. There is also the added complication that sodium can also form $^{24}$Na via a (n,γ) reaction. Therefore, magnesium and aluminum can only be quantified if it is independently known that only magnesium or only aluminum is in the sample, and in either case there is also no sodium present.

Since multiple activated isotopes can also decay by electron-capture or positron emission, both of which produce a positron, the positron-electron annihilation line at 511 keV cannot be used to quantify or identify an element.

### 2.3.2. Custom standard analysis

Two sets of custom eWaste standards were generated, one containing the elements iron, copper, aluminum, and silicon (samples A1 to A3) and one containing the elements tin, gold, arsenic, cadmium, chromium, palladium, nickel, magnesium, and neodymium (samples B1 to B3).

For the samples A1 - 3, all four elements were identified by detecting their respective radionuclide gamma peaks from $^{56}$Mn, $^{66}$Cu, $^{24}$Na, and $^{29}$Al regardless of the gamma spectrometer count time or sample mass. Note, in this sample it is known that the $^{56}$Mn peak

comes from iron vs. manganese as manganese was not included in the sample. The peaks of $^{27}$Mg, $^{38}$Cl, and $^{28}$Al were also identified. $^{27}$Mg is represented by three distinct peaks and formed because of either a $^{27}$Al(n,p)$^{27}$Mg or a $^{30}$Si(n,α)$^{27}$Mg nuclear reaction. Since these standards contained both silicon and aluminum, it is not possible to determine which element and reaction contributed to the peaks, as it is likely a combination of the two. $^{38}$Cl is represented by only one peak and results from the reaction $^{37}$Cl(n,γ)$^{38}$Cl. The source of the chlorine in the samples is the chloride counterion used in $FeCl_3$. $^{28}$Al is also represented by only one peak and results from the reactions $^{27}$Al(n,γ)$^{28}$Al and $^{28}$Si(n,p)$^{28}$Al. Once again, since both aluminum and silicon were present, the peak is a combination of the signal generated from both elements.

For the samples B1 - 3, all nine elements of interest were identified by detecting their respective radionuclide gamma peaks of $^{111m}$Cd, $^{123m}$Sn, $^{109m}$Pd, $^{149}$Nd, $^{198}$Au, $^{76}$As, $^{58}$Co, $^{24}$Na, and $^{52}$V. As demonstrated by Fig. 2.2.25-27, not all elements were identified in each spectrum. There were three spectra generated for each of the three samples, at a count time of two, five, and 10 minutes. The variety in count times aimed to assist in the identification of the different radionuclides by taking their varying half-lives into account. Those with shorter half-lives would have been more likely to be detected in the two-minute collection, whereas those with longer half-lives should be more prevalent after the five- or 10-minute collection.

The radionuclide that this affected most was $^{58}$Co, which has a half-life of 70.86 days. $^{58}$Co was only detectable in samples where the count time was 10 minutes. Still, the peak was quite small and would have been easier to detect and measure if the collection were extended further. This is also the case with $^{76}$As, with a half-life of 1.09 days, which could only be detected with five- and 10-minute count times. $^{76}$As shows up in five-minute runs, unlike $^{58}$Co, because if its shorter half-life. This was the trend for the other harder-to-detect radionuclides, $^{109m}$Pd and $^{149}$Nd. Obviously, increasing the sample size would make detection of long-lived isotopes easier at short count times.

In addition to the radionuclides of interest, the following radioisotopes were detected: $^{27}$Mg, $^{125m}$Sn, $^{56}$Mn, $^{29}$Al, and $^{28}$Al (Table 2.2.5). $^{27}$Mg generated three peaks and was formed as the result of the nuclear reactions of $^{26}$Mg(n,γ)$^{27}$Mg, $^{27}$Al(n,p)$^{27}$Mg , and/or $^{30}$Si(n,α)$^{27}$Mg. The

fact that all three of these reactions can generate $^{27}Mg$ indicates why $^{27}Mg$ cannot be used to quantify magnesium, silicon, or aluminum if at least two of these are present in the same sample. In the case of these samples (B1 - 3), no silicon or aluminum were added. Thus, it would be most likely that the $^{27}Mg$ peak came from the magnesium present. However, as evident by the $^{29}Al$ and $^{28}Al$ peaks, silicon, if not also aluminum, must also be present. This is because $^{29}Al$ would only be formed via the nuclear reaction $^{29}Si(n,p)^{29}Al$, indicating silicon's presence and $^{28}Al$ can be formed by either the reaction $^{27}Al(n,\gamma)^{28}Al$ or $^{28}Si(n,p)^{28}Al$, further confirming silicon's presence and the potential presence of aluminum. Hence, the $^{27}Mg$ could not have been used to identify and quantity the magnesium in the sample due to the presence of contaminants contributing to the gamma signal.

There are various sources for this contamination, which include reagent impurity, contamination from environmental sources, etc. Since the lids of the cryovials were made of silicone, they would have caused interference with the $^{29}Al$ peak if they were irradiated. Efforts were made to use new vials when placing the irradiated samples in the gamma spectrometer. If the lids were mixed up, this interference could have occurred. Since silicon and/or aluminum contamination cannot be ruled out, the accuracy of the magnesium qualification is poor. This is because $^{24}Na$ was used to identify magnesium, which can be formed by either the nuclear reaction $^{24}Mg(n,p)^{24}Na$ or $^{27}Al(n,\alpha)^{24}Na$. Therefore, it is unknown if the $^{27}Mg$ from magnesium is being interfered by the presence of silicon and/or aluminum. The peaks of $^{125m}Sn$ and $^{56}Mn$ were also identified. Simply, $^{125m}Sn$ was formed by the reaction $^{124}Sn(n,\gamma)^{125m}Sn$, which confirms the presence of tin in the sample. As for $^{56}Mn$, it was formed by the reaction $^{56}Fe(n,p)^{56}Mn$. This demonstrates that there was also some form of iron contamination in these samples, with sample preparation being the most likely culprit.

Similar to the varying success in identifying elements, their qualifications also experienced some difficulties. For samples A1 - 3, there was an average discrepancy in determining the mass of silicon of 137%, 12% for iron, 6% for copper, and 219% for aluminum (Table 2.2.6). A potential reason for the significantly higher discrepancy in the mass determination for aluminum and silicon is that the form that these elements were present in ($Al_2O_3$ and $SiO_2$) were not water soluble. This is important as the original standard mixture for

these samples was generated by adding all the compounds, dissolving them in water, and evaporating off the solvent to adsorb them onto activated carbon. Since these compounds were not water soluble, they would not have been as easily distributed throughout the mixture during this preparation. Thus, when generating the aliquots of the standard to create samples A1 - 3, the amounts of silicon and aluminum present were likely not representative of the whole mixture. By contrast, the masses of copper and iron were more accurate due to the better mixing of their respective compounds. Interestingly, the discrepancy regarding silicon and aluminum increased as the mass of the sample increased, whereas the discrepancy regarding iron and copper decreased (Table 2.2.6). For copper and iron, since they were more likely to be properly mixed, this decrease in discrepancy is likely the result of the larger sample mass leading to an increase in the gamma signals, which would have increased the signal to noise ratio. This would have allowed for a more accurate mass determination, as there would be a better distinction between the peaks of interest and the background noise. For silicon and aluminum, since they were likely not properly mixed, an increase in sample size may simply have led to a larger nonrepresentative sample.

For samples B1 - 3, there was similar variability in the discrepancy associated with mass determination. As per the main source of discrepancy with the samples A1 - 3, these samples would have also been subject to the discrepancies associated with improper mixing. This accounts for why there is such a large discrepancy between the calculated and expected quantity of each element. This also explains why some elements had shown an increase in discrepancy as the sample size increased, while others showed a decrease. Unlike samples A1 - 3, the discrepancy associated with these samples does not seem to be related to the solubility of the mixture's components. Out of the compounds mixed to form the samples, only $As_2O_3$, $Nd_2O_3$, and Pd/C were insoluble in water. Compared to the water-soluble compounds, there is not a noticeable difference in the determined discrepancy, thus making it unlikely that the water solubility of these compounds contributed to their variation in mass discrepancy. The discrepancy then is likely due to the lack of homogeneity in the mixtures and sample aliquots that do not have the same composition.

While the idea of creating a custom standard as a stand-in reference for eWaste was good, the inability to independently validate its homogeneity and element concentrations prevented it from being an accurate tool for validating the effectiveness of this analytical technique. One would need to determine an effective way to produce a homogeneously mixed standard to make it a useful tool for this investigation.

### 2.3.3. Heterogeneous mixture analysis

For the heterogeneous mixtures (*i.e.* those containing the elements of interest, unmixed), four samples were prepared. Two contained aluminum, silicon, copper, and iron (C1 and C2) while the other two contained magnesium, tin, cadmium, neodymium, nickel, arsenic, chromium, palladium, and gold (D1 & D2). Unlike the custom standards, these samples were prepared with various relative compositions, as shown in Table 2.1.2, to generate distinct samples. The exact masses in each mixture were recorded to compare to the NAA results to get a more accurate assessment of the effectiveness of the analytical method under variable compositions.

For samples C1 and C2, all four peaks of interest were identified, regardless of gamma count times. These included peaks for $^{56}$Mn, $^{66}$Cu, $^{29}$Al, and $^{24}$Na. Other than these, three peaks for $^{27}$Mg, one peak for $^{38}$Cl, and one peak for $^{28}$Al were present. The $^{27}$Mg peaks are the result of the nuclear reactions $^{27}$Al(n,p)$^{27}$Mg or $^{30}$Si(n,α)$^{27}$Mg, which are possible due the presence of both aluminum and silicon in the samples. The reaction $^{37}$Cl(n,γ)$^{38}$Cl gives rise to the $^{38}$Cl peak, due to the presence of chlorine in $FeCl_3$. Finally, $^{28}$Al was produced by the reactions $^{27}$Al(n,γ)$^{28}$Al and $^{28}$Si(n,p)$^{28}$Al, due to the presence of both aluminum and silicon. Since the vials that these samples were irradiated in were placed directly into the gamma spectrometer for collection, there was also some signal contribution from the vials towards the $^{27}$Mg, $^{24}$Na, $^{29}$Al, and $^{28}$Al peaks. An estimation of this contribution was determined by irradiating and then analysing an empty vial with the gamma spectrometer (Fig. 2.2.37). These contributions were subtracted from the peaks generated by the samples to compensate for the peak inflation. As mentioned in Table 2.2.10, while this adjustment increased the accuracy of the results, they are just approximations as not all vials contain the same quantity of silicon and aluminum.

For samples D1 and D2, eight of the nine radionuclides of interest were identified regardless of the gamma count time: $^{123m}$Sn, $^{109m}$Pd, $^{149}$Nd, $^{111m}$Cd, $^{198}$Au, $^{76}$As, $^{24}$Na, and $^{52}$V. $^{58}$Co, however, did not appear in either the two- or the five-minute collections of D1, but did appear in the 10-minute collection and in all D2 collections. Peaks representing $^{27}$Mg, $^{75}$Ge, $^{117}$Cd, $^{196}$Au, $^{125m}$Sn, $^{72}$Ga, $^{38}$Cl, and $^{28}$Al were also detected (Table 2.2.8). The $^{27}$Mg is most likely due to the presence of magnesium in the sample via the reaction $^{26}$Mg(n,γ)$^{27}$Mg. It however can also be due to the presence of aluminum and silicon from the vial itself, via the reactions $^{27}$Al(n,p)$^{27}$Mg and $^{30}$Si(n,α)$^{27}$Mg. $^{75}$Ge was produced by the presence of arsenic in the sample through the reaction $^{75}$As(n,p)$^{75}$Ge. $^{117}$Cd was produced by the presence of tin through the reaction $^{120}$Sn(n,α) $^{117}$Cd. $^{196}$Au was produced by the presence of gold through the reaction $^{197}$Au(n,2n)$^{196}$Au. $^{125m}$Sn was produced by the presence of tin through the reaction $^{124}$Sn(n,γ)$^{125m}$Sn. $^{72}$Ga was produced by the presence of arsenic via the reaction $^{75}$As(n,α) $^{72}$Ga. $^{38}$Cl was produced by the presence of chloride counterions in the iron, tin, and magnesium salts via the reaction $^{37}$Cl(n,γ)$^{38}$Cl. Finally, $^{28}$Al was produced by the presence of aluminum and silicon in the vial via the reactions $^{27}$Al(n,γ)$^{28}$Al and $^{28}$Si(n,p)$^{28}$Al. There was also some activity arising from previously irradiated gold wire (Fig. 2.2.32 & 2.2.34). This wire was also used when generating the gold standard curves and due to $^{198}$Au and $^{196}$Au long half-lives (2.7 to 6.2 days), there was some of each radioisotope still present in the samples. As per the silicon and aluminum contamination from the vials, any $^{198}$Au and/or $^{196}$Au contamination was approximated and subtracted from the sample's peaks.

Since samples A1 - 3 contained the same elements as samples C1 - 2, the average discrepancy in the mass determinations were compared. For samples C1 - 2, silicon was found to have an average discrepancy of 5%, 14% for copper, 9% for iron, and 20% for aluminum (Table 2.2.10). This is compared to 137% for silicon, 12% for copper, 6% for iron, and 219% for aluminum across samples A1 – 3 (Table 2.2.6). For both silicon and aluminum, there was a significant decrease in the average mass discrepancy when analysing samples C1 - 2. This is due to the elimination of the discrepancies associated with having an improperly mixed sample. The discrepancies are wildly different for silicon and aluminum when comparing the C samples with the A samples. This is attributed to the inhomogeneity of the A samples that was caused by

improper mixing and the lack of solubility leading to grossly inaccurate estimations of composition for those two elements. For iron and copper, the discrepancies are roughly the same when comparing the two sets of samples. This is consistent with the fact that the copper and iron salts had a more even distribution in the total mixture, and a more accurate estimation of the quantities of each element in the sample aliquot.

In relation to the samples containing the other 13 elements, samples D1 - 2 demonstrated lower average mass discrepancy when compared to samples B1 - 3. This can be seen in the average discrepancy of magnesium decreasing from 51% to 1%, tin from 22% to 16%, cadmium from 30% to 10%, neodymium from 62% to 6%, nickel from 95% to 26%, chromium from 31% to 11%, and gold from 259% to 24% (Tables 2.2.6 and 2.2.10). Some elements however show an increase in discrepancy, as there was an increase in arsenic from 17% to 35% and palladium from 33% to 40%. For arsenic, this increase is likely due to the masses of the arsenic salt detected in the samples D1 - 2 being larger than the range of the arsenic standard curve, leading to a decrease in accuracy and an increase in discrepancy. For palladium, there is some discrepancy present in its concentrations, as the 5% (w/w) has some variability in the manufacturing process. Pd/C is also very hygroscopic, which may have affected the accuracy of weighing out Pd/C. As per the comparison between samples A1 - 3 with C1 - 2, the improvement in the mass discrepancy is most attributed to eliminating the inaccurate estimation of the sample's contents, as the exact contents of samples D1 - 2 were known, and thus no estimation was required.

While investigating the differences in the results between the custom standard samples (A1 - 3 and B1 - 3) and the heterogeneous samples (C1 - 2 and D1 - 2), additional findings were drawn. In both the set of custom standard samples and the set of heterogenous samples, 62% of all calculated masses were above what was expected or initially measured. For the samples A1 - 3 and C1 - 2, the samples A1 - 3 overestimated 83% of the time, while samples C1 - 2 were overestimated 75% of the time. This decrease is likely to be related to the increase in the masses used for samples C1 - 2. Since the quantity of each compound used was larger, the signal to noise ratio of their respective gamma spectra also increased. This allowed for easier peak integration and decreased the amount of noise that was included. With a lower amount of

noise incorporated, the number of peaks that were above expected value decreased. For the samples B1 - 3 and D1 - 2, samples B1 - 3 were overestimated 52% of the time, and samples D1 - 2 were overestimated 53% of the time. Thus, while the average discrepancy for most of the elements in these samples decreased, the number of elements that were overestimated remained the same.

Reasons for overestimation include incorporating some of the background noise when integrating the peaks and detecting masses significantly above the upper range of the standard curve. The accidental incorporation of background noise was more prevalent in the low sample mass (palladium and gold) and low signal (nickel) elements. Reasons for underestimation include not being able to detect very much of certain radioisotopes, due to small peaks compared to the background noise.

### 2.3.2. Circuit board analysis

Since the circuit board samples were comprised of random fragments from a variety of electronic devices, the elemental mass and concentration data are not inherently useful for testing the effectiveness of this project's methods. If the circuits from the devices were first homogenized before they were analysed, the data generated would have given rise to significant findings as they would indicate the total quantity of each element and its actual concentration in the device. These data could then have been compared to those obtained using a different method to evaluate the relative effectiveness of each method.

## 2.4. Conclusion

In summary, neutron activation analysis has been applied to eWaste samples and custom samples made from a variety of valuable but toxic elements. It can detect the variety of elements on which this research focused: silicon, iron, aluminum, copper, magnesium, chromium, cadmium, arsenic, nickel, neodymium, tin, palladium, and gold. Standard curves may be easily generated for quantification of these elements. While there are some limitations regarding the accuracy of the quantification, the elements tested had calculated masses within 40% of their true value. Most of the calculated values were an overestimation of either the

expected or the true mass values (62%). The main contributing factors to the decrease in accuracy are a) the accidental inclusion of background noise when integrating the radionuclide gamma spectra peaks (overestimation) and b) the inability to detect much of a radionuclide's gamma signal due to a low signal to noise ratio in small samples or samples containing radionuclides with half-lives substantially longer than the gamma count time (underestimation). An additional limitation of this technique is that many elements produce the same radionuclides during neutron activation, leading to the inability to quantify a particular element if many contributing elements are present in the sample (i.e. silicon, aluminum, and magnesium all produce $^{27}$Mg).

Further research should be done to better assess the accuracy of this technique by analysing certified reference standards. Decreasing the percent discrepancy in mass quantification, especially with samples containing a large variety of low abundance elements, should also be investigated. This could be done by increasing the irradiation time to allow for more of each radionuclide to form, which may allow for better peak size. Increasing the gamma count time would allow for the radionuclides with longer half-lives to produce more signal, further increasing the peak size. Investigating the elemental mass limits of this technique should also be done, as upper limits, lower limits, and the linear range are not known.

## 3. References

(1) Bookhagen, B.; Obermaier, W.; Opper, C.; Koeberl, C.; Hofmann, T.; Prohaska, T.; Irrgeher, J. Development of a Versatile Analytical Protocol for the Comprehensive Determination of the Elemental Composition of Smartphone Compartments on the Example of Printed Circuit Boards. *Analytical Methods* 2018, *10* (31), 3864–3871. https://doi.org/10.1039/C8AY01192C.

(2) Manikandan, S.; Inbakandan, D.; Valli Nachiyar, C.; Karthick Raja Namasivayam, S. Towards Sustainable Metal Recovery from E-Waste: A Mini Review. *Sustainable Chemistry for the Environment* 2023, *2*, 100001. https://doi.org/10.1016/j.scenv.2023.100001.

(3) Agbim, A.; Schumacher, K. A.; Sharp, N.; Paul, R.; Corzo, R. Elemental Characterization of Electronic Waste: A Review of Research Methodologies and Applicability to the Practice of e-Waste Recycling. *Waste Management* 2024, *187*, 91–100. https://doi.org/10.1016/j.wasman.2024.07.009.

(4) Limbeck, A.; Bonta, M.; Nischkauer, W. Improvements in the Direct Analysis of Advanced Materials Using ICP-Based Measurement Techniques. *J. Anal. At. Spectrom.* 2017, *32* (2), 212–232. https://doi.org/10.1039/C6JA00335D.

(5) Schuster, J.; Ebin, B. Investigation of Indium and Other Valuable Metals Leaching from Unground Waste LCD Screens by Organic and Inorganic Acid Leaching. *Separation and Purification Technology* 2021, *279*, 119659. https://doi.org/10.1016/j.seppur.2021.119659.

(6) Otsuki, A.; Gonçalves, P. P.; Stieghorst, C.; Révay, Z. Non-Destructive Characterization of Mechanically Processed Waste Printed Circuit Boards: X-Ray Fluorescence Spectroscopy and Prompt Gamma Activation Analysis. *Journal of Composites Science* 2019, *3* (2), 54. https://doi.org/10.3390/jcs3020054.

(7) Buczkó, N. A.; Maróti, B.; Gméling, K.; Szentmiklósi, L. Elemental Composition Analysis of Electronic Waste Using Neutron-Based Analytical Techniques: A Novel Approach to Assessing Environmental and Resource Recovery Potential. *J. Anal. At. Spectrom.* 2025, *40*, 2385-2396. https://doi.org/10.1039/D5JA00233H.

(8) Greenberg, R. R.; Bode, P.; De Nadai Fernandes, E. A. Neutron Activation Analysis: A Primary Method of Measurement. *Spectrochimica Acta Part B: Atomic Spectroscopy* 2011, *66* (3), 193–241. https://doi.org/10.1016/j.sab.2010.12.011.

(9) Munita, C.; Glascock, M.; Hazenfratz, R. Chapter 5 - Neutron Activation Analysis: An Overview. In *Recent Advances in Analytical Techniques*; Atta-ur-Rahman; Ozkan, S., Eds.; Bentham Science Publishers, 2019, 3, pp 179–227.

(10) Hevesy, G.; Levi, H. Artificial Radioactivity of Dysprosium and other Rare Earth Elements. *Nature*, 1935, 136, 103. https://doi.org/10.1038/136103a0.

(11) Žikovský, L.; Galinier, J.-L. Calculation of Primary Nuclear Interferences Occurring in Neutron Activation Analysis with a Slowpoke Reactor. *J. Radioanal. Chem.* 1981, *67* (1), 193–203. https://doi.org/10.1007/BF02516241.

(12) Grynpas, M. D.; Pritzker, K. P. H.; Hancock, R. G. V. Neutron Activation Analysis of Bulk and Selected Trace Elements in Bones Using a Low Flux SLOWPOKE Reactor. *Biol. Trace. Elem. Res.* 1987, *13* (1), 333–344. https://doi.org/10.1007/BF02796644.

(13) Kriváň, V.; Münzel, H. Activation Analysis with Fast Neutrons Using a Cyclotron. *J. Radioanal. Chem.* 1973, *15* (2), 575–583. https://doi.org/10.1007/BF02514274.

(14) Münzel, H.; Michel, F.; Coetzee, P. P.; Krivan, V. Utilization of Cyclotron Produced Fast Neutrons in the Activation Analysis for Oxygen. *J. Radioanal. Chem.* 1977, *37* (1), 267–273. https://doi.org/10.1007/BF02520532.

(15) Das, B.; Islam, M. A.; Tamim, U.; Ahmed, F. T.; Hossen, M. B. Heavy Metal Analysis of Water and Sediments of the Kaptai Lake in Bangladesh: Contamination and Concomitant Health Risk Assessment. *Applied Radiation and Isotopes* 2024, *210*, 111358. https://doi.org/10.1016/j.apradiso.2024.111358.

(16) Vichi, S.; Zagni, F.; Cicoria, G.; Infantino, A.; Riga, S.; Zeller, M.; Carzaniga, T. S.; Nesteruk, K. P.; Braccini, S.; Marengo, M.; Mostacci, D. Activation Studies of a PET Cyclotron Bunker. *Radiation Physics and Chemistry* 2019, *161*, 48–54. https://doi.org/10.1016/j.radphyschem.2019.04.001.

(17) Benavente-Castillo, J. A.; Lacerda, M. A. S.; Ferreira, A. V.; Dalle, H. M.; Da Silva, T. A. Assessment of the Neutron Radiation Field with Activation Foils and Intermittent Irradiations around a PETtrace Biomedical Cyclotron. *Applied Radiation and Isotopes* 2019, *153*, 108823. https://doi.org/10.1016/j.apradiso.2019.108823.

(18) Huston, D. A.; Samuleev, P.; Kelly, F.; Corcoran, E. C. Characterization of Flux Distribution in the Pool of the RMC SLOWPOKE-2. *Applied Radiation and Isotopes* 2024, *207*, 111262. https://doi.org/10.1016/j.apradiso.2024.111262.

(19) Campbell, M.; Tikka, A. Low-Cost Target System for Neutron Activation Using a Medical Cyclotron. Application to the Non-Destructive Analysis of Gold and Silver. *Applied Radiation and Isotopes* 2022, *184*, 110117. https://doi.org/10.1016/j.apradiso.2022.110117.

(20) Types of Radioactive Decay. In *Radioactivity Radionuclides Radiation*; Springer-Verlag: Berlin/Heidelberg, 2005; pp 59–87. https://doi.org/10.1007/3-540-26881-2_4.

(21) *Livechart - Table of Nuclides - Nuclear structure and decay data*. https://www-nds.iaea.org/relnsd/vcharthtml/VChartHTML.html (accessed 2025-04-23).

(22) Radioactivity and Nuclear Reactions. In *Radioactivity Radionuclides Radiation*; Springer-Verlag: Berlin/Heidelberg, 2005; pp 43–57. https://doi.org/10.1007/3-540-26881-2_3.

(23) Deo, K.; Kumar, R.; Devan, K.; Umasankari, K. Chapter 10 - Experimental and Operational Reactor Physics. In *Physics of Nuclear Reactors*; Mohanakrishnan, P., Singh, O. P., Umasankari, K., Eds.; Academic Press, 2021; pp 571–633. https://doi.org/10.1016/B978-0-12-822441-0.00014-5.

(24) Vainionpaa, J. H.; Chen, A. X.; Piestrup, M. A.; Gary, C. K.; Jones, G.; Pantell, R. H. Development of High Flux Thermal Neutron Generator for Neutron Activation Analysis. *Nuclear Instruments and Methods in Physics Research Section B: Beam Interactions with Materials and Atoms* 2015, *350*, 88–93. https://doi.org/10.1016/j.nimb.2014.12.077.

(25) Beck, J. N.; Lamberty, C. M. Thermal Neutron Activation Analysis – An Important Analytical Tool. *Applied Spectroscopy Reviews* 2002, *37* (1), 19–55. https://doi.org/10.1081/ASR-120004372.

(26) Laine, P.; Vickery, J. H.; Braun-Sand, S.; Dietrich, D.; Essman, L.; Charlton, W.; Alvarado, C.; Lewis, J. Prompt Gamma Activation Analysis as a Means for Quantitative, Non-Destructive, Non-Invasive Measurement of Mercury in Steel from Oil and Gas Operations. *Nuclear Instruments and Methods in Physics Research Section A: Accelerators, Spectrometers, Detectors and Associated Equipment* 2023, *1045*, 167550. https://doi.org/10.1016/j.nima.2022.167550.

(27) Frontasyeva, M. V. Neutron Activation Analysis in the Life Sciences. *Phys. Part. Nuclei* 2011, *42* (2), 332–378. https://doi.org/10.1134/S1063779611020043.

(28) Sandia National Laboratories, 2025, InterSpec, version 1.0.7 from https://github.com/sandialabs/InterSpec

# 4. Appendix

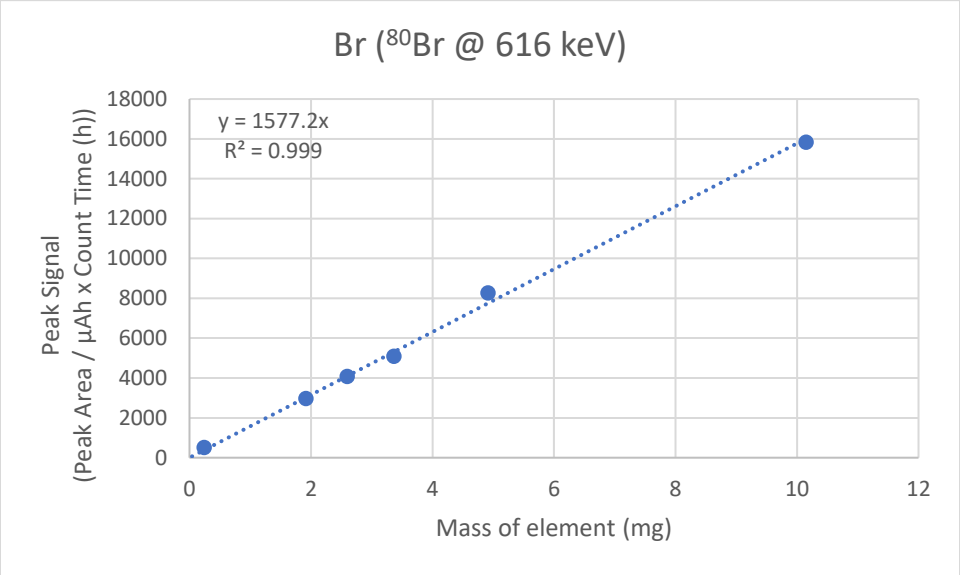


Fig. 4.1. Standard curve based on mass of bromine, in the form of NaBr. Peak area values corrected for proton beam exposure (µAh), spectrometer count time (h), and radionuclide decay (DCF). $T_{1/2}$ is 17.68 minutes. Cyclotron operated at 24 MeV. Samples were irradiated for an average of nine minutes, with an average nominal beam current of 100 µA. Sample placed directly on detector.

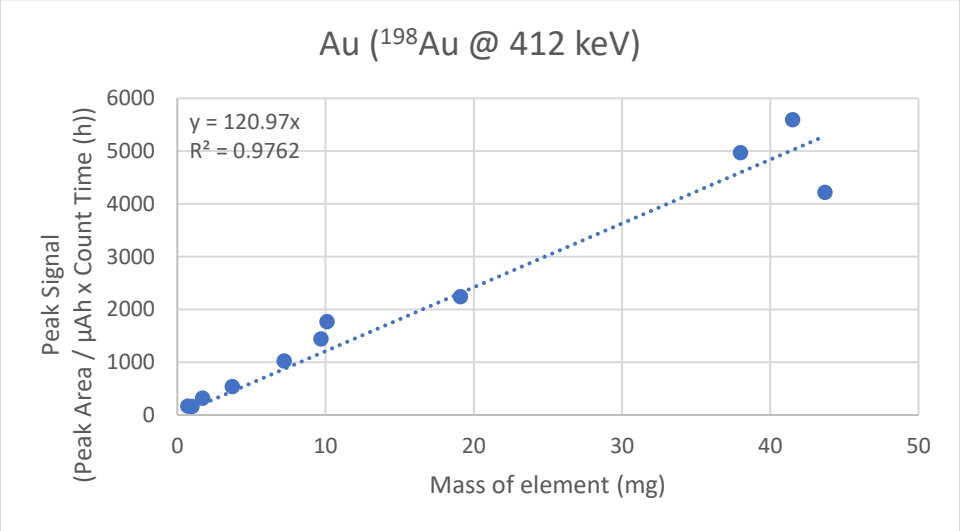


Fig 4.2. Standard curve based on mass of gold, in the form of gold wire. Peak area values corrected for proton beam exposure (µAh), spectrometer count time (h), and radionuclide decay (DCF). $T_{1/2}$ is 2.69 days. Cyclotron operated at 18 MeV. Samples were irradiated for an average of 11 minutes, with an average nominal beam current of 91 µA. Sample placed directly on detector.

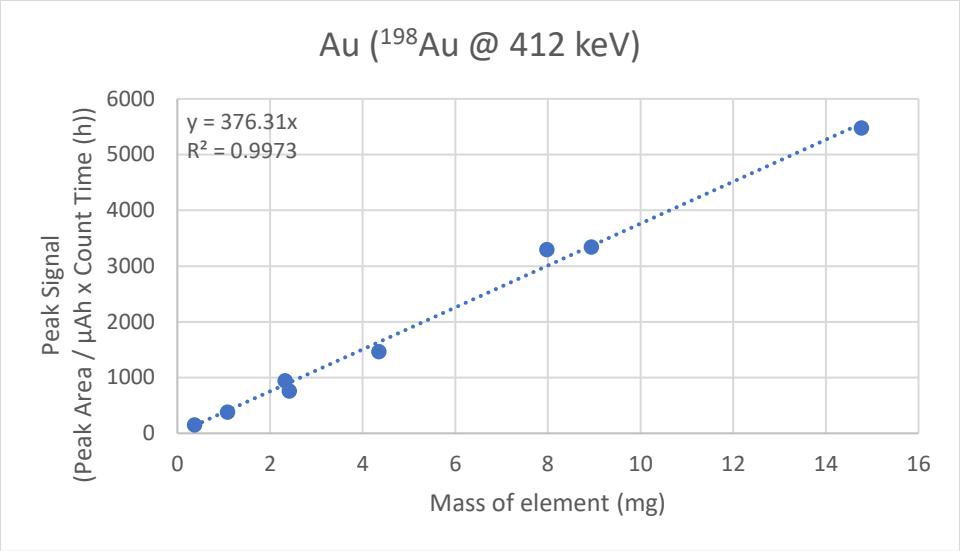


Fig 4.3. Standard curve based on mass of gold, in the form of gold wire. Peak area values corrected for proton beam exposure (µAh), spectrometer count time (h), and radionuclide decay (DCF). $T_{1/2}$ is 2.69 days. Cyclotron operated at 24 MeV. Samples were irradiated for an average of 11 minutes, with an average nominal beam current of 91 µA. Sample placed directly on detector.

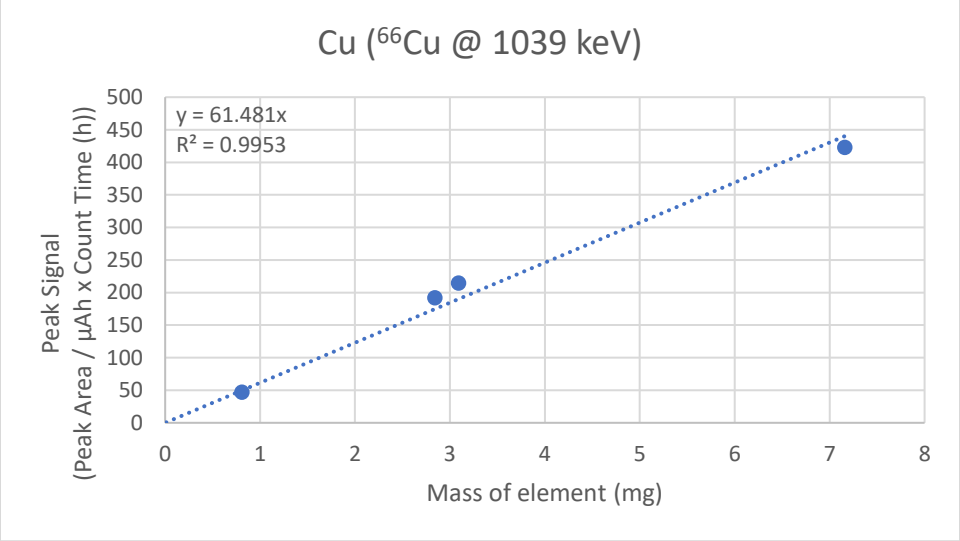


Fig 4.4. Standard curve based on mass of copper, in the form of copper wire. Peak area values corrected for proton beam exposure (µAh), spectrometer count time (h), and radionuclide decay (DCF). $T_{1/2}$ is 5.12 minutes. Cyclotron operated at 18 MeV. Samples were irradiated for an average of nine minutes, with an average nominal beam current of 102 µA. Sample placed directly on detector.

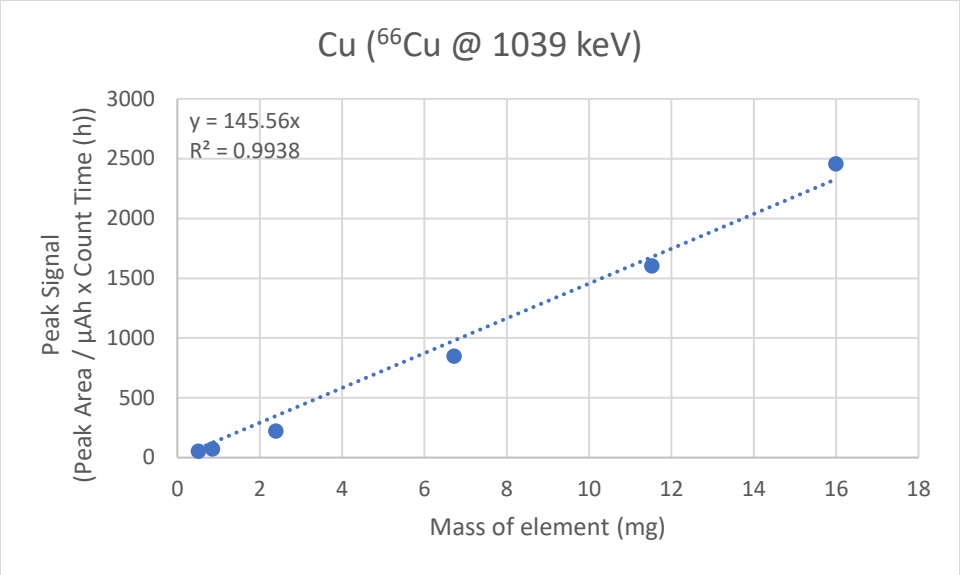


Fig 4.5. Standard curve based on mass of copper, in the form of copper wire. Peak area values corrected for proton beam exposure (µAh), spectrometer count time (h), and radionuclide decay (DCF). $T_{1/2}$ is 5.12 minutes. Cyclotron operated at 24 MeV. Samples were irradiated for an average of eight minutes, with an average nominal beam current of 106 µA. Sample placed directly on detector.

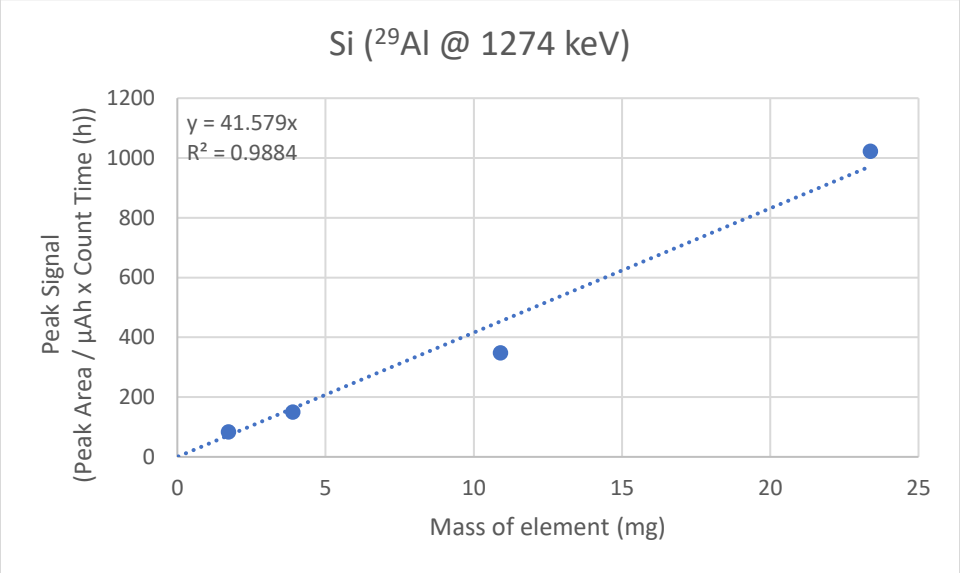


Fig 4.6. Standard curve based on mass of silicon, in the form of $SiO_2$. Peak area values corrected for proton beam exposure (µAh), spectrometer count time (h), and radionuclide decay (DCF). $T_{1/2}$ is 6.56 minutes. Cyclotron operated at 18 MeV. Samples were irradiated for an average of nine minutes, with an average nominal beam current of 112 µA. Sample placed directly on detector.

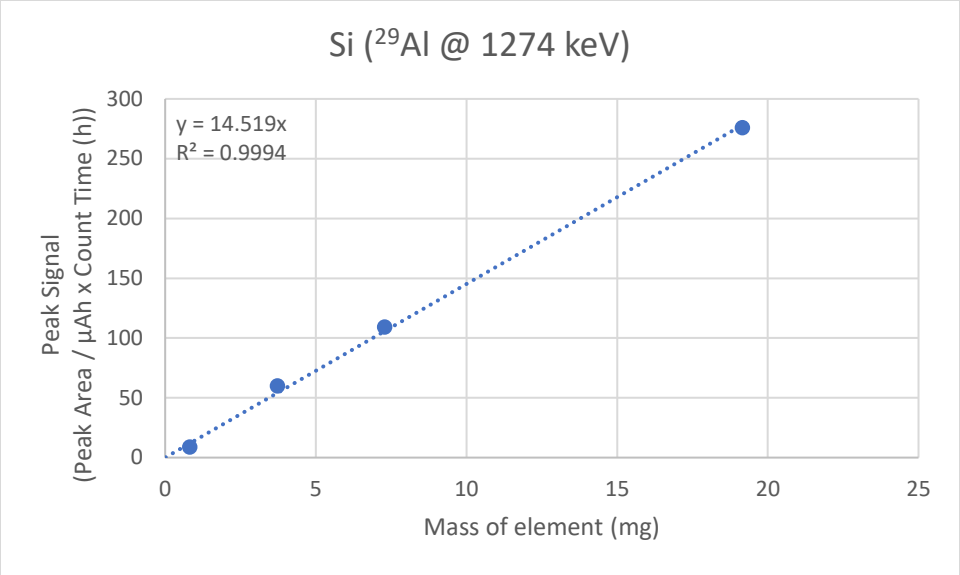


Fig 4.7. Standard curve based on mass of silicon, in the form of $SiO_2$. Peak area values corrected for proton beam exposure (µAh), spectrometer count time (h), and radionuclide decay (DCF). $T_{1/2}$ is 6.56 minutes. Cyclotron operated at 24 MeV. Samples were irradiated for an average of nine minutes, with an average nominal beam current of 107 µA. Sample placed directly on detector.

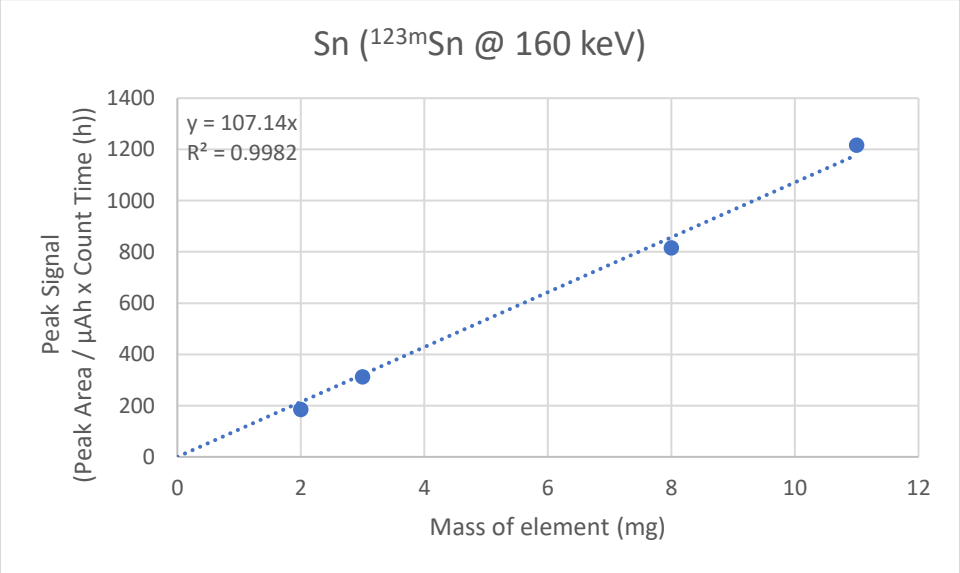


Fig 4.8. Standard curve based on mass of tin, in the form of tin flakes. Peak area values corrected for proton beam exposure (µAh), spectrometer count time (h), and radionuclide decay (DCF). $T_{1/2}$ is 40.06 minutes. Cyclotron operated at 18 MeV. Samples were irradiated for an average of 10 minutes, with an average nominal beam current of 102 µA. Sample placed directly on detector.

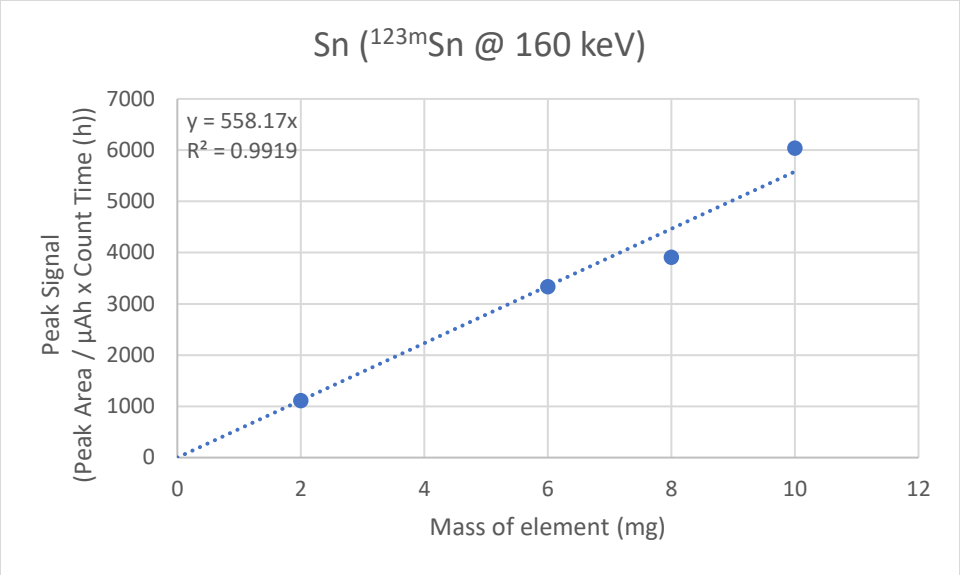


Fig 4.9. Standard curve based on mass of tin, in the form of tin flakes. Peak area values corrected for proton beam exposure (µAh), spectrometer count time (h), and radionuclide decay (DCF). $T_{1/2}$ is 40.06 minutes. Cyclotron operated at 24 MeV. Samples were irradiated for an average of 13 minutes, with an average nominal beam current of 83 µA. Sample placed directly on detector.